THE UNIVERSITY OF MANITOBA

THE EFFECTS OF BONDING PARAMETERS ON ISOTHERMAL SOLIDIFICATION RATE AND MICROSTRUCTURE OF TLP BONDED IN 738LC SUPERALLOY

By

OLUWASEUN AYODEJI IDOWU

A thesis submitted to the Faculty of Graduate Studies in partial fulfillments of the requirements for the degree of Master of Science

DEPARTMENT OF MECHANICAL AND MANUFACTURING ENGINEERING
WINNIPEG, MANITOBA
FEBRUARY 2005

THE UNIVERSITY OF MANITOBA

FACULTY OF GRADUATE STUDIES

*****

COPYRIGHT PERMISSION

THE EFFECTS OF BONDING PARAMETERS ON ISOTHERMAL SOLIDIFICATION RATE AND MICROSTRUCTURE OF TLP BONDED IN 738LC SUPERALLOY

BY

OLUWASEUN AYODEJI IDOWU

A Thesis/Practicum submitted to the Faculty of Graduate Studies of The University of Manitoba in partial fulfillment of the requirement of the degree

Of

Master of Science

ACKNOWLEDGEMENT

I acknowledge my supervisor Dr M.C. Chaturvedi for granting me the opportunity to work on this project. I am sincerely grateful for his timely advice and support throughout the duration of this work. I acknowledge Dr N.L. Richards, for his encouragement and guidance. Thanks are also due to Dr O.A. Ojo, for his input through many useful discussions.

I acknowledge the financial support provided for this research project by Standard Aero Ltd, Bristol Aerospace, Boeing Canada Technologies Ltd, Manitoba Aerospace Association, NSERC etc. I also appreciate financial support in form of research assistantship and graduate fellowship from the University of Manitoba. I am grateful to John Van Dorp, Dan McCooeye, Don Mardis and Mike Boskwick for their technical assistance. Thanks are also due to Krutika and other members of the materials research group for their support and friendliness. I sincerely appreciate the love and support from Mr and Mrs Adegunju, 'sola Adeyinka, 'dotun, and my family members; 'seyi, 'bode, 'timi, Dr and Mrs A.A. Idowu. Finally, I am very grateful to Elshaddai, the source of my wisdom and understanding.

ABSTRACT

This thesis reports the results of an investigation of the effects of bonding temperature and joint gap size on isothermal solidification rate, and on the nature of interfacial/grain boundary particles formed during the transient liquid phase (TLP) bonding of IN 738LC superalloy using a ternary Ni-Cr-B filler alloy, Nicrobraz 150.

The microstructure of the bonded samples was examined using optical metallography and then a JEOL 5900 Scanning Electron Microscope (SEM) equipped with an ultra thin window Oxford energy dispersive x-ray spectrometer (EDS).

In contrast to the solidification behavior predicted by the current TLP models, isothermal solidification occurred under two separate regimes, depending on the bonding temperature and joint gap size. The rate of isothermal solidification in the first regime was faster than in the second regime. This led to a deviation in isothermal solidification completion time from that predicted by a conventional TLP model. The change in solidification rate was attributed to the substantial enrichment of the liquid interlayer with the base alloy solute elements and its continuous modification during isothermal solidification. These factors also influenced the nature of the phases formed in the centerline eutectic constituents subsequent to the incomplete isothermal solidification.

Also, in addition to eutectic constituents, which were observed at the centerline of a 100 μm joint that was bonded for 1 hr at 1067°C, nickel-rich and chromium-rich boride

particles were observed at the original substrate/insert interface. The formation of these particles was however prevented by brazing at a suitable temperature and/or gap size. Furthermore, an extensive amount of chromium-rich boride and Ni-Al-Ti rich particles were observed on the substrate grain boundaries of 100 μm joints that were bonded for 1 hr at 1067°C and 1160°C. However, brazing at 1175°C resulted in the localized liquation of the Ni-Al-Ti rich particles, as resolidified fine γ/γ' eutectic type products were observed around some of the dispersed Cr-rich boride particles.

TABLE OF CONTENTS

LIST OF FIGURES

LIST OF TABLES

Chapter 1

INTRODUCTION

Inconel 738 superalloy is a vacuum melted, vacuum cast, precipitation-strengthened nickel base superalloy. It possesses excellent high temperature creep-rupture strength combined with hot corrosion resistance, which is superior to that of many high-strength superalloys. It derives its strength primarily by the precipitation of ordered $L1_2$ intermetallic $Ni_3(Al,Ti)$-type γ' phase in the γ solid solution-strengthened matrix. Due to its excellent properties, it has found a wide range of applications in power generating and aerospace industries for making gas turbine jet engine components, such as blades and vanes. However, the requirements for improved efficiency of the aero-engines and power generation turbines have necessitated the turbine components to withstand higher stresses and temperatures, causing a more rapid degradation of these components by enhanced level of creep, fatigue and oxidation etc [1]. This damage necessitates the repair of these components in order to extend their total life. The most widely used repair process is welding. However, Inconel 738, like most precipitation hardened Ni-base superalloys that contain substantial amounts of Al and Ti are generally considered to be difficult to weld due to their high susceptibility to heat affected zone (HAZ) cracking during welding and post-weld heat treatment [2, 3, 4]. In view of this, Duvall et al [5] developed the transient liquid phase (TLP) bonding process, also referred to as diffusion brazing process, which is a hybrid process that combines the beneficial features of liquid phase joining and diffusion bonding techniques [6]. This process eliminates the need for the application of substantial pressure during bonding [5], and can be successfully used in joining of heat

resistant alloys that are inherently susceptible to hot cracking or post-weld heat treatment cracking [5, 7, 8].

Successful application/optimization of the TLP bonding process involves a proper control of parameters which include, bonding temperature, time, filler alloy thickness and composition. This is to obtain a joint whose microstructure and mechanical properties are comparable to those of the base alloy [9]. In this regard, several attempts have been made to predict the time required to complete the TLP bonding process by using both analytical and numerical models over the past decades. These models were based on hypothetical binary phase relationships between the base and filler alloys. However, recent studies [10, 11] have suggested that the presence of second solute element in the filler, may affect the rate of isothermal solidification. It should be noted that this has not been implicitly considered in the existing TLP bonding models. Furthermore, significant volume fractions of precipitate particles usually form along the interface and the substrate grain boundaries of TLP-bonded joints. These particles are known to have detrimental effects on the corrosion resistance and mechanical properties of the bonded assembly [12, 13]. However, the mechanism and the preclusion of their formation are still emerging subjects in the literature.

In view of the above, the present work was designed to investigate the effects of bonding temperature and joint gap size on isothermal solidification rate, since these may affect the composition of the liquid interlayer during the TLP bonding of a multicomponent Inconel 738LC superalloy, using a Ni-Cr-B ternary filler alloy. Furthermore, the effects of

bonding temperature and joint gap size on the nature of interfacial particles, and the effects of bonding temperature on the nature of particles, which formed along the substrate grain boundaries of IN 738LC superalloy TLP-bonded joints were also investigated.

The results obtained have provided a better understanding of the factors that can affect the isothermal solidification rate during TLP bonding process; most especially when multicomponent alloys are involved. This, coupled with a better understanding of the microstructural development during TLP bonding of IN 738 superalloy, as provided by this work, will be a significant tool for future work on the optimization of the TLP bonding process.

In this dissertation, the physical metallurgy of Inconel 738 is reviewed along with the various available joining techniques, and past work that has been done on the brazing of superalloys. The results and discussions of the above mentioned investigations are subsequently presented.

Chapter 2

LITERATURE REVIEW

2.1 Alloy Inconel 738

With the advent of World War II, the gas turbine became an important driver for alloy development or adaptation, and there has been a keen race towards making metal alloys available for the insatiable thirst of the designer for improved high-temperature strength capability [14]. Thus, over the past years a lot of nickel-, iron-nickel-, and cobalt-base alloys, which can generally be used at temperatures above 540°C have been developed. Alloy Inconel 738 is one of the nickel-base superalloys, which was developed in this regard. It is designed to provide the gas turbine engine components with good creep strength up to 982°C combined with the ability to withstand long time exposure to the hot corrosive environments associated with an aircraft engine [15]. It derives its high temperature strength primarily by the precipitation of ordered $L1_2$ intermetallic $Ni_3(Al,Ti)$-type γ' phase in the γ solid-solution matrix and that of carbides at the grain boundaries. Table 2.1 shows the nominal chemical compositions of two versions of cast Inconel 738 alloy that are available in the market. IN 738C superalloy usually has a high carbon concentration in the range of 0.15 – 0.20 wt%, while IN 738LC is the low carbon version with a carbon concentration of between 0.09 – 0.13 wt%. The mechanical and physical properties of IN 738 superalloy are listed in Table 2.2.

Table 2.1: Nominal composition of alloy IN 738 [15]

Element	**High carbon IN 738C wt%**	**Low carbon IN 738 wt %**
Carbon	0.17	0.11
Cobalt	8.50	8.50
Chromium	16.00	16.00
Molybdenum	1.75	1.75
Tungsten	2.60	2.60
Tantalum	1.75	1.75
Niobium	0.90	0.90
Aluminum	3.40	3.40
Titanium	3.40	3.40
Boron	0.010	0.010
Zirconium	0.10	0.05
Iron	LAP*	LAP
Manganese	LAP	LAP
Silicon	LAP	LAP
Sulphur	LAP	LAP
Nickel	Balance (61)	Balance (61)

*Low As Possible

Table 2.2: Mechanical and physical properties of IN 738 superalloy [15]

Physical properties		**Mechanical properties**					
Melting Range	1232-1315^{0}C	**Temperature (^{0}C)**	**Ultimate Tensile Strength (MPa)**	**Yield Strength (MPa)**	**Elongation (%)**	**Poisson's Ratio**	0.29
Density	8.11gm/cm^3	21	1096	951	5.5	**Young Modulus**	200.2 Gpa
		649	1055	910	7.0		
Coefficient of Thermal Expansion	15.36 X 10^{-6}/^{0}C	760	965	793	6.5	**Shear Modulus**	78 Gpa
		871	772	552	11.0		
Electron Vacancy Number	<2.36	982	455	345	13.0		
		Stress Rupture Properties					
		Temperature (^{0}C)	**Stress (Psi)**	**Life (hr)**	**Elongation (%)**	**Reduction of Area (%)**	
		732	90,000	212	6	8	
		816	40,000	3314	5	5	
		927	33,000	95	8	14	
		982	22,000	66	12	18	

2.2 The Role of various Alloying Elements

The FCC nickel lattice is known to have a large solubility for many other elements due to its electronic structure [16]. IN 738 contains a variety of alloying elements that are required to produce the desired metallurgical effects and properties, which are summarized in Table 2.3.

2.3 The Microstructure of As Cast IN 738:

IN 738 has a very complex microstructure, which is influenced by several factors such as: elemental composition, melting and casting route, final heat treatment, and service exposure. It has a coarse grain size ranging from 500 - 800μm. Also, as shown in the optical micrograph in Fig. 2.1, IN 738 has well serrated grain boundaries. This is known to impede grain boundary sliding and thus promote intragranular deformation instead [17]. The cast alloy essentially consists of extensive precipitates of ordered γ' intermetallic phase within the dendrite core and in the interdendritic region [4]. Smaller volume fractions of various kinds of carbides/Carbonitrides, predominantly MC type carbide, boride, sulphocarbide and γ-γ' eutectic, which form during ingot solidification are also present along the interdendritic region [18].

2.3.1 The Gamma (γ) matrix:

The matrix of IN 738 is austenitic FCC solid solution of nickel-cobalt-chromium and several other alloying elements. It also contains a dispersion of ordered intermetallic particles of $Ni_3(Al,Ti)$-type γ' precipitates. It derives some of its strength from the presence of extensive amounts of substitutional solid solution elements such as Co, Cr,

Table 2.3: Role of alloying elements in IN 738 superalloy [14, 15]

Effect	**Element**
Solid solution strengtheners	Co, Cr, Mo, W, Ta
Carbide formers	
MC	W, Ta, Ti, Mo, Nb
$M_{23}C_6$	Cr, Mo, W
M_6C	Mo, W, Nb
Forms γ' $Ni_3(Al,Ti)$	Al, Ti
Raises solvus temperature of γ'	Co
Promotes the formation of hardening precipitates and/or intermetallics	Al, Ti, Nb
Oxidation resistance	Al, Cr
Sulfidation resistance	Cr, Co, Si
Improves creep properties	B, Ta
Inhibit carbide coarsening; improve grain boundary strength; improve creep strength and ductility	B, Zr
Causes embrittlement by grain boundary segregation	Impurity elements: S, P, Si
Promote formation of undesirable TCP phases of σ, μ and Laves etc	Cr, Mo, W, Co

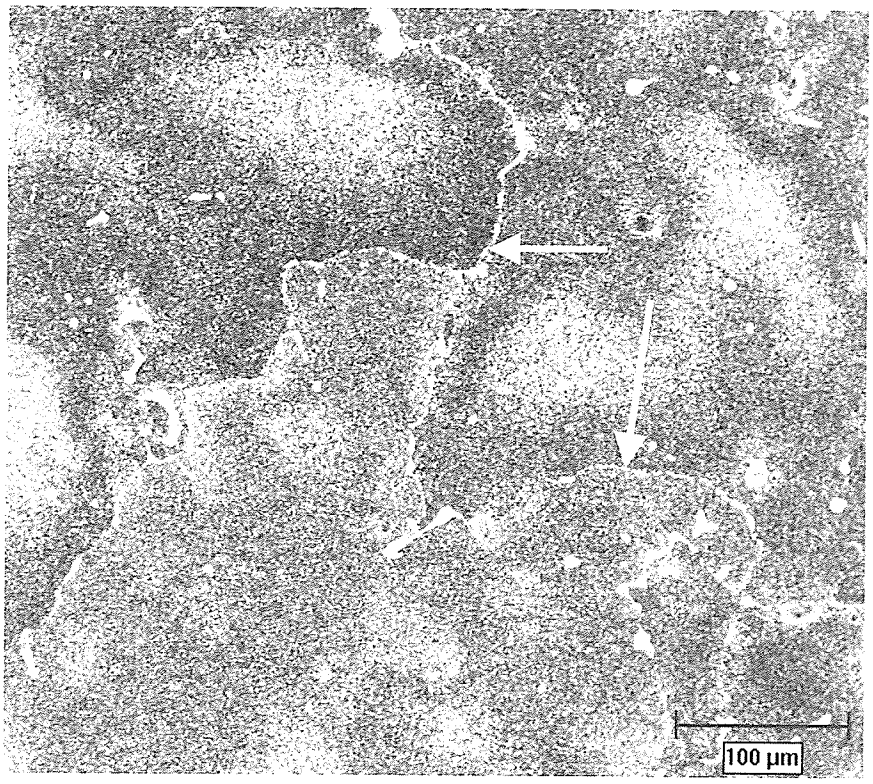

Fig. 2.1: Optical micrograph showing serrated grain boundary in as cast IN 738 alloy.

Mo and W. These elements differ with nickel in atomic diameter up to about 10%, thus their solubility in the nickel matrix results in the distortion of the lattice [19], which typically gives rise to a spherically symmetrical stress field surrounding the solute atoms. This stress field can interact with the stress field of a dislocation, giving rise to solute atom – dislocation interaction, and thus strengthen the γ-matrix.

2.3.2 Gamma Prime (γ') Precipitates

This is the principal high temperature-strengthening phase in IN 738. It is formed when the solubility limits of titanium and aluminum are exceeded in the γ-matrix, resulting in the precipitation of $L1_2$ intermetallic $Ni_3(Al,Ti)$-type γ' particles. These precipitates, whose distribution is shown in Fig. 2.2, contain some other elements in smaller amounts, and their composition in IN 738 has been suggested [20] to be given by: $(Ni_{.922}Co_{.058}Cr_{.017}Mo_{.002}W_{.002})_3(Al_{.518}Ti_{.352}Ta_{.046}Nb_{.41}W_{.014}Cr_{.027})$. While the γ matrix has a FCC crystal structure, γ' has an ordered FCC structure with lattice parameter very close to that of γ. The γ' precipitates are therefore coherent with the matrix, and a cube – cube orientation relationship exists between the two of them [21]. However, the difference in the lattice parameter between the two phases, although small, commonly called the "misfit" or "mismatch" is usually not zero [19]. This is known to have a significant importance in determining the morphology of γ' precipitates and the strength of the alloy. It has been observed that γ' tends to form as spheres for 0 to +/- 0.2% mismatch, becomes cuboidal for the mismatch of about +/- 0.5 to 1%, and is platelike at the mismatch of above about +/- 1.25% [14]. Figs. 2.3 a, b, and c show the TEM bright field image and

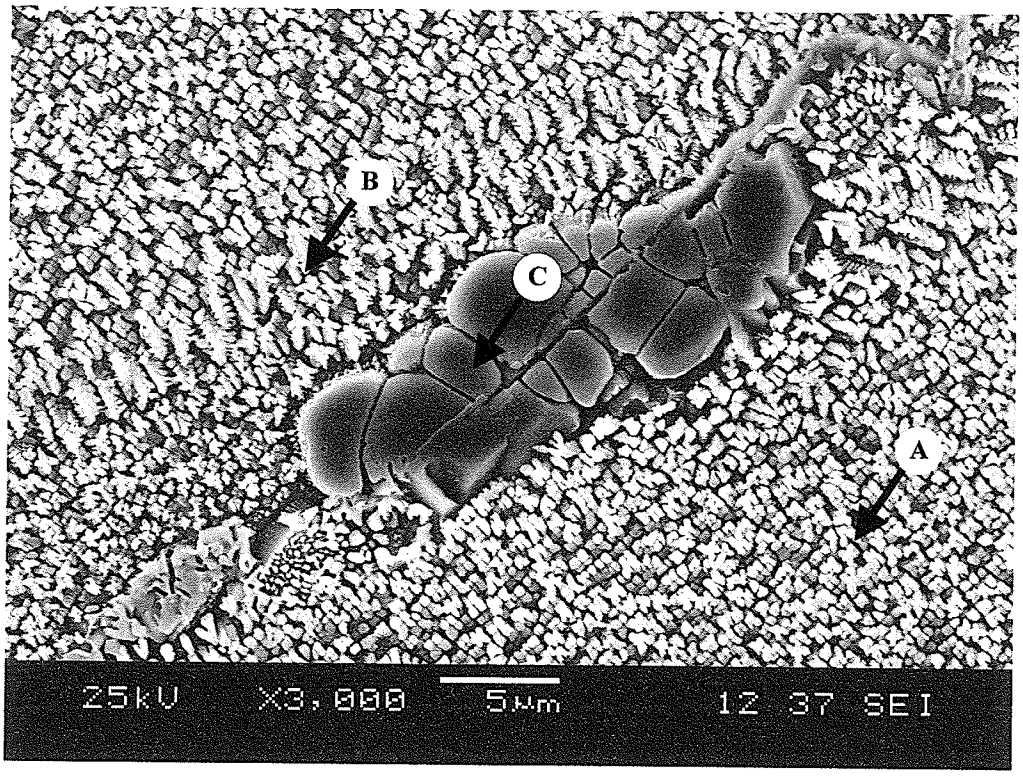

Fig. 2.2: SEM micrograph showing the distribution of γ' precipitates in as cast IN 738 alloy; A) dendritic γ' B) interdendritic γ' C) grain boundary γ'.

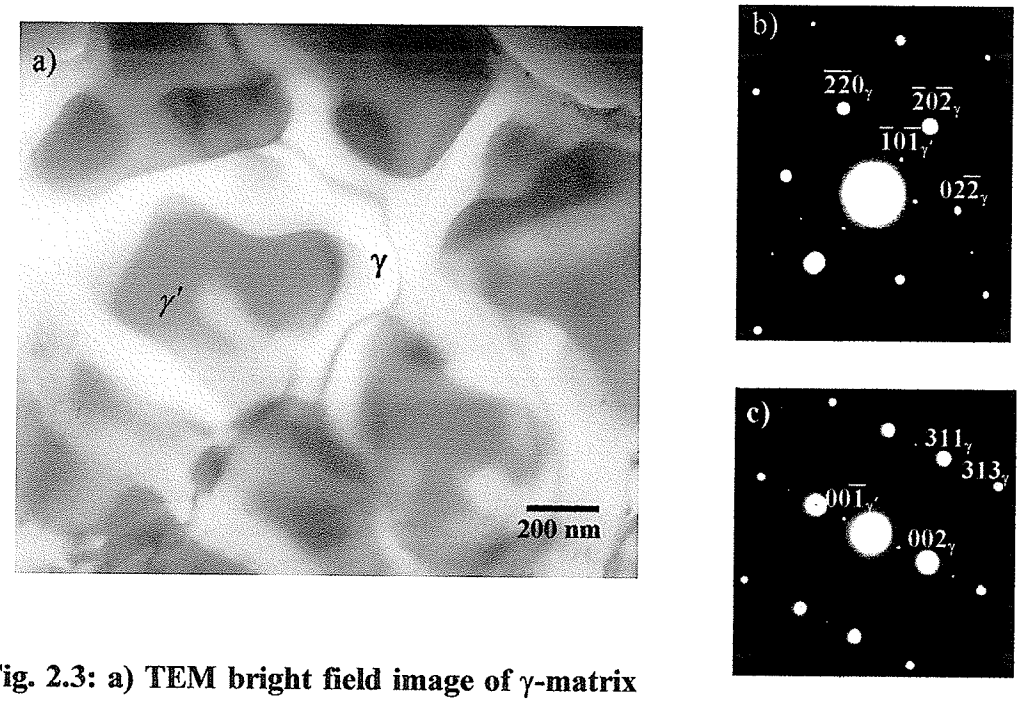

Fig. 2.3: a) TEM bright field image of γ-matrix and γ' precipitates. b) SADP from $[\bar{1}11]$ zone axis c) SADP from $[\bar{1}30]$ zone axis; showing superlattice reflections of γ' precipitates.

selected area diffraction patterns (SADP) from γ matrix and γ' precipitates. Observed in addition to the fundamental reflections from γ' and γ matrix on the SADP taken from $[\bar{1}11]$ and $[\bar{1}30]$ zone axes, is the presence of weak superlattice spots from $L1_2$ ordered intermetallic γ' precipitates. The precipitation strengthening due to γ' particles depends on the following:

1. **Lattice mismatch between γ' and γ:**

The degree of γ/γ' lattice mismatch has a significant effect on the mechanical strength of nickel-base superalloys [22]. A coherent particle whose lattice parameter differs from that of the matrix produces a coherency strain field, which interacts with dislocations and subsequently makes a significant contribution to the overall hardening of the alloy. However, a large value of mismatch increases the driving force for particle coarsening, which can have detrimental effect on high temperature strength of the alloy [19]. The mismatch between the γ'/γ in IN 738 is in the favorable range of 0 to +/- 1%, thus making it possible to pack more γ' precipitate (approximately 40% volume fraction) in the γ matrix.

2. **Precipitate Order:**

There is a significant increase in the amount of energy required for dislocations to pass through the γ' precipitates due to their ordering. It is known that ordered precipitates posses an energy (Antiphase Domain Boundary or APB), which represents the extra energy associated with ordered atom positions versus normal disordered or random

positions [14]. The higher the APB energy associated with the precipitates, the higher will be the corresponding force required for dislocations to shear them.

2.3.3 Carbides

IN 738LC is known to have a nominal carbon composition of 0.11wt% [15], therefore, a significant amount of predominantly MC type carbides are formed, both intergranularly and transgranularly, in the as cast alloy. The distribution of these carbides along the grain boundaries of as cast IN 738LC superalloy is shown in Fig. 2.4. Also, Figs. 2.5 a, b, c and d show the TEM images (bright and dark field) and SADPs from a carbide precipitate, which was extracted on a carbon replica from the γ matrix of Inconel 738LC superalloy. MC carbides form from the melt during solidification as a result of the reaction of carbon with reactive and refractory elements such as Ti, Ta, Nb, Mo and W. They may also be precipitated from the supersaturated solid solution at high temperatures, in excess of 1038°C, and usually exhibit a coarse, random, globular, or blocky morphology, with an ordered FCC lattice structure and their size ranges from fraction of one micron to hundreds of microns. It has been suggested [20] that MC carbides have the formula: $(Ti_{.5},Ta_{.2},Nb_{.2},W_{.04},Mo_{.03},Cr_{.02})C$, and a typical TEM/EDS spectrum from an MC carbide particle is shown in Fig. 2.6.

MC carbides tend to degenerate during heat treatment and service, resulting in the generation of other carbides such as $M_{23}C_6$ and/or M_6C. Fig. 2.7 shows a thin film of $M_{23}C_6$ that formed along a grain boundary of IN 738LC after a standard solution heat treatment of 1120°C for 2 hours, followed by aging at 845°C for 24 hours. Thakur [17]

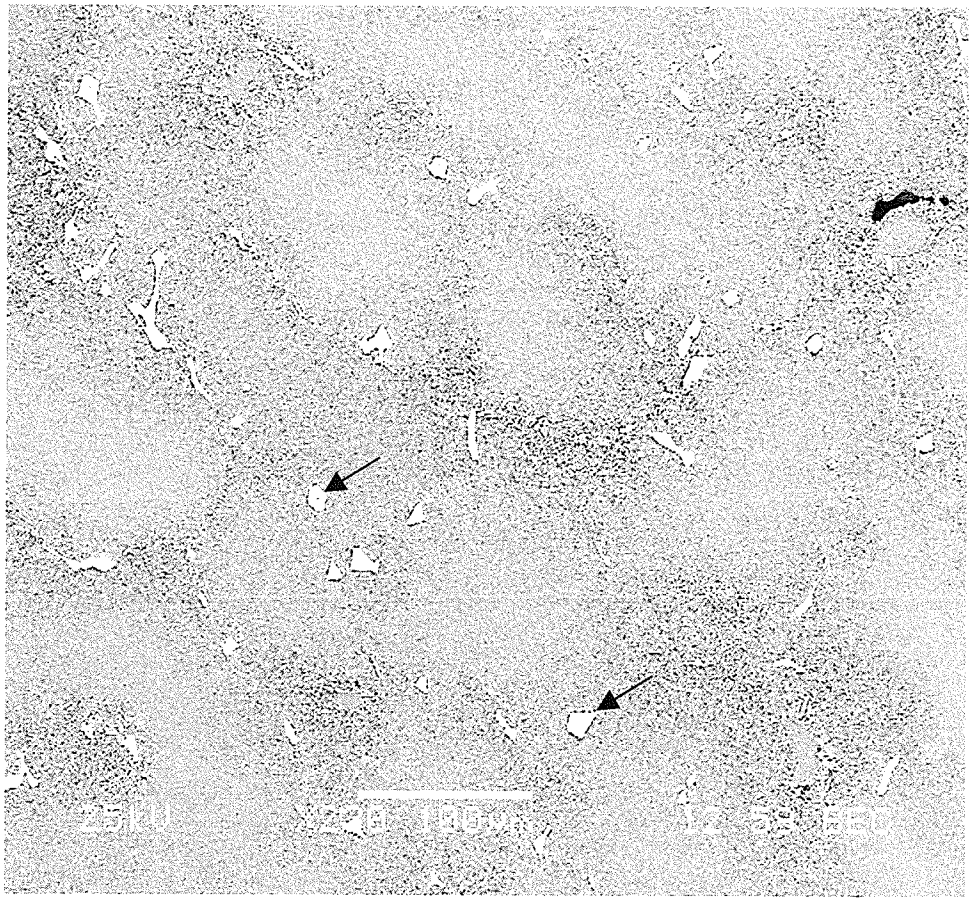

Fig. 2.4: SEM backscattered electron image showing MC carbide particles in as cast IN 738LC alloy.

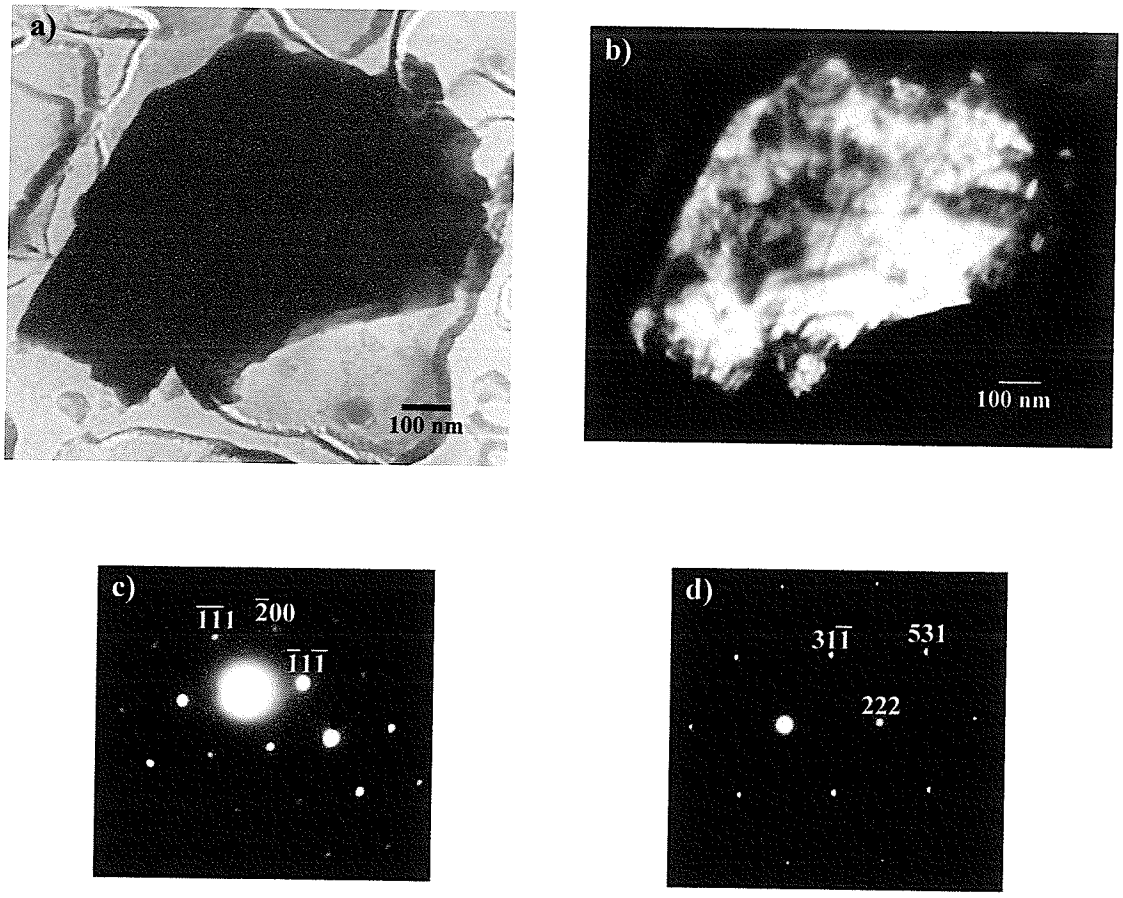

Fig. 2.5: TEM a) bright field image b) dark field image ($g = (02\bar{2})$) of extracted carbide precipitate with lattice parameter a = 4.36Å c) SADP from [011] zone axis d) SADP from [$\bar{1}2\bar{1}$] zone axis.

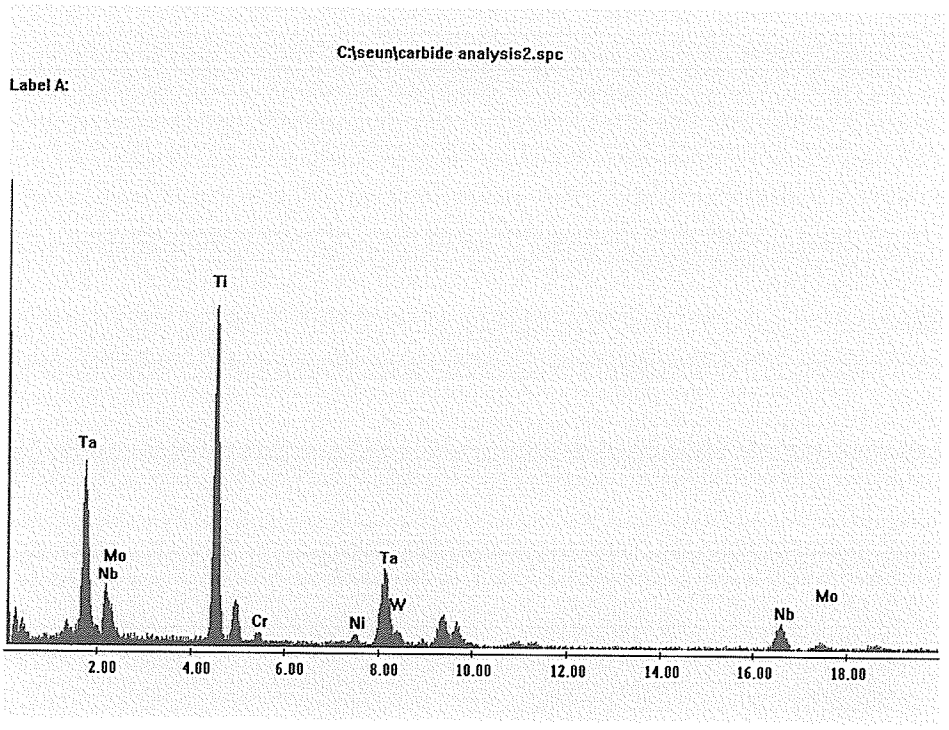

Fig. 2.6: TEM/EDS spectrum from a MC-type carbide particle.

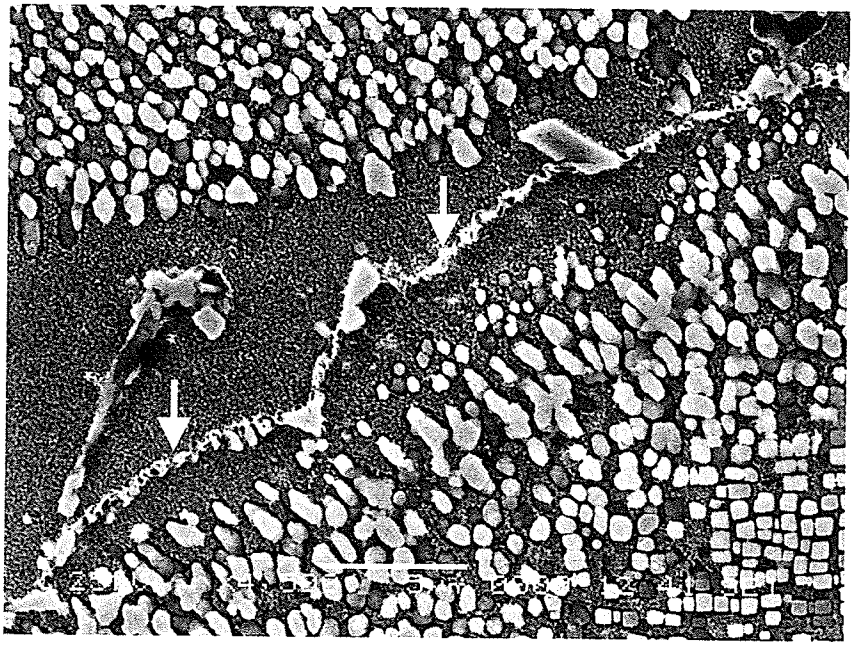

Fig. 2.7: SEM microstructure of intergranular $M_{23}C_6$ carbide formed in IN-738LC after solution heat treatment at 1120°C/2hrs and aging at 845°C/24hrs.

has also reported the formation of discrete grain boundary $M_{23}C_6$ carbides in IN 738 that was heat-treated under the same conditions as above. The degeneration of MC carbides, which results in the formation of $M_{23}C_6$ carbides, occurs by the reaction [21]:

$MC + \gamma \rightarrow M_{23}C_6 + \gamma'$ or

$(Ti,Mo)C + (Ni,Cr,Al,Ti) \rightarrow Cr_{21}Mo_2C_6 + Ni_3(Al,Ti)$

$M_{23}C_6$ (for example $Cr_{23}C_6$) carbides have complex cubic structure and readily form in alloys with moderate-to-high chromium content [14] at a favorable temperature range of 760 °C to 816 °C, although they may form at a temperature that is as high as 982 °C. They can also form from unused free carbon when cast ingot cools through the $M_{23}C_6$ solvus range (1000°C to 1050°C). The carbides encountered in this alloy serve three principal functions:

1. When properly formed at the grain boundaries, they strengthen and prevent or retard grain boundary sliding, and permit stress relaxation. $M_{23}C_6$ carbides are known to improve the creep life of the alloy if present in discrete form along the grain boundaries. However, they have a detrimental effect on the alloy properties if they form a continuous network along the grain boundaries, as this will enhance crack propagation by boundary-matrix decohesion.
2. They may provide dispersion strengthening to the γ-matrix if they are precipitated as fine carbides.
3. Carbides can tie up certain elements that would otherwise promote phase instability during service.

2.3.4 The γ-γ' Eutectic

Dendritic solidification of an alloy leads to compositional differences within the as-cast alloy. These differences occur as a result of the segregation of solute elements between the cores and tips of the dendrites. It is known that the extent of segregation depends on the partition coefficient k ($=\frac{C_s}{C_l}$, i.e. the ratio of the equilibrium concentrations of the solid and the liquid) of each element, which is present in the molten alloy undergoing solidification [23, 25], and on the conditions of solidification and subsequent cooling. The formation of the non-equilibrium γ-γ' eutectic product is one of the effects of microsegregation during ingot solidification [25, 26] of IN 738 alloy. The γ-γ' eutectic islands consist of lamellar structure of continuous γ' platelets, or rafts [17], as shown in Fig. 2.8. During solidification, the solute-rich liquid pool is expected to commence solidification first as γ, and then transforms to γ-γ' eutectic product on reaching the eutectic temperature [4]. It has been suggested that the γ-γ' eutectic product forms in such a way that their "crown" region protrudes into the last liquid to solidify [27]. In the interdendritic spaces, where the last liquid solidifies, segregation can also lead to the formation of new secondary phases [19]. For example, the formation of boride and Zr-Ni rich phases are often observed along with the γ-γ' eutectic product formed in as cast IN-738 (as shown in Figs. 2.9 and 2.10). These secondary phases, which form in the interdendritic spaces, can have deleterious effects on the mechanical properties of the alloy considering their massive morphology, which can aid in initiating cleavage fracture.

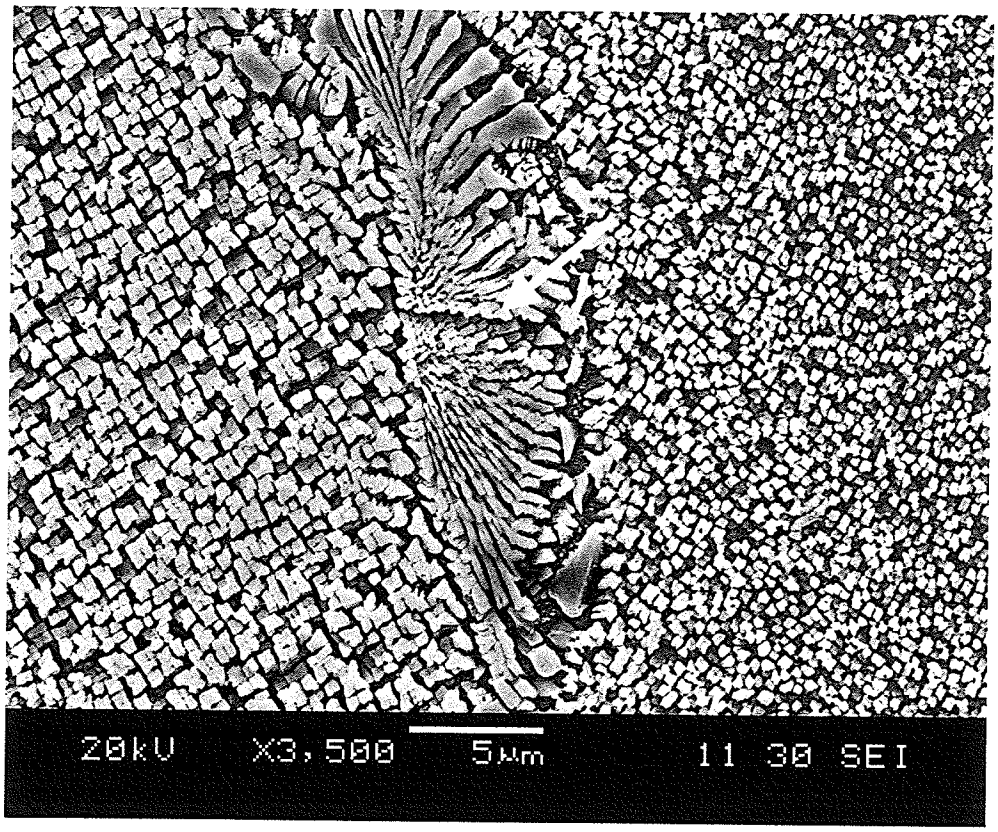

Fig. 2.8: SEM microstructure of γ-γ' eutectic island in as cast IN 738LC alloy.

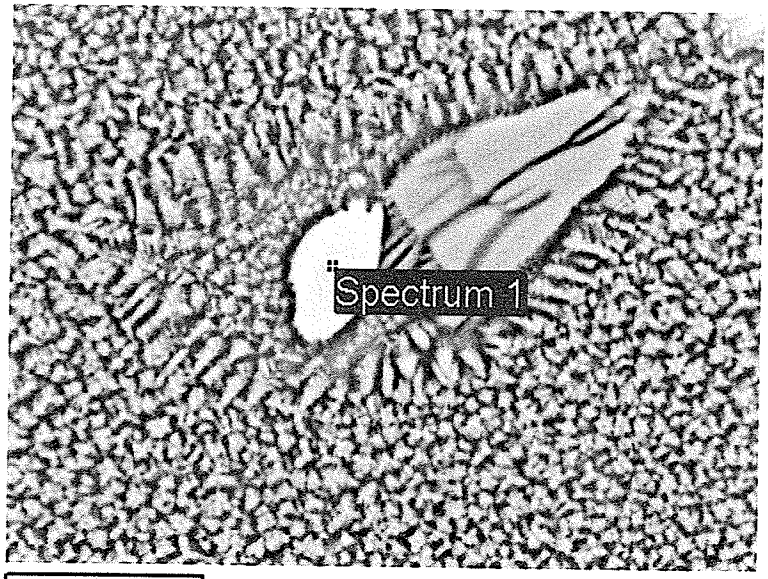

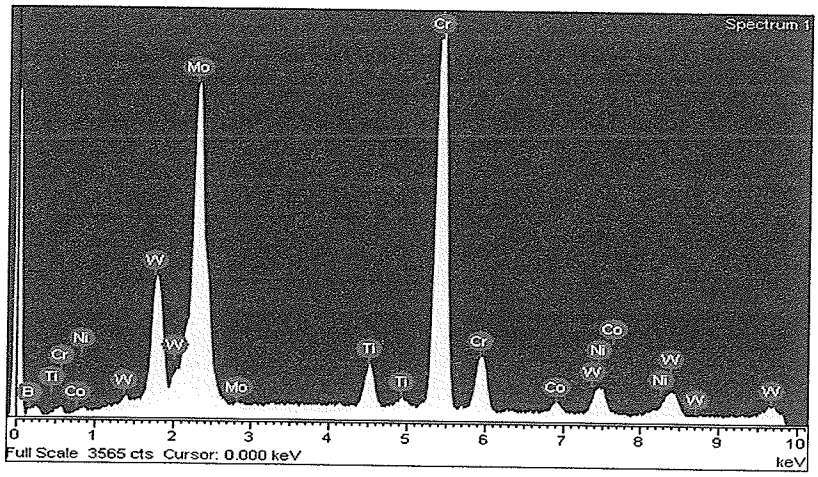

Element	App Conc.	Intensity Corrn.	Weight%	Weight% Sigma	Atomic%
Ti K	2.60	0.8784	3.13	0.09	4.72
Cr K	35.00	0.9258	39.88	0.26	55.43
Co K	1.50	0.9020	1.75	0.13	2.15
Ni K	4.32	0.9666	4.71	0.17	5.80
Mo L	22.01	0.6946	33.43	0.30	25.18
W M	11.75	0.7245	17.11	0.22	6.72
Totals			100.00		

Fig. 2.9: SEM backscattered electron image (BEI) and EDS analysis of a boride particle observed ahead of a γ-γ' eutectic island.

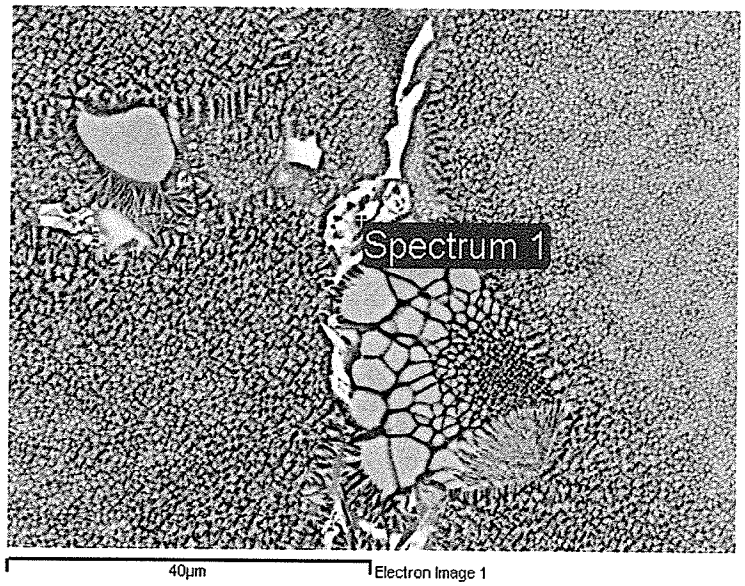

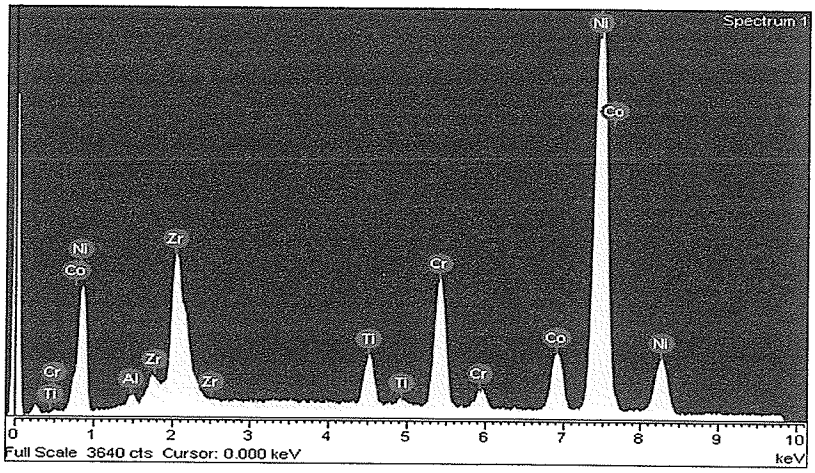

Element	App Conc.	Intensity Corrn.	Weight%	Weight% Sigma	Atomic%
Al K	0.32	0.3606	0.82	0.09	1.84
Ti K	3.06	0.9319	3.05	0.09	3.84
Cr K	11.25	1.0109	10.32	0.14	11.99
Co K	8.48	0.9405	8.36	0.19	8.57
Ni K	65.22	0.9883	61.24	0.32	63.01
Zr L	9.97	0.5707	16.21	0.29	10.74
Totals			100.00		

Fig. 2.10: SEM backscattered electron image (BEI) and EDS analysis of a Zr-Ni rich phase observed ahead of a γ-γ' eutectic island.

2.3.5 The Topologically Closed Packed (TCP) Phases

These are usually platelike or needlelike phases such as σ, μ and Laves. They may form in alloys of some compositions and under certain conditions, for example, after a long time exposure of the alloy in service. It has been well established that σ phase precipitation generally occurs when the γ matrix reaches a critical electron vacancy concentration (N_v) range [28]. The electron vacancy number for IN 738LC was estimated to be 2.31 [15], which is less than the critical value of 2.36. Also, it has been reported that σ phase was not present in the heat-treated IN 738C of optimum composition, even after more than 5000 hours of stress-rupture testing at a temperature of 816°C and at a stress of 40,000Psi [15]. The TCP phases are very brittle, thus they can have very serious detrimental effect on the mechanical properties of the alloy if present in more than trace amounts.

2.4 The Standard Heat Treatment

If the optimum precipitation-hardening effects in IN 738 alloy are to be achieved, then the alloy has to be solution heat-treated at a temperature more or less above the γ' solvus. This is to dissolve the γ' particles in the γ-matrix, resulting in the supersaturation of the γ-matrix with γ'-forming elements when the solution heat-treated alloy is rapidly cooled to the room temperature. The solution heat treatment is then followed by an aging heat treatment, which is employed in order to optimize the distribution of γ' in γ-matrix, and to promote transitions in other phases [14].

2.4.1 The Solution Heat Treatment

IN 738 alloy has a standard solution heat treatment temperature of 1120°C /2 hours. This results in almost a complete dissolution of primary γ' in the dendritic core, with little, if any dissolution of the particles in the interdendritic regions [4]. Fig. 2.11 shows the distribution of γ' precipitates in solution treated IN 738 superalloy. It is seen that after the solution heat treatment operation, the alloy mostly consists of fine (~ 1μm) spheroidal secondary γ' particles, which are distributed in the interdendritic region, but more predominantly in the dendritic core. These form during cooling from the solution heat treatment temperature. Also, the dendritic core is outlined by a ring of large γ' particles due to very rapid growth of these particles that contain higher aluminum and titanium content, immediately before solutioning. Furthermore, fairly regular distribution of coarse cuboidal primary γ' particles with size range of 0.6 – 0.8μm is also observed along the interdendritic region (as shown in Fig. 2.11).

2.4.2 The Aging Treatment

The second stage of the standard heat treatment operation, namely; aging at 845°C/24 hours followed by air-cooling, increases the particle sizes of both spheroids and cuboids γ' particles, but no appreciable change in the particle morphology occurs. Fig. 2.12 shows the distribution of γ' precipitates in solution treated and aged IN 738LC superalloy. It is seen that the microstructure of the aged sample consists of large cuboids and smaller spheroids. It has been established that the precipitation of γ' in γ matrix is a continuous process involving three classical stages of nucleation, growth and ripening [28, 29].

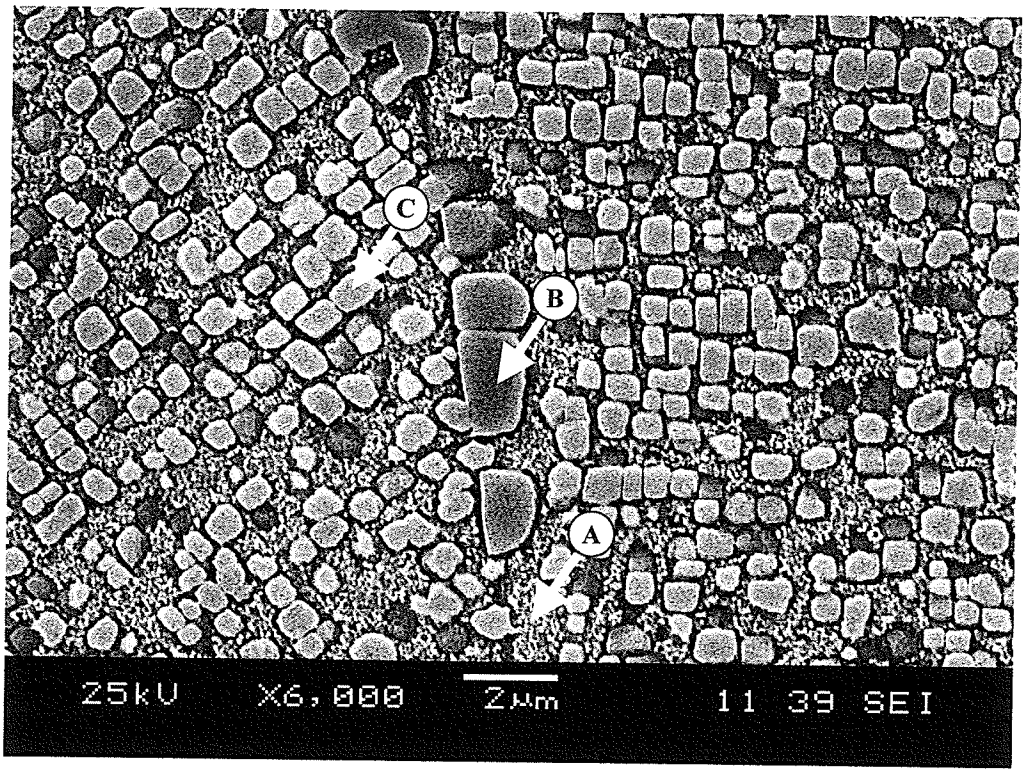

Fig. 2.11: SEM micrograph showing the distribution of γ' precipitates in solution treated alloy (1120°C/2 hrs), (A) secondary γ' (B) grain boundary γ' (C) primary γ'.

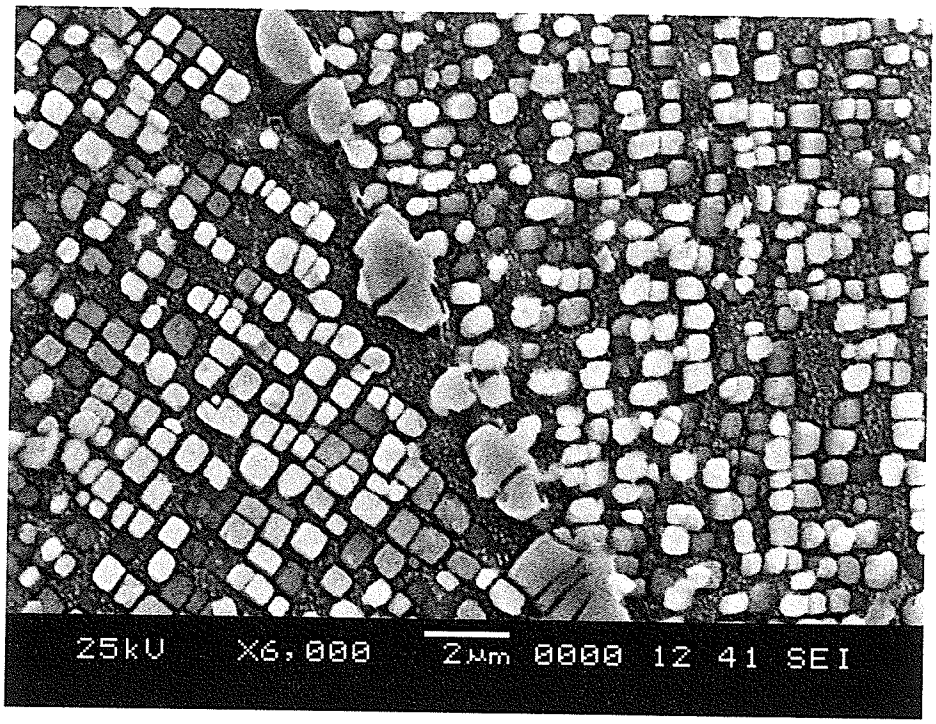

Fig. 2.12: SEM micrograph showing the distribution of γ' in solution treated (1120°C/2 hours) and aged IN 738LC alloy (845°C/24 hours).

However, the disparity in dissolution behavior and size distribution of the core and interdendritic γ' is as a result of microsegregation that occurs during solidification of the alloy [4]. Segregation, particularly of titanium, into the interdendritic regions raises the γ' solvus in these regions, and results in larger particle sizes after continuous cooling compared to particles in the core, owing to the precipitation occurring at higher temperatures [25].

2.5 Joining/Repair Techniques

Over the past years, there has been an increased emphasis on the development and optimization of various repair processes in order to offset the cost that would be incurred in the replacement of service-degraded turbine engine components. Thus, a great deal of research work is currently being carried out that is aimed at satisfying the quest for the production of a perfect joint, whose microstructure and mechanical properties are indistinguishable from those of the parent materials. Up to date, some processes such as diffusion bonding can achieve results that are very close to these ideal conditions; however, they are either expensive or restricted for use to repair components made of just a few materials [30]. Nevertheless, it should be noted that a material could be joined in several ways; however, many factors have to be considered when selecting a joining/repair technique. These include, service requirements (such as, service temperature), environment (e.g. corrosive, oxidizing), mechanical properties requirements (e.g. fatigue resistance, impact resistance, and other cyclic conditions), and manufacturing considerations (such as cost, equipment required, and other assembly details).

This section discusses the fundamentals of some of the available joining/repair techniques, which include: fusion welding, diffusion bonding, brazing, and Transient Liquid Phase (TLP) bonding Processes. Emphases are also placed on their inherent advantages and limitations.

2.5.1 Fusion Welding

This involves fusion of the joint surfaces by controlled melting through a localized application of heat and subsequent solidification of the molten pool. Commonly employed heating sources include, electron beam, plasma arc, electrical resistance, and laser. Furthermore, the use of filler metals has become commonplace, most especially when the joint gap is wide and of variable width. In this situation, the filler is often chosen to have a marginally lower melting point than the components in order to ensure that it melts completely [6] and flows easily in the joint. Notwithstanding the fact that welding process has been used on the macroscopic scale over a long period of time, it still has its inherent limitations, which invariably limit its use as a repair/joining process. These limitations include:

1. The detrimental effect of the heating cycle, involving very rapid heating and cooling, on the microstructure and, hence, the properties of the components over a region around the joint, called the heat affected zone (HAZ). For example, most precipitation-hardened nickel base superalloys that contain substantial amounts of aluminum and titanium are considered to be difficult to weld due to their high susceptibility to HAZ cracking during welding and post-weld heat treatment [2]. This has been attributed to:

- The large shrinkage stress occurring as a result of rapid precipitation of γ' particles during cooling from the welding temperature [3],
- Combination of thermally induced welding strains and very low ductility in the alloy due to localized melting at grain boundaries [4]

2. The distortion of the components in the region of the HAZ. This is as a result of the thermal gradients developed through the use of a concentrated heat source in melting the joint surfaces.
3. Welding cannot be used widely in the joining of metals to non-metals.
4. The mechanical properties, most especially fatigue resistance, of the welded joints are usually inferior to those of the base alloy. This is due to the stress concentrations produced by the high thermal gradients that develop during joining.
5. It may be difficult to repair components with complex geometries, as the joint surfaces may not be easily accessible to the concentrated heat source.

2.5.2 Diffusion Bonding

This is a solid-state welding process that allows joining of a variety of structural materials, both metals and non-metals [31]. This process is controlled by thermally activated migration of atoms towards and across the joint interface [32]. Therefore, a necessary requirement for diffusion bonding is that the joint surfaces be placed in intimate contact with one another. This is usually achieved by an extensive preparation of the mating surfaces, and the compressive loading of the mating parts, such that plastic deformation of the surface asperities occurs on a microscopic scale. Fig. 2.13 shows the sequence of metallurgical stages that are involved in the diffusion bonding process.

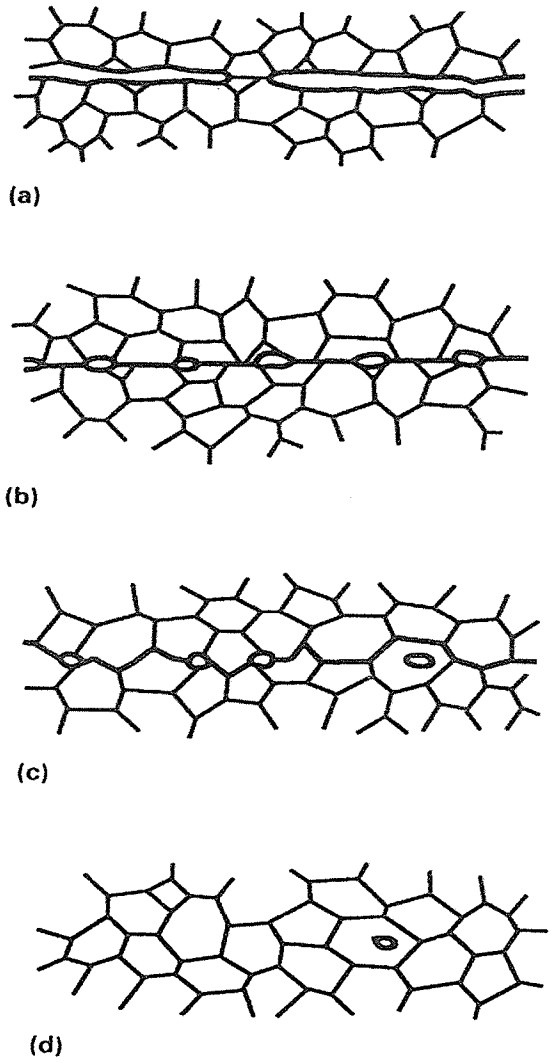

Fig. 2.13: Sequence of metallurgical stages in diffusion bonding process [32].

a) Initial contact: limited to a few asperities (room temperature).
b) First stage: deformation of surface asperities by plastic flow and creep.
c) Second stage: grain boundary diffusion of atoms to the voids and grain boundary migration.
d) Third stage: volume diffusion of atoms to the voids.

Advantages of Diffusion Bonding:

The diffusion bonding process is widely used due to the following reasons:

1. The generation of thermal expansion mismatch stresses, most especially when joining dissimilar components, is reduced, since the process is carried out at relatively low temperatures.
2. It sidesteps the need for wetting and spreading of fillers, which imposes the use of controlled atmosphere during TLP bonding process [6].
3. Diffusion bonded joints have higher remelting temperatures. Thus, repaired components can be used at a much higher service temperature.

Limitations of Diffusion Bonding:

The use of diffusion bonding as a joining/repair process tends to be of limited applications due to the following reasons:

1. The need for high bonding pressures (e.g. 500 – 5000 psi), exacting mating surface preparation and fit-up, and some deformation in the parts during bonding can make the process uneconomical in many situations [5].
2. Diffusion bonding is limited in application to specific combinations of materials that provide adequate diffusion without a consequential formation of voids (Kirkendall porosity) or embrittling phases in the joint [6].
3. Aluminum-, iron-, nickel-, and cobalt-base alloys, which exhibit very low solubility for interstitial elements are not readily diffusion bondable.
4. A severe limitation can be imposed on the joint design because the process is not tolerant to joints of variable width.

5. Diffusion bonding has the least tolerance to poor mating of the joint surfaces when compared to all other joining methods.
6. Diffusion bonding process is controlled by the solid-state diffusion of atoms across the interface; therefore, it is a relatively slow process.

2.5.3 Brazing

Brazing encompasses a group of joining processes that produce coalescence of joint surfaces through the heating of the materials to the brazing temperature in the presence of a filler metal, which has a liquidus temperature above 450°C but below the solidus temperature of the base material [33]. During the brazing process, the materials being joined are heated to a temperature approximately 50 - 55°C above the liquidus temperature of the filler metal. The molten filler metal, which is held in the joint by surface tension, then spreads into the joint by capillary action and wets the base metal surfaces. Metallurgical reactions occur between the liquid filler and the joint surfaces, which result in the erosion of the original surfaces of the components on a microscopic scale. Finally, the parts are cooled in order to solidify or "freeze" the filler metal.

Advantages of Brazing Process:

Brazing has some distinct advantages, among which include the following:

1. Strong, uniform and leak proof joints can be made rapidly, and even simultaneously.
2. Components with complex geometries and/or combinations of thick and thin sections can usually be brazed together.
3. It preserves the protective metal coating on the materials being joined.

4. The entire part can be brought up to the same brazing temperature. This prevents localized heating that causes distortion during fusion welding. Thus, multicomponent assemblies can be joined with low distortion and good resistance to thermal shock.
5. Cast and wrought alloys can be turned into integral components by a single treatment through a brazing furnace.
6. The mere fact that brazing does not involve any substantial melting of the base metal offers several advantages over the fusion welding process. It is generally possible to maintain closer assembly tolerances, preserve special metallurgical characteristics of metals, and produce a cosmetically neater joint without costly secondary operations [31].

Limitation of Brazing Process:

The formation of intermetallic phases in a brazed joint during the brazing process can adversely affect the physical, chemical and mechanical properties of the joint. In fact, there are many applications for which superalloy brazements do not possess adequate elevated temperature mechanical and physical properties as a result of the heterogeneous nature of the joints.

2.5.4 Transient Liquid Phase (TLP) Bonding

Transient Liquid Phase (TLP) bonding process (also known as diffusion brazing) is a hybrid process that combines the beneficial features of liquid phase joining and diffusion bonding techniques [6]. It is a relatively new process that is currently being used economically in producing high strength diffusion bonds in most difficult-to-weld heat

resistant alloys. It also excludes a need for the application of substantial pressure during bonding [5]. It has been extensively used for the repair of aero-engine turbine blades [34] and joining of electronic circuit components [35].

During the TLP bonding process (as shown in Fig. 2.14), a thin interlayer alloy, containing a melting point depressant (MPD), is clamped between the well-cleaned mating surfaces of the joint metal. Thereafter, the entire assembly is then placed in a vacuum or an argon atmosphere, and heated up to the bonding temperature. This results in melting of the filler metal (at a temperature below the solidus temperature of the base metal) and/or its reaction with the base metal to form a liquid zone, which subsequently fills the gap between the joint surfaces. While the parts are still held at the bonding temperature, rapid interdiffusion of alloying elements occurs between the liquid interlayer and the base metal [5], which results in a change in the compositions of the solid and liquid phases, until equilibrium is established at the joint's interface. Further diffusion of the MPD into the parent metal raises the melting temperature of the liquid filler alloy, resulting in its isothermal solidification. Thus, a complete isothermal solidification is achieved if the joint is kept for a sufficient time at the brazing temperature before cooling to the ambient temperature. Following solidification, the joint region is homogenized both in composition and microstructure by keeping it for a longer period of time at the bonding temperature, or at some lower temperature at which interdiffusion of solute elements will be fast enough. It should be noted that the diffusion brazing process is not limited to alloys with binary eutectics, but can also be applied to

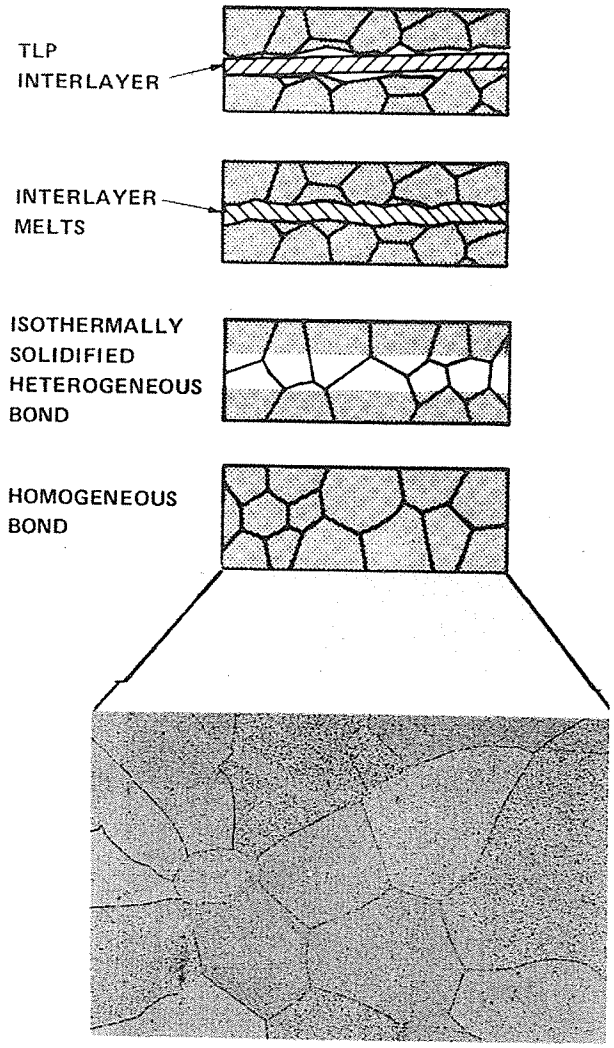

Fig. 2.14: Diagrammatic illustration of TLP bonding process [5].

any system where the parent metal or alloy will form a relatively low melting phase, which has solubility for the MPD [36].

Advantages of TLP Bonding Process:

1. It has the advantage of not requiring the rather high pressure needed in typical solid-state diffusion bonding process [37].
2. It can be used successfully in joining of heat resistant alloys that are inherently susceptible to hot cracking or post-weld heat treatment cracking [5, 7, 8].
3. Complex-shaped parts can be joined using simple tooling and mating surface preparation. Also, TLP bonding can be used for the production of sound joints between varieties of materials ranging from similar/dissimilar alloy combinations, to metal-matrix composites etc.
4. Process cost can be significantly reduced, as diffusion brazing allows for mass production of parts.
5. Joints having microstructural and mechanical properties similar to those of the base metal can be produced. Also, the quality of the brazed joint can be improved by employing an adequate post-braze diffusion heat treatment.
6. The process parameters and interlayer design are quite flexible and can be tailored towards a particular requirement of a given alloy for a particular application [32].
7. In contrast to diffusion bonding, diffusion brazing can be suitably used for joining intermetallic base materials, which have stable oxide surface films [38]; are highly sensitive to microstructural changes; and have poor low temperature ductility [39, 40].

Limitations of TLP Bonding Process:

Although TLP bonding process has a wide range of applications, its limitations include the following:

1. Very slow solidification process, typically requiring several hours. This is because the isothermal solidification stage is controlled by the solid-state diffusion of solute element from the liquid interlayer into the adjoining base metal.
2. Brittle phases may form in the joint if a complete isothermal solidification of the liquid interlayer is not achieved during holding at the bonding temperature [41, 42]. These brittle phases generally have detrimental effects on the mechanical and chemical properties of the joint.
3. The diffusion of the melting point depressant from the liquid interlayer into the substrate results in the precipitation of second phase particles at the brazed joint interface and along the grain boundaries of the substrate. These particles can have detrimental effects on the mechanical properties and corrosion resistance of the brazed assembly.

2.5.4.1 Key Parameters of TLP Bonding Process

The quality of a diffusion-brazed joint depends on the appropriate combination of a number of key parameters. These range from the characteristics of the filler/base alloy, to the processing conditions. The relevant factors include the joining atmosphere employed, the condition of the solid surfaces (e.g. nature of any oxides or coatings, surface roughness etc.), the metallurgical reactions involving the filler and base alloys, and the process temperature/time. These factors are discussed in the subsections below.

2.5.4.1.1 Joining Atmosphere

For molten filler metal to wet and bond to a base metal surface, the latter must be free from non-metallic surface films [6]. Although it is possible to ensure that this condition is met at the beginning of the heating cycle, by prescribed surface cleaning treatments; however, significant oxidation will generally occur if the components are heated in air. Therefore, steps must be taken to either prevent oxidation or remove the oxide film as fast as it forms. In view of this, diffusion brazing atmosphere is usually controlled in order to prevent the formation of oxides during brazing, and to reduce the oxides present, so that there will be no impediment to the wetting and flow of the liquid interlayer on the clean base metal [43]. The controlled atmospheres normally employed include:

a) Vacuum Atmosphere:

Most nickel base superalloys containing titanium and aluminum have been successfully brazed in vacuum atmosphere of around 10^{-4} torr. Any gas that evolves during heating to the brazing temperature can be removed to a suitably low pressure through the use of a vacuum pumping system that is attached to the brazing furnace. Thus, it is possible to obtain very clean surfaces even prior to bonding. A vacuum atmosphere is mostly useful when brazing metals that react chemically with hydrogen. Vacuum brazing has the following advantages and disadvantages as compared to brazing carried out under high purity atmospheres:

- Certain oxides that form on the base metal dissociate in vacuum at brazing temperatures.

- Volatile impurities and gases are removed as a result of the low pressure existing around the base and filler metals at elevated temperatures. This therefore eliminates the necessity of purifying the supplied atmosphere.
- It is not advisable to use filler metals with volatile constituents, as these can corrode the vacuum chamber, degrade its seals, and contaminate the pumping oils. Also, extreme care has to be taken when bonding base metals with very high vapor pressure, as brazing at high temperature under a high vacuum can result in their evaporation.

b) Pure dry hydrogen Atmosphere:

Here, dry hydrogen with a dew point of –51°C is used as a protective atmosphere during brazing. This dissociates the oxides of most elements found in heat-resistant alloys, except those of aluminum and titanium.

c) Inert Atmosphere:

An atmosphere of non-reactive gases such as helium and argon is usually employed, since these gases do not form compounds with metals. Also, the evaporation rate of volatile elements in vacuum atmosphere can be significantly reduced by the use of an inert atmosphere. It should be noted however that some elements such as zinc and cadmium vaporize in pure dry inert atmospheres [42].

2.5.4.1.2 Surface Cleaning and Preparation

Damaged hot section aero-engine components are usually contaminated with oxidation products, wear debris, and sometimes sulphidation and carbonaceous deposits resulting from incomplete combustion during service [44]. Thus, it is imperative that all the contaminants (including any film of grease, oil or wax) be thoroughly removed in order to prevent obstruction to the wetting, flow, and interdiffusion of solute elements across the solid base metal/liquid filler metal interface during TLP bonding. The surface cleaning methods that are usually employed individually or collectively include:

a) Chemical Cleaning Method:

This is the most effective means of removing all traces of oil or grease by the use of degreasing solutions, which include stabilized perchloroethylene. The parts are degreased by soaking, spraying or suspending them in a hot vapor of the aforementioned chemicals. Likewise, anodic and cathodic electrolytic cleaning can also be employed. However, surface oxides and scale that cannot be eliminated by these solutions are removed by using other chemical means e.g. the immersion of the components in phosphate acid cleaners or acid pickling solutions. Thereafter, the chemically cleaned components are cleaned ultrasonically in alcohol or clean hot water in order to ensure the removal of all the traces of previous cleaning solutions.

b) Mechanical Cleaning Methods:

These methods are usually employed in cleaning components with heavy tenacious oxide films prior to repair brazing. Mechanical cleaning involves the use of processes like grit

blasting, abrasive grinding, wire brushing and filing. These processes result in the cleaning and slight roughening of the surfaces to be brazed. It is well known that for each parent material, there exists an optimum surface roughness in which the spreading of the liquid filler can be maximized [45]. If the texturing is too deep, then capillary dams can be formed, which will impede the spreading of the filler metal.

c) Fluoride Cleaning Method:

In order to produce a high quality repair of thermal fatigue cracks and other narrow cracks, which are not easily accessible, the oxide layer on the cracked surfaces needs to be removed effectively. This is easily done by heating the part, most especially nickel- and cobalt-base alloys with low Al and Ti contents (i.e. less than 1wt%) in a hydrogen-rich atmosphere. However, oxides of alloys containing a considerable amount of these elements usually exhibit a high degree of thermodynamic stability. Therefore, they are cleaned by exposing them at elevated temperature to fluoride ions in a reducing atmosphere. During this process, not only are the Al and Ti oxides reduced, the surface of the parent material also becomes depleted in these elements, and this prevents the possibility of reoxidation prior to repair brazing.

Components requiring fluoride ion cleaning are firstly preheated up to a temperature of 950°C in a hydrogen atmosphere. This is then followed by the introduction of either a fluorocarbon such as PTFE or a metallic fluoride (e.g. chromium fluoride) into the hot zone at a controlled rate. The cleaning action then occurs as a result of the following reactions [45]:

Decomposition of PTFE:

$$(C_2F_4)_n \rightarrow nC_2F_4 \uparrow$$

Generation of HF:

$$C_2F_4 + 6H_2 \rightarrow 4HF + 2CH_4$$

Decomposition of metallic fluoride:

$$CrF_2 + H_2 \rightarrow 2HF + Cr$$

Reduction of the surface oxide:

$$6HF + Al_2O_3 \rightarrow 2AlF_3 \uparrow + 3H_2O$$

It should be noted that the process needs to be properly controlled in order to ensure adequate cleaning of deep narrow cracks, and at the same time avoiding excessive surface depletion, intergranular attack or deposition of soot.

2.5.4.1.3 Filler Alloy Characteristics

For a filler alloy to be compatible with a particular base alloy, it must exhibit the following characteristics:

1. It must have a liquidus temperature that is less than the solidus temperature of the base alloy. Generally, heat-resistant alloys are brazed with nickel- or cobalt-base filler alloys containing boron, silicon, and/or phosphorus, which serve(s) as melting point depressant (MPD). These elements are added to the filler alloy in specific amounts in order to depress its melting point. However, it is very important that the MPD has a significant diffusivity and solubility in the base alloy in order to ensure reasonable bonding times.

2. The filler used should be able to produce a joint that not only has the required mechanical properties, but also desirable chemical properties (e.g. oxidation/corrosion resistance). In view of this, apart from the MPD, chromium is often added to the filler alloy in an amount that can be as high as 20%. This improves the oxidation and corrosion resistance of the brazed joint. In fact, some filler alloys contain small additions of some transition elements like lanthanum, which are known to improve the oxidation properties of the brazed joints.
3. The filler alloy must not contain constituents or impurities that might embrittle or otherwise weaken the resulting joint. Therefore, a careful selection of the bonding interlayer composition is necessary in order to form a single-phase microstructure upon solidification. Certain elements (e.g. aluminum, titanium and carbon) are either deliberately excluded or restricted in amount in the interlayer because they were found to form very stable interfacial phases during bonding [5].
4. It must have proper fluidity at the brazing temperature to ensure wetting and flow by capillary action. In this regard, Gale and Wallach [46] showed in their work that the ultimate control of spreading of boron and phosphorus bearing nickel base fillers is affected by their chromium content, which is consistent with a fluidity associated process suggested by Ambrose et al [47]. Furthermore, filler alloys having eutectic composition are often regarded as having the best spreading characteristics when compared to those with hypo- and hyper-eutectic compositions [48]. The results of a study on a Ag/Ag-20wt%Cu/Ag sandwich joint by Tuah-Poku et al [37] also showed that the use of an alloy close to the eutectic composition as an interlayer material shortened the TLP processing time substantially. Therefore, filler alloys having

eutectic compositions are always preferred, not only because of their improved fluidity, but also because of the reduction in the bonding time associated with their use.

5. It must be capable of producing a joint at temperatures that will not be detrimental to the properties of the base alloy. This is very important because some work-hardened and precipitation-hardened alloys loose their beneficial mechanical properties at elevated temperatures.
6. More importantly, the filler alloy must be available in a form, which will make it to be easily applied to the damaged surfaces that are being repaired. Available forms of American Welding Society (AWS) classified and proprietary brazing filler alloys include, powder, paste, tape, foil, etc.

a) Brazing Powders/Paste:

These are normally produced by inert gas atomization. They are sold in a range of specified particle sizes, which ensures their uniform heating and melting during the brazing cycle. The powders can be mixed with plasticizers or organic cements/binder in order to facilitate their positioning on the base substrate. A filler metal in the paste form is simply a premixed powder and binder.

b) Brazing Tape:

This is made up of powders uniformly applied to a flexible organic backing strip. The braze metal density is typically 55% and the organic content 45%. Brazing tapes are

approximately 0.15mm thick and can be produced with an adhesive backing to ease application [44].

c) Brazing Foils:

Brazing foils are amorphous in nature. They are usually made by rapid solidification during melt spinning operations, although, some gold-containing brazing foils are sufficiently ductile to be manufactured by rolling. Foils are made in thickness ranging from 0.025 – 0.6 mm, and up to 50 mm in width. Brazing foils and tapes are best suited for applications requiring a large joint area, good fit-up, or where brazing flow and wettability may be a problem [43].

2.5.4.1.4 Base Alloy Characteristics

In principle, most metals can be TLP bonded by using a suitable interlayer [49]. However, in order to have a joint whose properties are comparable to those of the parent metal, some of the physical properties of the base metal need to be considered. These include, the melting temperature, strength at temperature, and the ability to diffuse away bonding elements (i.e. MPD). The solidus temperature of the base metal must be such that it is considerably higher than the liquidus temperature of the filler metal. Also, the base alloy should be thermodynamically stable at the bonding temperature and should have an extensive solubility for the MPD. These considerations suggest that superalloys would be ideal candidates for TLP bonding, as they are intrinsically stable close to their melting temperature, thus allowing for rapid diffusion and hence shorter bonding times.

2.5.4.1.5 Process Temperature/Time

The temperature-time parameters used for bonding a given component are dependent on the quality of bond required and the effect of the bond cycle on the properties of the base metals being joined [5]. It is therefore important to have an understanding of both the physical metallurgy of the base material and its interaction with the filler alloy. The exposure of some alloys to brazing temperatures that are higher than their normal solution heat treatment temperatures can be detrimental to their properties. For example, a brazing temperature of 1010°C or above would result in grain growth and a corresponding decrease in stress-rupture properties in IN 718, which cannot be recovered by subsequent heat treatment [43]. Therefore, the brazing temperature should be such that it is sufficiently high to promote melting, wetting, and alloying of the filler alloy, and at the same time minimizing its effects on the physical metallurgy of the base metal.

The time at brazing temperature is also very important. If the most desirable metallurgical and mechanical properties are to be achieved, the joint should be kept for a sufficient time required for achieving complete isothermal solidification and subsequent homogenization [33]. This time is a function of the diffusivity and phase relationships between the MPD and the base metal, both of which are dependent on the bonding temperature [36].

2.5.4.1.6 Joint Gap Size

The joint gap at the process temperature influences both the joint filling and the resulting properties of the joint. The smaller the joint gap size, the easier it is for the distribution of

the liquid interlayer (by capillary action) throughout the joint area, and a smaller likelihood of the formation of voids or shrinkage cavities as the liquid interlayer solidifies. However, an increase in the gap size will result in a corresponding increase in the time required for a complete isothermal solidification and joint's homogenization. This is because much longer time will be required for the MPD to be fully diffused away from the joint into the base metal.

2.5.5 Mechanisms controlling the TLP Bonding Process

MacDonald and Eagar [49] in their work have described two types of the TLP bonding processes. The type I process utilizes a pure interlayer, whereas in the type II process, the interlayer has a eutectic composition [50]. Tuah-Poku et al [37] did an extensive amount of work on the TLP bonding of a Ag/Cu/Ag sandwich (a type I based process) and divided the TLP process into four stages, namely, dissolution of the pure interlayer, homogenization of the liquid, isothermal solidification, and homogenization of the joint region. However, MacDonald and Eagar [49] described the TLP bonding as a five-stage process; a fifth stage termed 'stage 0' was included in their description, which accounts for the effects of a less than instantaneous heating rate on the filler alloy, as discussed by Niemann and Garret [51], and Nakagawa et al [52]. From the earlier work of Duvall et al [5], which was based on the type II process, the TLP bonding process was considered to comprise of four different stages, namely, melting of the interlayer, base metal dissolution, isothermal solidification, and joint homogenization. For the purpose of the theoretical description of the TLP stages as shown schematically in Figs. 2.15 a-e, it is convenient to use an interlayer having a eutectic composition of C_E. This is sandwiched

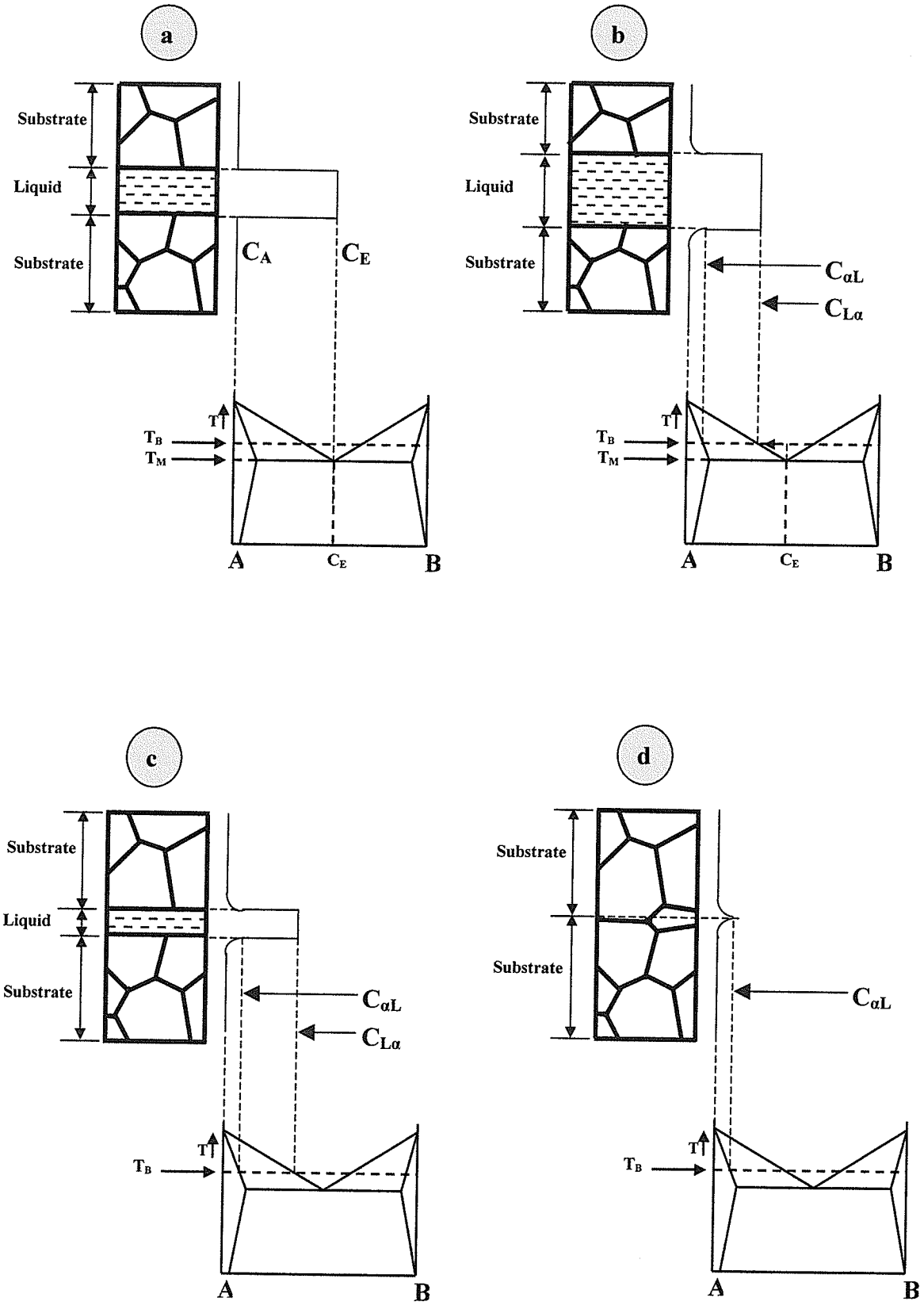
a
Substrate
Liquid
Substrate
C_A
C_E
T
T_B
T_M
A
C_E
B
b
Substrate
Liquid
Substrate
$C_{\alpha L}$
$C_{L\alpha}$
T
T_B
T_M
A
C_E
B
c
Substrate
Liquid
Substrate
$C_{\alpha L}$
$C_{L\alpha}$
T
T_B
A
B
d
Substrate
Substrate
$C_{\alpha L}$
T
T_B
A
B

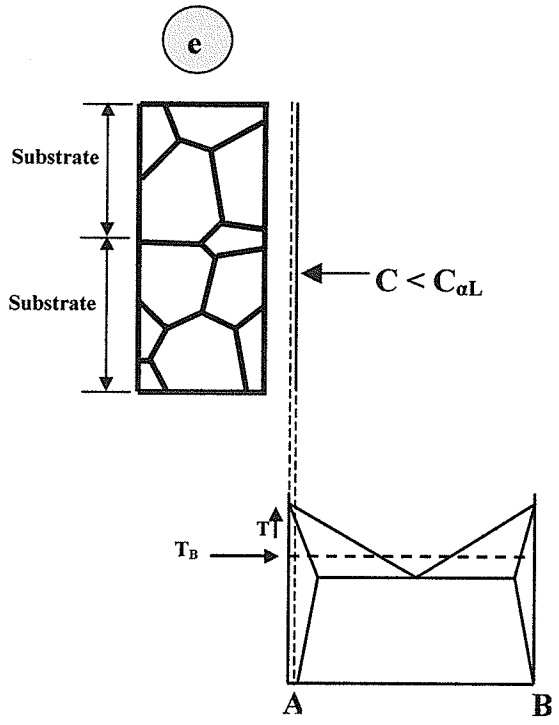

Fig. 2.15: Schematic of the mechanisms controlling TLP bonding process [54]:

a) melting of the interlayer
b) base metal dissolution
c) isothermal solidification
d) completion of isothermal solidification
e) joint homogenization

between two pure A base metal, each with composition C_A. Thus, the assembly is a A/A-B/A system, where B acts as a melting point depressant.

a) Melting of the Interlayer (Stage 1):

During this stage (Fig. 2.15 a), the bulk assembly is heated to the bonding temperature T_B, which is above the eutectic temperature T_M of the filler alloy. Therefore, the interlayer melts and fills the joint region.

b) Base Metal Dissolution (Stage 2):

The diffusion of the MPD (atoms of B) from the liquid into the base metal increases the concentration of B at the base metal mating surfaces to values greater than $C_{\alpha L}$, therefore, some melting of the adjoining base metal occurs [53]. The local melt back of the mating surfaces continues until equilibrium is achieved across the solid/liquid interface (i.e. interfacial concentrations of B atoms in the solid reaches $C_{\alpha L}$, while that in the liquid reaches $C_{L\alpha}$) as shown in Fig. 2.15 b.

c) Isothermal Solidification (Stage 3):

At this point, further melting of the base alloy ceases and isothermal solidification of the liquid starts. During isothermal solidification at temperature T_B, the composition of the liquid remains at $C_{L\alpha}$ and is in equilibrium with composition $C_{\alpha L}$ of the adjacent solid surfaces (Fig. 2.15 c). However, because of the continuing diffusion of the MPD into the base metal, the volume of liquid which can be maintained at the composition $C_{L\alpha}$ gradually decreases in order to satisfy the solute mass balance across the interface, thus,

solidification occurs inward from both mating surfaces [5]. The isothermal solidification stage is very slow because it is controlled by the solid-state diffusion of the MPD in the base metal. Once diffusion has reduced the maximum joint region MPD concentration to $C_{\alpha L}$, then isothermal solidification is completed and the basic bond has been formed (Fig. 2.15 d).

d) Joint Homogenization (Stage 4):

Solid-state redistribution of the solute elements occurs in the joint region when the brazed assembly is kept for an additional time at the homogenization temperature, which is not necessarily the same as the bonding temperature. The concentration of the MPD in the joint region decreases and at the same time, some base metal solute elements diffuse into the joint. In the ultimate, the joint will be identical both in chemistry and microstructure to the base metal (Fig. 2.15 e).

2.5.6 Modeling of Isothermal Solidification Kinetics

A great deal of effort has been put into the modeling of TLP bonding process over the past years. All the works that have been done so far, were geared towards the common goal of successfully:

- Predicting the completion times required for each stage of the process (i.e. base metal dissolution, isothermal solidification, and homogenization). It should be noted however, that the majority of the work has been done in modeling the isothermal solidification stage. This is simply because isothermal solidification kinetics is controlled by the slow solid state diffusion of solute element in the base

metal, thus, the time required for its completion is much more prolonged than that required for other stages. Due to this, a reasonably good estimation of the completion time for the isothermal solidification stage may be used as an approximation for the whole process [55, 56].

- Selecting the optimum filler alloy (chemistry, thickness) and bonding parameters (e.g. time and temperature), which will ensure that the TLP bonding process is completed within a reasonable time frame [57].
- Predicting the solute concentration distribution, both in the solid and liquid phases, throughout the TLP bonding process.

This section reviews some of the past research that have been done in modeling the isothermal solidification stage, which were essentially premised upon some fundamental assumptions, including:

- Assuming that a local equilibrium condition exists at the migrating solid/liquid interface [5], such that the composition of each phase at the interface is as dictated by the phase diagram. However, Langer and Sekerka [58] have pointed out that this is only an approximation, as local equilibrium is generally not attained at the solid/liquid interface.
- Assuming that the effect of convection in the liquid is negligible due to the small thickness of the interlayer. Therefore, the problem can be considered as one of pure diffusion [37].
- The interdiffusion coefficients in the solid and liquid (D_s and D_L) are assumed to be independent of composition [37].

- According to Nakagawa et al [52], solute distribution in the liquid can be considered to be uniform during the isothermal solidification stage. Therefore, solute diffusion in the liquid can be ignored. Also, the base metal is assumed to be semi-infinite in dimensions because of the relatively slow solute diffusion in the solid.

Subsequent to the above assumptions, two major approaches have been used in analytically modeling isothermal solidification completion time [37, 59-64]. In one, the system is treated as a two-phase semi-infinite diffusion-controlled moving solid/liquid interface, while the other, treats it as a single-phase semi-infinite diffusion-controlled system, with the base metal surface maintained at a constant solute concentration $C_{\alpha L}$ [65] (see Fig. 2.16).

In the work of Tuah-Poku et al [37], which was based on the "single-phase" model, an error function solution was employed in describing the solute distribution in semi-infinite base metal (see Shewmon, 1989 [66]), as given below:

$$C(x,t) = C_{\alpha L} + (C_M - C_{\alpha L})\, erf\left(\frac{x}{\sqrt{4D_s t}}\right) \qquad (1)$$

Where, $C_{\alpha L}$ is the solute concentration at the surface of the base metal

C_M is the initial solute concentration in the base metal

D_s is the solute diffusivity in the base metal

t is the solidification time

x is the distance along the specimen length from the surface

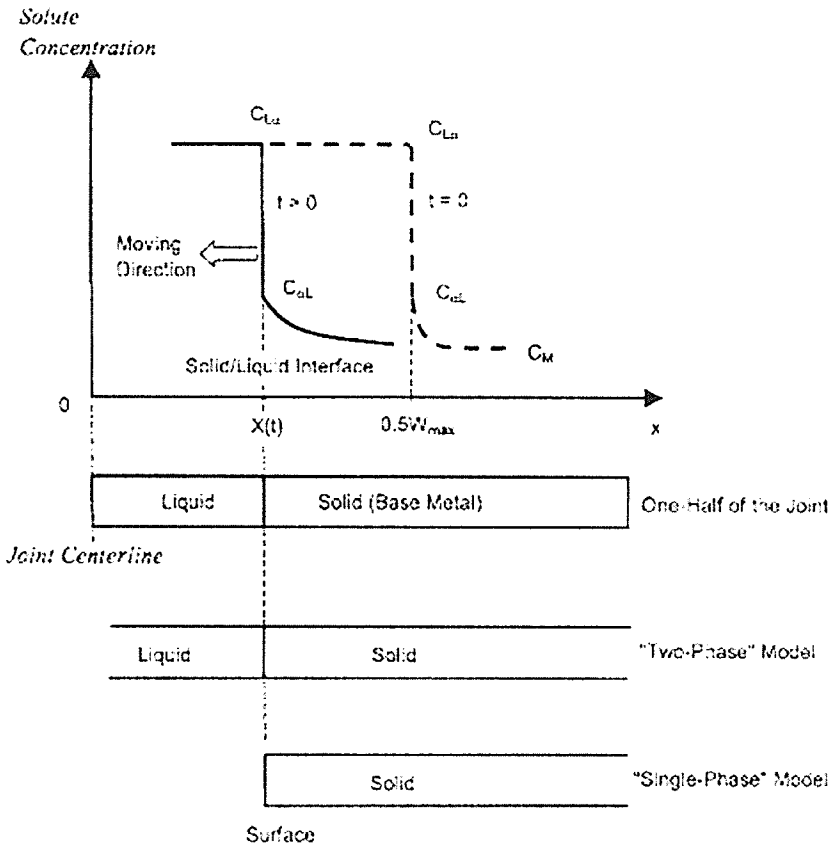

Fig. 2.16: Schematic showing solute distribution during isothermal solidification process in TLP bonding, and the two analytical models used to simulate the process [65].

Using the above error function solution, the total amount of solute (M_t) diffused into the base metal at time (t) is given by:

$$M_t = \int_0^t D_s \frac{dc}{dx} dt = 2(C_{\alpha L} - C_M)\sqrt{\frac{D_s t}{\pi}} \qquad (2)$$

Assuming the amount of solute diffused into the base metal during the heating and dissolution stages is ignored, the total amount of solute diffused into the base metal at the completion of isothermal solidification equals the original solute concentration of the filler metal [56], such that:

$$C_E W_o = 4(C_{\alpha L} - C_M)\sqrt{\frac{D_s t}{\pi}} \qquad (3)$$

Where C_E and W_o are the original solute concentration and the initial width of the filler metal, respectively.

Isothermal solidification completion time can therefore be calculated using the following expression:

$$t = \frac{\pi}{16 D_s}\left(\frac{C_E W_o}{C_{\alpha L} - C_M}\right)^2 \qquad (4)$$

Onzawa et al [59], Ikawa et al [60], and Nakao et al [62] have also used the above approach in modeling the isothermal solidification process.

Lesoult's [61] work was based on the "two-phase" model. In a more rigorous treatment of the problem, a general error function solution was assumed for solute distribution in the solid phase [57] as given below:

$$C(x,t) = A_1 + A_2 erf\left\{\frac{x}{\sqrt{4D_s t}}\right\} \qquad (5)$$

Where, A_1 and A_2 are constants determined by the specific boundary conditions:

When $x \to \infty$, $C(\infty, t) = A_1 + A_2 = C_M$ (6)

and at the moving solid/liquid interface, i.e. x = X(t)

$$C(X(t), t) = A_1 + A_2 erf\left\{\frac{X(t)}{\sqrt{4D_s t}}\right\} = C_{\alpha L} \quad (7)$$

Where $C_{\alpha L}$ is the solute concentration of the solid phase at the interface.

Since equation (7) above must be satisfied for all values of t, X(t) must be proportional to to $t^{\frac{1}{2}}$ i.e.,

$$X(t) = k\sqrt{4D_s t} \quad (8)$$

Where, k is a constant.

Mass balance at the interface produces the following expression:

$$(C_{L\alpha} - C_{\alpha L}) \bullet \frac{dX(t)}{dt} = D\left(\frac{\partial C(x,t)}{\partial x}\right)_{x=X(t)} \quad (9)$$

Where $C_{L\alpha}$ is the solute concentration in the liquid phase at the moving solid/liquid interface.

Solution of equations (5) and (9) gives:

$$\frac{k(1 + erf(k))\pi^{\frac{1}{2}}}{\exp(-k^2)} = \frac{C_{\alpha L} - C_M}{C_{L\alpha} - C_{\alpha L}} \quad (10)$$

Solutions, similar to the above were also derived by Sakamoto et al [67] and Ramirez and Liu [63]. Using equation (8), the time required for the completion of isothermal solidification is given by:

$$t = \frac{W_{\max}^2}{16k^2 D} \quad (11)$$

Where, W_{max} is the maximum liquid width calculated using the mass balance method [37], and the value of k can be determined by solving equation (10) numerically.

It was however established in the work of Tuah-Poku et al [37] that equation (4), which was based on the "single-phase" solution, grossly overestimated the isothermal solidification completion time. According to them, the solidification process could have been accelerated as a result of the ledge-type interface migration, and also due to grain boundary grooving. However, in a recent work, Zhou [65] suggested that apart from the reasons given by Tuah-Poku et al [37] for the overestimated value resulting from the use of equation (4), the error might have been as a result of the major assumption made during its derivation. Since it is known that the liquid/solid interface actually migrates during the isothermal solidification stage, the assumption of a stationary interface, which led to the application of equation (1) (which is only exact for a stationary interface) in predicting solute distribution in the solid base metal may be unsuitable. It should be noted however, that isothermal solidification completion time could be approximated using equation (4) only when the value of k is very small [37]. This occurs when the values of C_M and $C_{\alpha L}$ are very small as compared to that of $C_{L\alpha}$. In that case, isothermal solidification rate will be very slow, thus, the migrating solid/liquid interface can be approximated by a "stationary interface" [56].

In a different approach, Gale and Wallach [68, 69] assumed that the base metal dissolution, which leads to liquid homogenization, and the isothermal solidification stages occur simultaneously rather than sequentially. This is contrary to the previous

models already discussed, which considered them as sequential processes. This assumption has been also suggested by Nakagawa et al [52] and Lee et al [70]. Subsequent to this, the solid substrate and liquid phase were treated as a continuum, which was modeled using the following equation [71]:

$$C(x,t) = C_M + \frac{1}{2}(C_E - C_M)\left\{erf\left[\frac{h+x}{\sqrt{4D_s t}}\right] + erf\left[\frac{h-x}{\sqrt{4D_s t}}\right]\right\} \qquad (12)$$

Where, C_M is the initial solute concentration in the base metal

C_E is the initial solute concentration in the interlayer

C(x,t) is the initial solute concentration as a function of distance from the center of the interlayer (x) and time (t).

Equation (12) above gives the solute distribution in a semi-infinite substrate for an unsteady state diffusion of a specie from a source with initial thickness 2h, which is of the order of diffusion distance $(Dt)^{\frac{1}{2}}$. It is known that at the completion of isothermal solidification stage, $C(x,t) = C_{\alpha L}$ at $x = 0$, i.e. solute concentration at the center of the interlayer is reduced to the solidus value $C_{\alpha L}$. Therefore, in order to estimate isothermal solidification completion time t_f, equation (12) can be reduced to:

$$C_{\alpha L} - C_M = (C_E - C_M)\left\{erf\left[\frac{h}{\sqrt{4D_s t_f}}\right]\right\} \qquad (13)$$

This approach has been reported to give a good agreement between the estimated and experimental values of t_f [68, 69].

Ojo et al, in a recent work [72] investigated the applicability of the two-phase model to the diffusion brazing of IN 738LC superalloy using a ternary Ni-Cr-B filler alloy. They also investigated the applicability of equation (13) above. Their results showed that isothermal solidification completion time could be successfully predicted using the two approaches, as the predicted times were in agreement with the experimentally observed times. Also, in their work, the activation energy (Q) and the frequency factor (D_o) for the diffusion of boron in IN 738 LC superalloy were experimentally determined to be 211 KJ/mol and 0.014 m^2/s, respectively. These values were found to be in good agreement with the values reported for nickel base polycrystalline superalloys by Nakao et al [62].

2.5.7 Transient Liquid Phase Bonding of Superalloys

The high performance requirements of aero-engines and power generation turbines have necessitated the use of superalloy materials for making turbine components. This is necessary in order for the turbine components to withstand high stresses, temperature, and corrosive environments to which they are exposed. However, with prolonged service exposure, a degradation of these materials occurs. According to Mattheij [68] a blade or vane usually exhibits a combination of the following types of damage:

- Degenerated base material
- Corrosion – oxidation, sulphidation and hot corrosion
- Foreign object damage
- Erosion
- Fatigue cracking

This therefore necessitates the repair of these components, in order to extend their total life at a price, which gives the greatest benefit in cost of ownership to the user of the gas turbine [73]. Although repair by welding techniques is widely used, it may be accompanied by defects, which may affect the service performance of the repaired parts [74]. Also, a poor weldability of most superalloys limits the use of fusion welding techniques as a repair process.

In view of the above, Duvall et al [5] developed the Transient Liquid Phase (TLP) bonding process, which has proven to be an alternative, widely used, and a cost effective repair process for damaged superalloy turbine engine components. In their work, after a complete isothermal solidification of the liquid filler, joint strength equivalent to base metal strength was achieved in a variety of nickel (Udimet 700, Inco 713C, IN-100, B-1900, Mar-M200 + Hf, Hastelloy X) and cobalt (Mar-M302, Stellite 31) base superalloys. However, a significant reduction in joint strength (tensile and stress rupture) was observed as a result of brittle and segregated phases, which formed in the joint due to incomplete isothermal solidification. Thus, microstructural and chemical homogeneities are requisite to having joints whose mechanical properties are comparable to those of the base metal. Nakao et al [62] worked on the TLP bonding of MM 007, Mar-M247, Alloy 713C, and Inconel 600 superalloys using MBF-80, MBF-60 and Ni-B filler alloys. They observed that a linear relationship exists between the residual eutectic width and the square root of holding time. They concluded that isothermal solidification was controlled by the solid-state diffusion of boron in the superalloys, and the activation

energies required for this were experimentally determined to be 219, 199, 211, and 209 KJ/mol respectively.

Also, TLP bonding process has been used in the joining of dissimilar superalloys. Le blanc and Mevrel [75] worked on the brazing of DS 247/BNi-3/Astrolloy ATGP3 assembly. After brazing at 1080^0C for 1 hr, they observed the formation of Ni_3B precipitates at the joint's centerline due to an incomplete isothermal solidification of the liquid interlayer. Also, boride particles were observed at the DS 247/BNi-3 and Astrolloy ATGP3/BNi-3 interfacial zones. Wu et al [76] brazed IN 718 to Inconel X-750 using AMS 4777 filler alloys. They reported that the presence of brittle intermetallic phases significantly reduced the achievable shear strength of the brazed assembly.

Furthermore, TLP bonding process has been used in joining of single crystal and oxide dispersion strengthened superalloys [8, 77, 78]. Nishimoto et al [8] brazed CMSX-2 Ni-base single crystal superalloy using MBF-80 filler alloy at a temperature in the range of 1373-1548 K for 0-19.6 Ks. Electron back scatter diffraction patterns (EBSD) revealed that the solid base alloy grew epitaxially into the liquid phase during isothermal solidification. Also, the microstructural properties of the joints were identical to those of the base alloy. The activation energy required for the solid-state diffusion of boron from the MBF-80 liquid interlayer into CMSX-2 was experimentally determined to be 266 KJ/mol.

In a recent work of Ojo et al [9] and Ojo [79], the effects of brazing parameters on microstructure and properties of diffusion brazed joints of IN-738 superalloy were investigated using two commercial brazing alloys, NB 150 and Amdry DF3. Centerline ternary eutectic constituents of γ-solid solution, Cr-rich borides, and Ni-rich borides were observed in NB 150 joints. The formation of these constituents was attributed to the athermal solidification of the residual liquid interlayer due to incomplete isothermal solidification at the brazing temperature. Also, MC carbide, Cr-rich borides and Ni_3Ti based intermetallics were observed in DF3 joints. Their work showed that the presence of second phases at the brazed joints and along their interfacial zones adversely affected the high temperature tensile strength properties of the brazed assemblies.

2.5.8 Scope of the Present Investigation

The preceding introduction and literature review indicates that a microstructural homogeneity of the brazed joint is required, in order to obtain a joint whose strength is comparable to that of the base metal. For this to be achieved not only should the liquid interlayer be completely solidified isothermally at the brazing temperature within a reasonable brazing time, but the interface of the brazed joint and substrate grain boundaries should also be free of second phase particles. Although it has been suggested that the presence of a second solute element (having a marked difference in diffusion coefficient and/or solubility) in the filler alloy may prolong the time required for complete isothermal solidification, it has not been implicitly considered that even if the starting composition of the filler alloy is properly controlled, the commercial alloys that

are brazed in industrial applications may act as the source of the aforementioned solute element(s) into the liquefied filler during brazing.

In view of the above, this work was designed to study the rate of isothermal solidification by varying the bonding temperature and joint gap size during the TLP bonding of a multicomponent IN 738LC superalloy using Nicrobraz 150 filler alloy. Furthermore, the effects of bonding temperature and joint gap size on the nature of interfacial particles, and the effects of bonding temperature on the nature of particles, which form along the substrate grain boundaries of IN 738LC superalloy TLP-bonded joints were also investigated. The results of this investigation are not only expected to contribute towards the optimization of TLP bonding of IN 738LC superalloy, but will also provide a better understanding of the possible effects of base alloy composition on isothermal solidification rate during TLP bonding process, most especially when multicomponent alloys are involved, as only few detailed publications have been found in the literature in this respect.

Chapter 3

MATERIALS AND EXPERIMENTAL PROCEDURES

3.1 Materials

Inconel 738LC superalloy, supplied by Hitchiner Manufacturing Co., Inc. in the form of 16 x 2.5 x 0.6 cm cast plates, was used in the as-cast condition as the base alloy in this investigation. Also, a commercial ternary Ni-Cr-B alloy (Nicrobraz 150), in the form of an amorphous foil, was used as the filler alloy. Table 3.1 shows the nominal chemical composition and the melting temperature range of the base and filler alloy.

3.2 Sample Preparation and Diffusion Brazing

15 x 7 x 7 mm coupons were sectioned from the as-received plates using a NC wire Electro-discharge Machine (EDM). Thereafter, the mating surfaces of the coupons were polished using 600 grade SiC paper. This was necessary in order to remove the recast layer produced by the EDM operation. After polishing, the coupons were ultrasonically cleaned for about 15 minutes in a solution of acetone. Subsequent to this, the filler alloy was placed between the mating surfaces of the cleaned coupons, and the edges of the coupons were tack-welded in order to keep the gap size fixed during brazing.

The TLP bonding operations were carried out in a vacuum furnace, operating at a vacuum of approximately 5 x 10^{-5} torr, using a temperature-time bonding cycle shown schematically in Fig. 3.1. The bonded samples were sectioned using EDM and mounted in bakelite. Thereafter, they were polished and electrolytically etched in 12 ml H_3PO_4 +

Table 3.1: Nominal composition of IN 738LC and Nicrobraz 150 filler Alloy.

Material	Composition (wt %)	Melting Temperature Range (°C)	
		Solidus	Liquidus
Filler Alloy (NB 150)	3.5B, 15Cr, Balance Ni	1055	1055
Base Alloy (IN 738LC)	0.11C, 15.84Cr, 8.5Co, 2.48W, 1.88Mo, 0.07Fe 0.92Nb, 3.46Al, 3.47Ti 1.69Ta, 0.001S, 0.04Zr 0.012B, Balance Ni	1232	1315

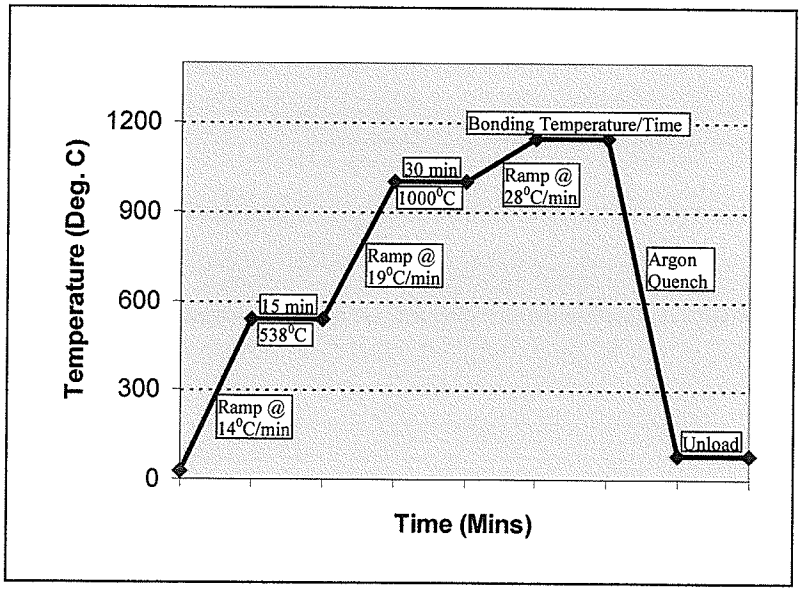

Fig. 3.1: Schematic of the TLP bonding cycle.

40 ml HNO_3 + 48 ml H_2SO_4 solution at 6V for 5 seconds.

3.3 Microscopic Examination

The microstructure of the bonded samples was examined using optical metallography and then a JEOL 5900 Scanning Electron Microscope (SEM) equipped with an ultra thin window Oxford energy dispersive x-ray spectrometer (EDS). Using the SEM, an average of 20 measurements were taken across the joint on each sample to determine the width of the eutectic zone in the bonded specimens. Semi-quantitative chemical compositional analyses of phases formed in the centerline eutectic constituents and along the interface/substrate grain boundaries of TLP bonded coupons were carried out by EDS equipped with INCA standardless analytical software.

Chapter 4

RESULTS AND DISCUSSION

4.1 Effects of Bonding Temperature on Isothermal Solidification Rate

4.1.1 Results

To study the effects of bonding temperature on the rate of isothermal solidification, 100 μm gap-sized Inconel 738LC superalloy coupons were vacuum TLP bonded for varying times ranging between 1-8 hrs using Nicrobraz 150 filler alloy at temperatures of 1130°C, 1145°C, 1160°C, and 1175°C, respectively. The microstructure of the samples after 1 hr of bonding at the respective temperatures, observed by SEM operating in secondary electron mode is shown in Figs. 4.1 a, b, c, and d. It is seen that the microstructure, at all the bonding temperatures, consisted of similar centerline eutectic constituent made up of three distinct phases. Figs. 4.2 a, b, and c show the EDS spectra of the phases present in a 100 μm gap-sized joint bonded for 1 hr at 1130°C. Boron was detected in two of the phases (as shown in Figs. 4.2 a and b). Although, its concentration could not be determined due to difficulty in quantifying the light elements with sufficient accuracy. The EDS compositional analyses of the rest of the elements (Table 4.1) suggest the two phases to be nickel-rich and chromium-rich boride phases. The third phase was identified to be nickel-base γ-solid solution phase. EDS analyses of the eutectic present in the joints bonded for 1 hr at 1145°C, 1160°C, and 1175°C revealed it to consist of the same phases. It has been established from previous work on diffusion brazing [5, 9, 80] that these phases formed during the athermal solidification of the residual liquid interlayer due to incomplete isothermal solidification at the bonding temperature. Thus, it is concluded

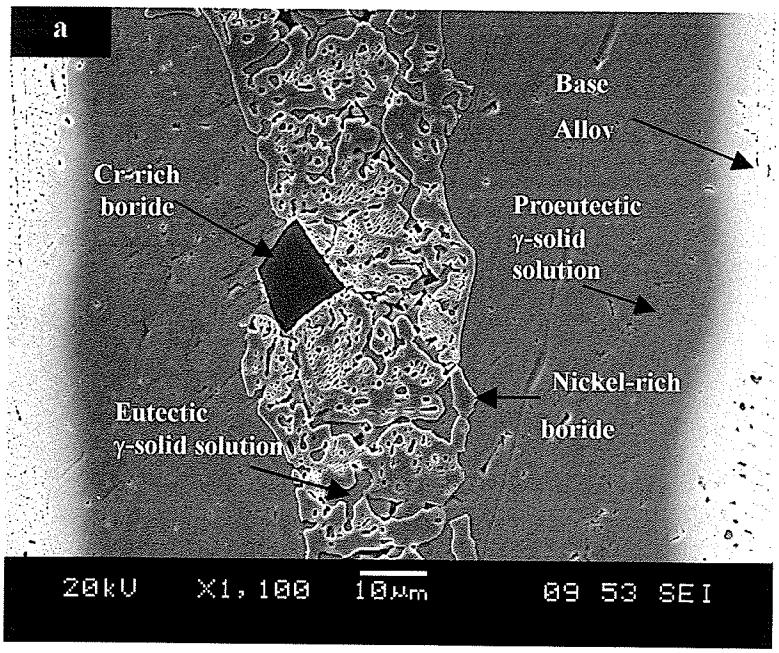

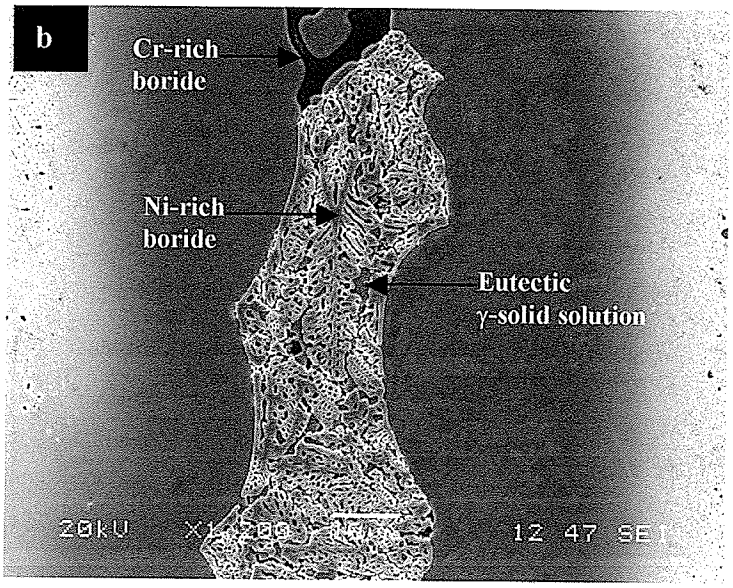

Fig. 4.1: SEM microstructure of 100 μm joint bonded for 1 hr at a) 1130°C, b) 1145°C, c) 1160°C and d) 1175°C.

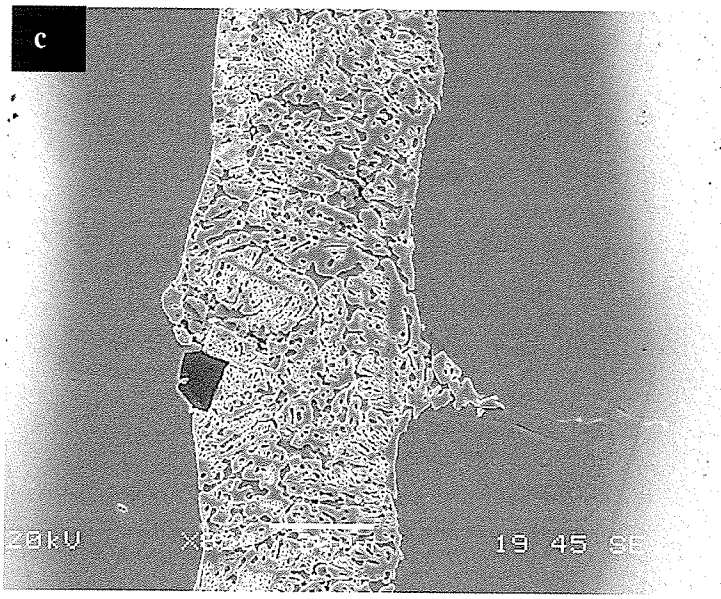
c
20kU
19 45

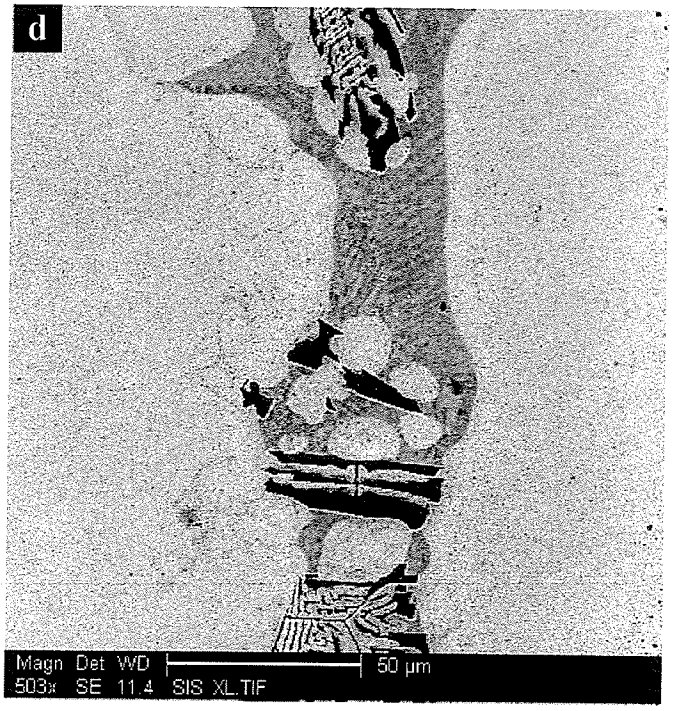
d
Magn Det WD
50 µm
503x SE 11.4 SIS XL.TIF

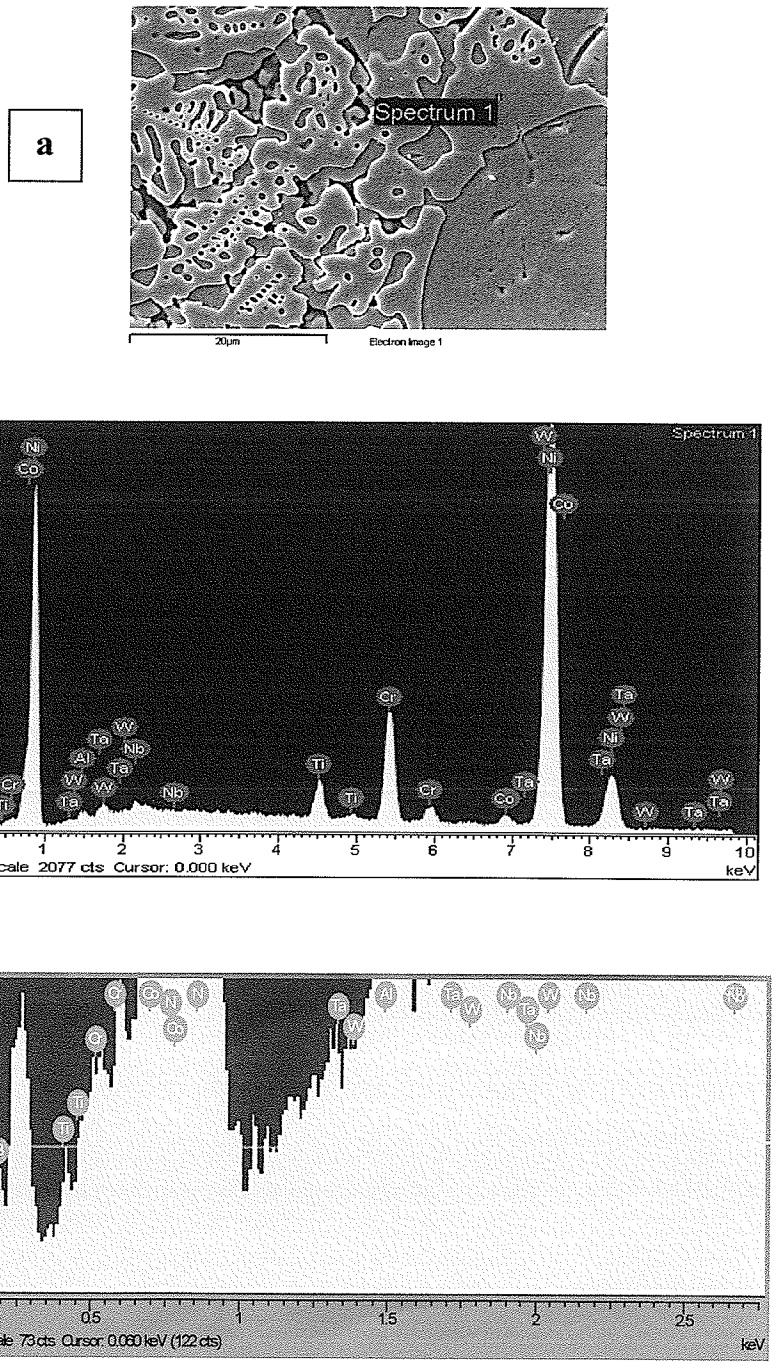

Fig. 4.2: EDS spectra of a) Ni-rich boride phase b) Cr-rich boride phase and c) γ-solid solution phase observed in the centerline eutectic constituents formed in 100 µm gap-sized joint bonded at 1130°C for 1hr.

b

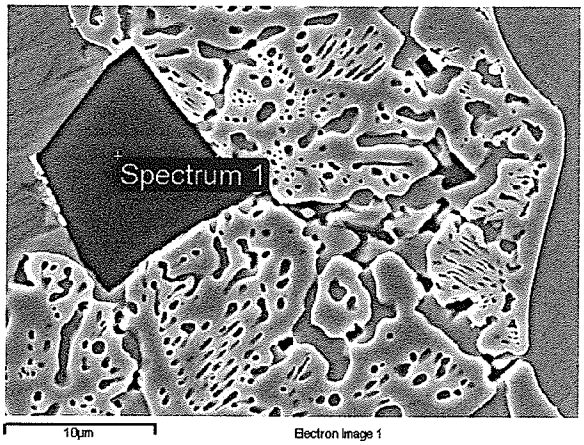
Spectrum 1
10µm
Electron Image 1

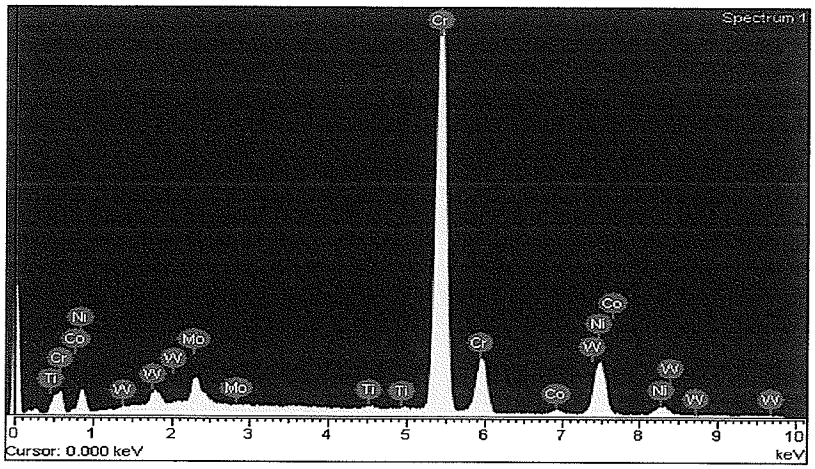
Spectrum 1
Cursor: 0.000 keV
keV

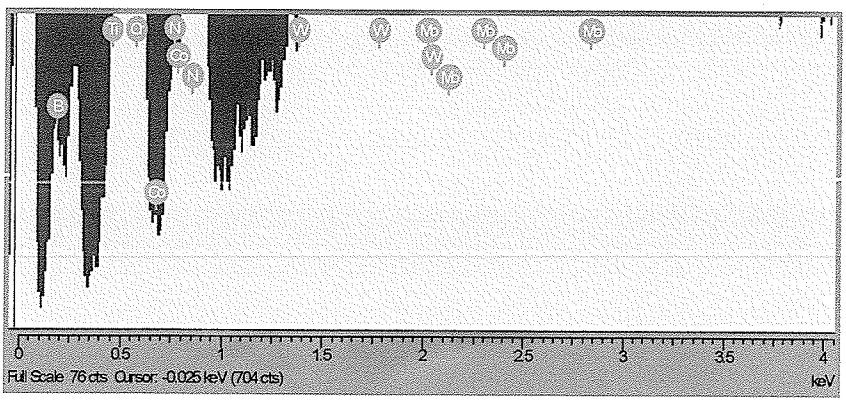
Full Scale 76 cts Cursor: -0.025 keV (704 cts)
keV

c

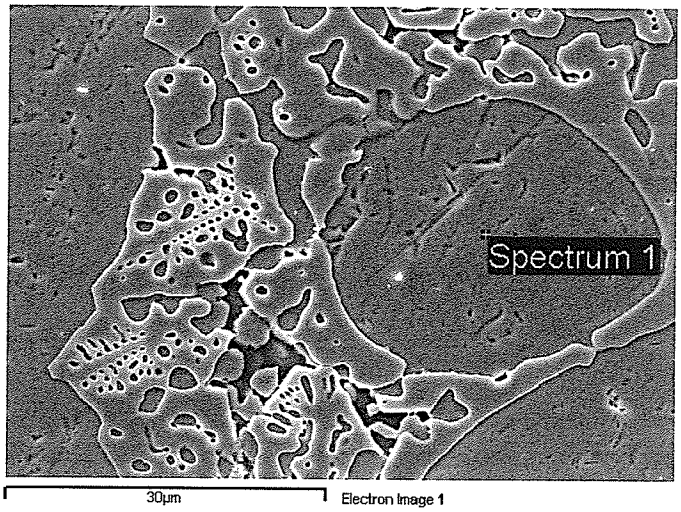
Spectrum 1
30µm
Electron Image 1

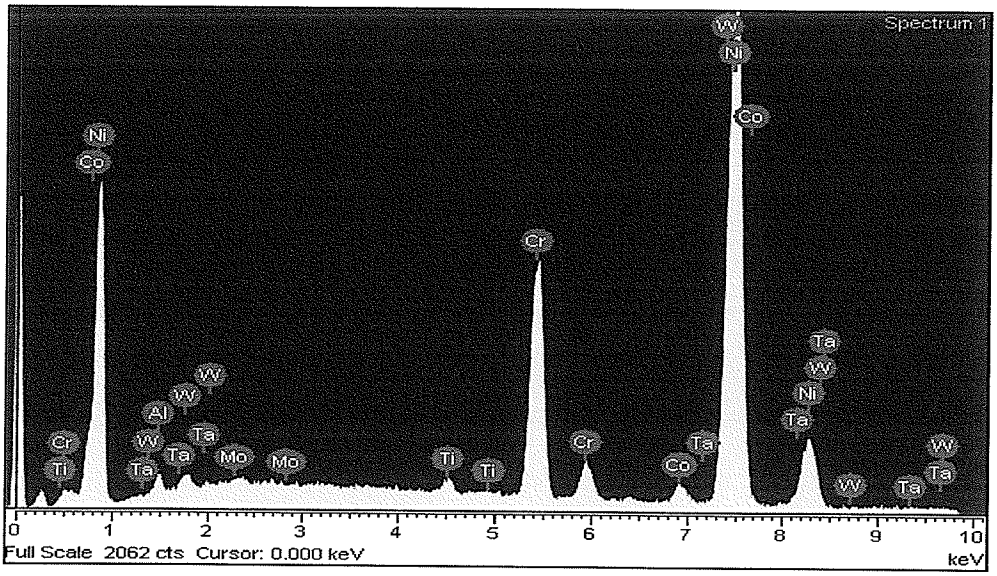
Spectrum 1
Ni
Co
Cr
W
Ni
Co
Ta
W
Ni
Ta
Al
W
Ta
Cr
Ti
Ta
Mo
Mo
Ti
Ti
Cr
Ta
Co
W
Ta
W
Ta
0
1
2
3
4
5
6
7
8
9
10
Full Scale 2062 cts Cursor: 0.000 keV
keV

Table 4.1: Composition of metallic constituents of centerline eutectic in 100 μm 'NB 150' joint bonded at 1130°C for 1 hr.

Element	Nickel rich boride phase (at %)	Chromium rich boride phase (at %)	γ-solid solution phase (at %)
Al	1.21	-	1.88
Ti	3.14	0.32	0.84
Cr	11.45	76.01	18.55
Co	1.82	1.26	2.34
Ni	81.23	18.92	75.41
Nb	0.39	-	-
Ta	0.45	-	0.26
W	0.30	1.00	0.41
Mo	-	2.49	-

that bonding a 100 μm - wide joint for 1 hr at 1130°C, 1145°C, 1160°C, and 1175°C is not sufficient for complete isothermal solidification of the liquid interlayer. Also, as shown in Figs. 4.1 a, b, c, and d, the centerline ternary eutectic constituents were bordered on the two sides adjacent to the base alloy by an isothermally solidified pro-eutectic region. The SEM-EDS compositional analysis revealed that this region has a composition similar to that of the nickel-base γ-solid solution phase present in the eutectic constituent.

Considering the proeutectic/eutectic interface to be the solid-liquid interface prior to athermal solidification at the end of each holding time, the average eutectic width was measured using SEM and plotted against the bonding time for each bonding temperature, as shown in Fig. 4.3. Each value is an average of 20 measurements. It is seen that the isothermal solidification rate increased as the bonding temperature increased from 1130°C to 1145°C, such that, a complete isothermal solidification of the joints was achieved within 6 hrs at 1130°C (Fig. 4.4 a) and after 5 hrs at 1145°C (Fig. 4.4 b), and the joints consisted of predominantly nickel-base γ-solid solution phase. However, after 5 hrs and 4 hrs of bonding time at 1130°C and 1145°C, respectively, (i.e. prior to the completion of isothermal solidification) centerline ternary eutectic constituents were observed. These were typical of those observed in the joints after 1 hr of bonding time. The increase in isothermal solidification rate with increase in bonding temperature from 1130°C to 1145°C is attributed to the increase in solid-state diffusion rate of boron with an increase in bonding temperature, since this is the rate-controlling factor during isothermal solidification process.

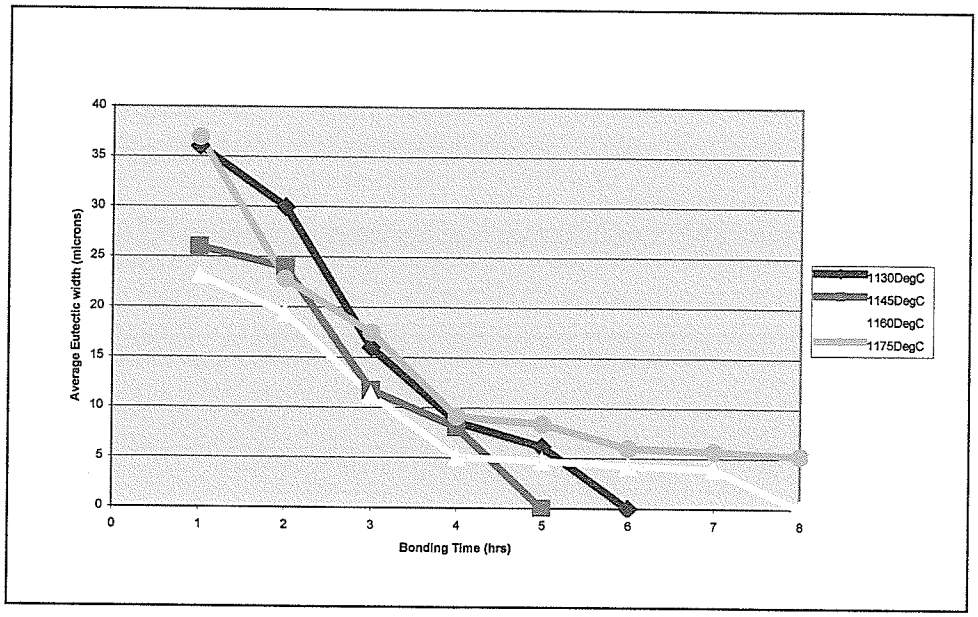

Fig. 4.3: Variation in average eutectic width with bonding time and temperature.

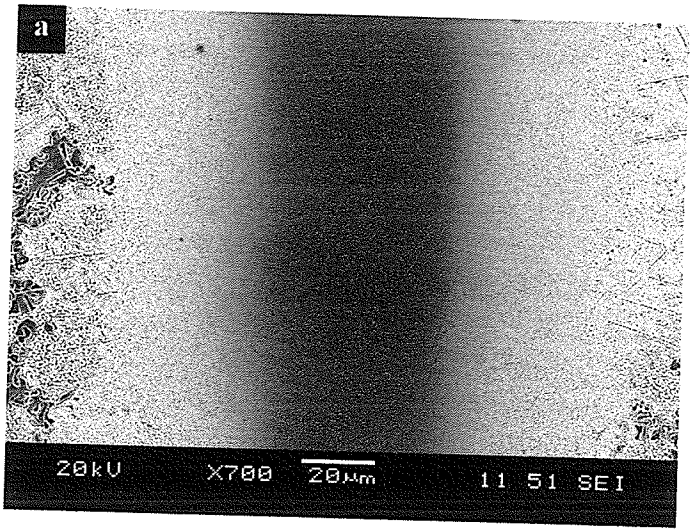

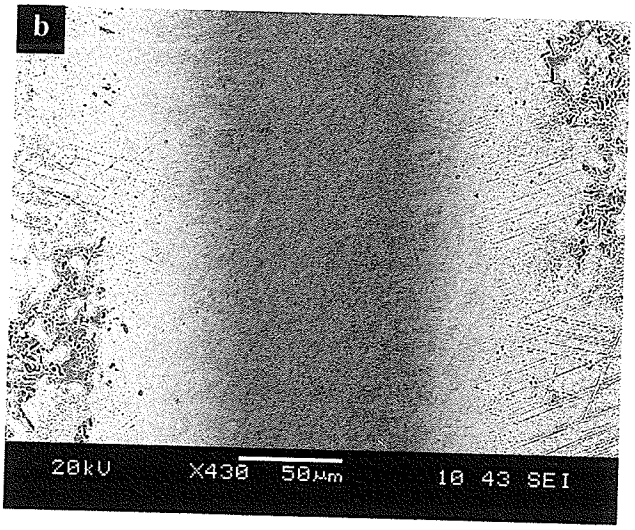

Fig. 4.4: SEM microstructure of completely isothermally solidified 100 µm joint bonded at a) 1130°C for 6 hrs and b) 1145°C for 5 hrs.

In the expectation that bonding at higher temperature would reduce the isothermal solidification time to a more industrially viable level, bonding was done at 1160°C, and 1175°C for times exceeding the time required for a complete isothermal solidification (t_f), as estimated by using the current TLP model developed by Gale and Wallach [69], and successfully applied by Ojo et al to diffusion brazing of IN 738LC superalloy using Nicrobraz 150 filler [72]. It was reported by Gale and Wallach [68, 69] that the diffusion of a solute from a source with initial thickness 2w, which is of the order of diffusion distance $\sqrt{Dt}$, into a semi-infinite solid substrate during TLP bonding may be represented by the analytical solution to Fick's second law of diffusion, given by Crank [71]:

$$C(x,t) = C_m + \frac{1}{2}(C_o - C_m)\left\{erf\frac{w-x}{\sqrt{4Dt}} + erf\frac{w+x}{\sqrt{4Dt}}\right\} \qquad (1)$$

Where,

C(x,t) = concentration of solute as a function of distance (x) from the center of the interlayer and time (t)

C_o = initial solute concentration in the interlayer

D = diffusion coefficient of the solute in the substrate.

From equation (1), the time t_f, in the present work, was predicted using the following equations [72]:

$$C_s - C_m = (C_o - C_m)\left\{erf\frac{w}{\sqrt{4Dt_f}}\right\} \qquad (2)$$

Where,

C_m = initial boron concentration in the base alloy (0.0628 at %)

C_o = 16.1 at % B

C_s = solidus concentration of boron (based on average value of solidus composition of 0.3 at % B in binary Ni-B system [69])

D = diffusion coefficient of boron in the substrate, which is given by the empirical equation, $D_o \exp\left(\frac{-Q}{RT}\right)$ (3)

The apparent activation energy (Q) for diffusion of boron and its frequency factor (D_0) in Inconel 738LC superalloy during the isothermal solidification stage were determined to be 211KJ/mole and 0.0144m^2/s, respectively, by Ojo et al [72], and was reported to be in good agreement with those that were previously reported for other nickel-base polycrystalline superalloys [62]. Ojo et al [72] found that equations 2 and 3 successfully predicted the value of t_f, during the diffusion brazing of IN 738LC superalloy with Nicrobraz 150 in the temperature range of 1100°C – 1150°C. Similarly, a good agreement between predicted and experimental values of t_f during the diffusion brazing of nickel substrates, using Ni-Si-B filler was also observed by Gale and Wallach [69]. Table 4.2 shows the predicted and experimental values of t_f for the present investigation. It is seen that there is a reasonable agreement between the predicted time of 5.5 hrs/ 4.5 hrs and experimentally observed time of 6 hrs / 5 hrs at bonding temperature of 1130°C / 1145°C. However, at 1160°C and 1175°C, a significant deviation in the experimentally observed isothermal solidification completion time from the predicted time of 4 hrs and 3 hrs, respectively, was observed. Figs. 4.5 and 4.6 show the SEM secondary electron images of the microstructure of 100 μm joints bonded for 5 hrs at 1160°C and 1175°C, respectively. At these bonding temperatures and time, the microstructure of the joints consisted of

Table 4.2: Predicted and experimentally observed bonding time for completion of isothermal solidification

Bonding Temperature (°C)	Approximate Isothermal Solidification Completion Time (hrs)	
	Predicted	Experimental
1130	5.5	6
1145	4.5	5
1160	4	8
1175	3	Not completed in 12 hrs

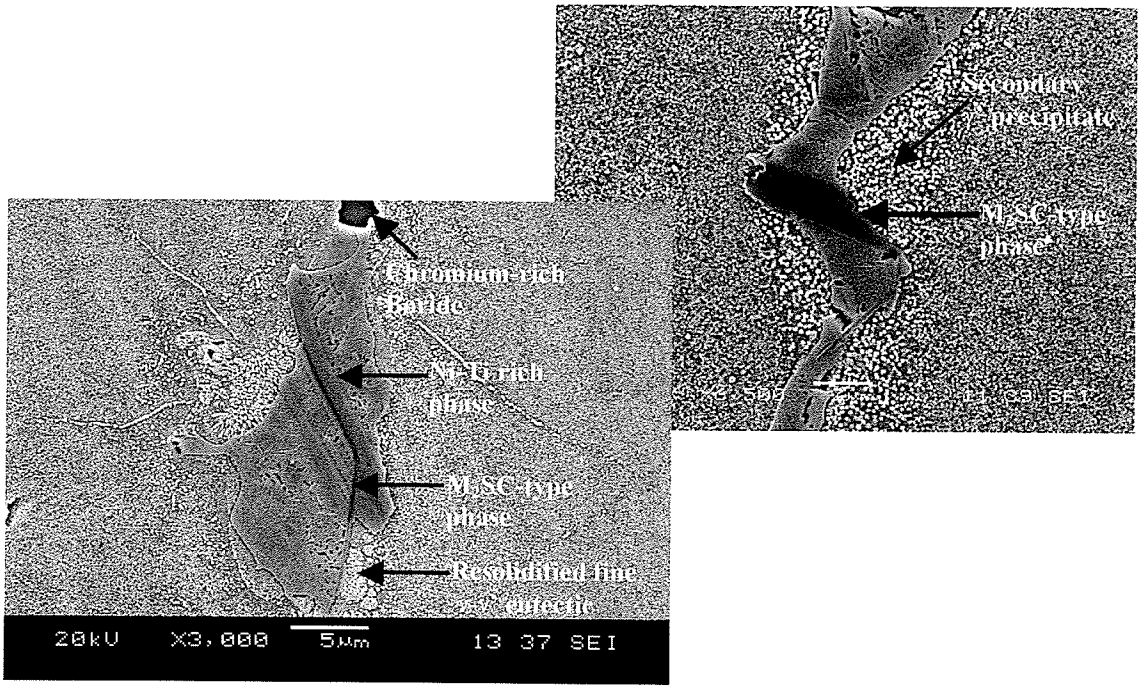

Fig. 4.5: Centerline eutectic constituents observed in 100 µm joint bonded for 5 hrs at 1160°C.

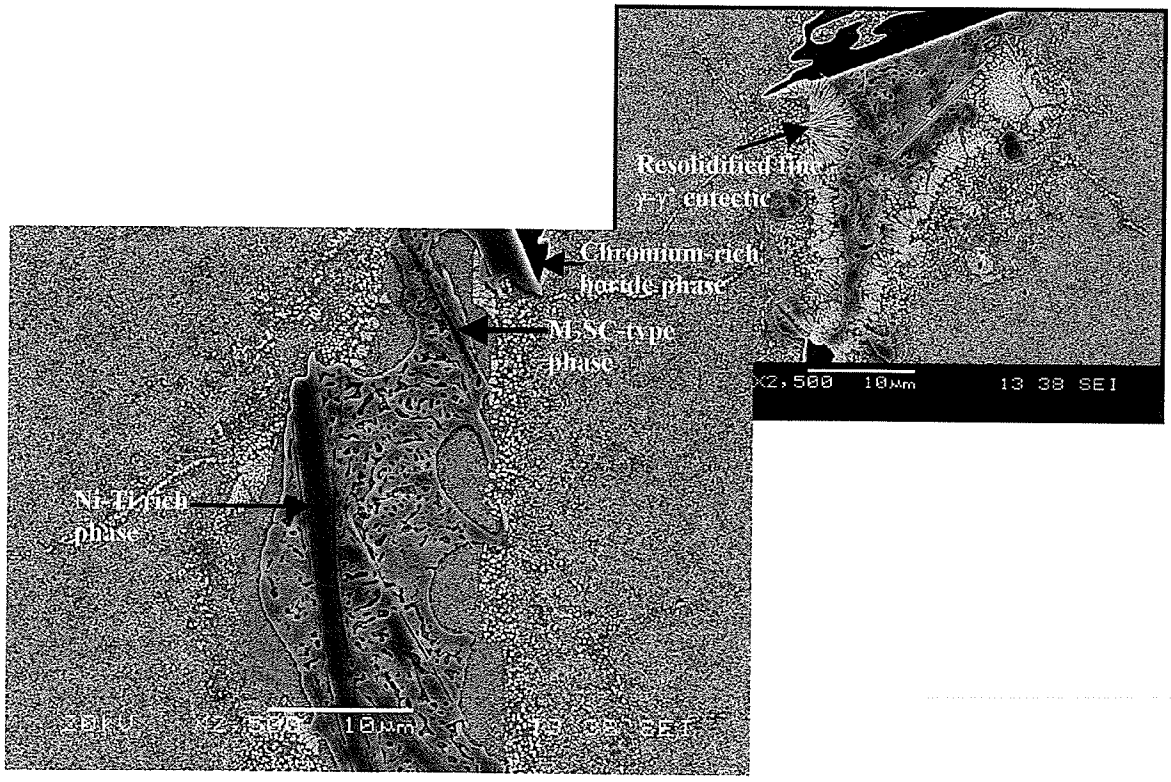

Fig. 4.6: Centerline eutectic constituents observed in 100 µm joint bonded for 5 hrs at 1175°C.

centerline eutectic constituents. This implied that isothermal solidification of the residual liquid was not complete. Furthermore, as seen in Fig. 4.3, a complete isothermal solidification of the joint could not be achieved until after 8 hrs of bonding at 1160°C. At 1175°C, however, even after 12 hrs of bonding, a complete isothermal solidification of the residual liquid did not occur. The SEM-EDS analysis of the isothermally solidified region revealed that the joints consisted of a considerable volume fraction of secondary γ' precipitates that formed within the γ-solid solution matrix, but were not observed at 1130°C and 1145°C. Figs. 4.7 a, b, and c show the EDS spectra of the distinct phases that were observed in the centerline of the joints bonded at 1160°C and 1175°C for 5 hrs. SEM-EDS compositional analyses (Table 4.3) suggest these phases to be a Ni-Ti rich phase, M_2SC-type sulphocarbide, and a chromium-rich boride phase. EDS X-ray mapping (Fig. 4.8) of the M_2SC-type sulphocarbide phase revealed that it was mostly rich in Ti, S, and Nb, and also contained an appreciable amount of Zirconium. Additionally, fine $\gamma - \gamma'$ eutectic-type resolidification products, with their "crown" region protruding inwards in the direction of solidification, were observed in the centerline of the joints (as shown in Figs. 4.5 and 4.6). These products have an eutectic morphology, which is characteristic of $\gamma - \gamma'$ eutectic product, which has been reported to be formed due to the microsegregation of elements, particularly Ti, during ingot solidification [25, 26] in as-cast Inconel 738LC superalloy. It should be noted that the solidification products (i.e. Ni-Ti rich phase, M_2SC-type sulphocarbide, chromium-rich boride, and $\gamma - \gamma'$ centerline eutectic) that were observed after 5 hrs of bonding at 1160°C and 1175°C are representative of the microstructure of 100 μm joints bonded at 1160°C for 4-7 hrs and at 1175°C for 3-8 hrs. After shorter bonding time, and at the respective temperatures,

a

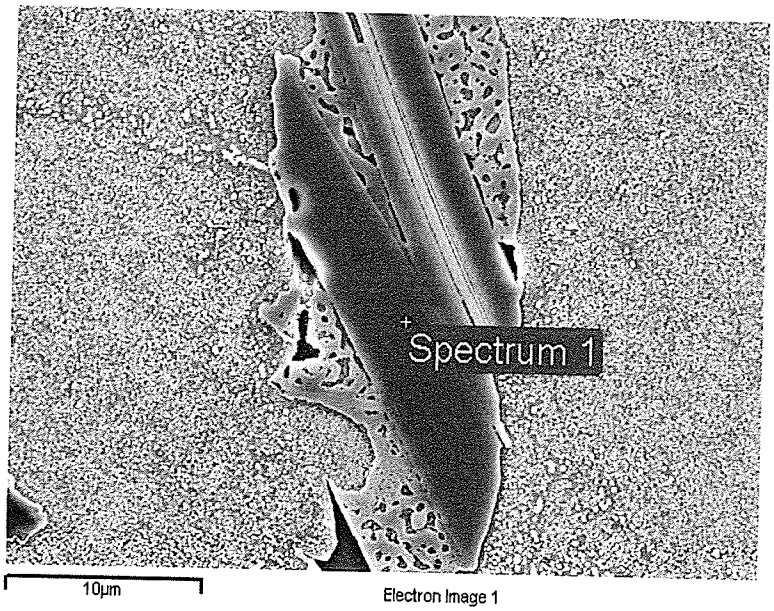

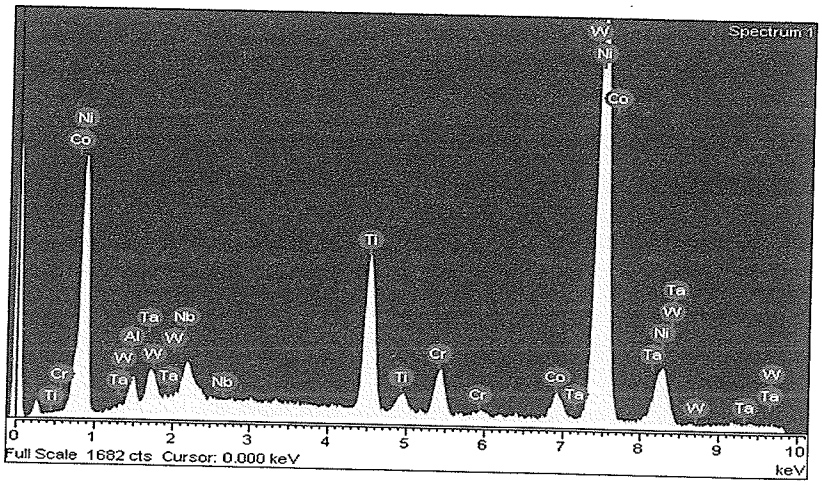

Fig. 4.7: EDS spectra of a) Ni-Ti rich phase, b) M_2SC-type phase and c) Chromium-rich boride phase observed in the centerline eutectic constituents formed in 100 µm gap-sized joint bonded at 1175^{0}C for 5 hrs.

b

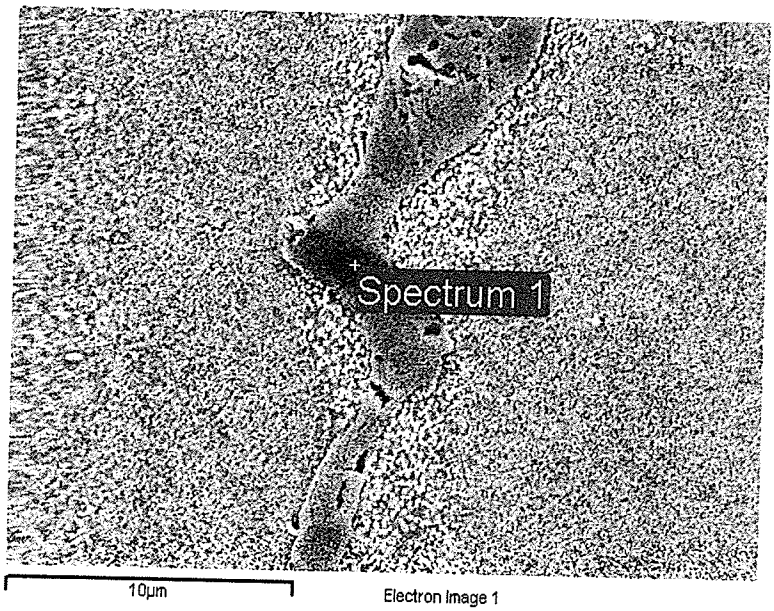
Spectrum 1
10µm
Electron Image 1

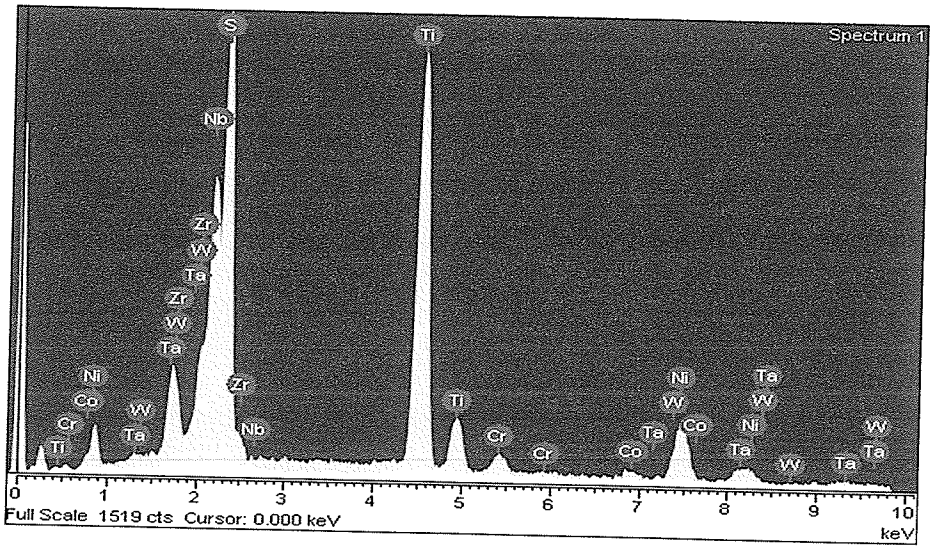
Spectrum 1
S
Ti
Nb
Zr
W
Ta
Ni
Co
Cr
0 1 2 3 4 5 6 7 8 9 10
Full Scale 1519 cts Cursor: 0.000 keV
keV

c

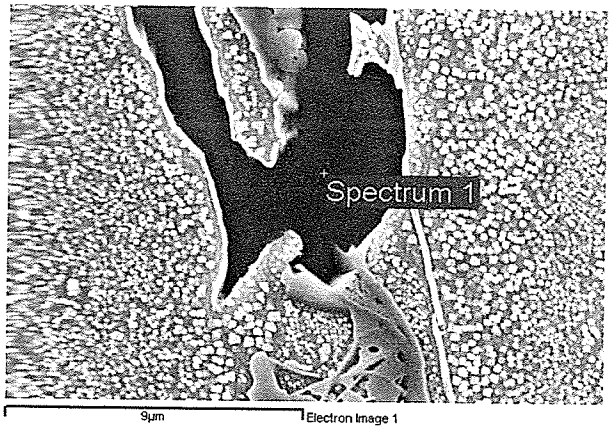
Spectrum 1
9µm
Electron Image 1

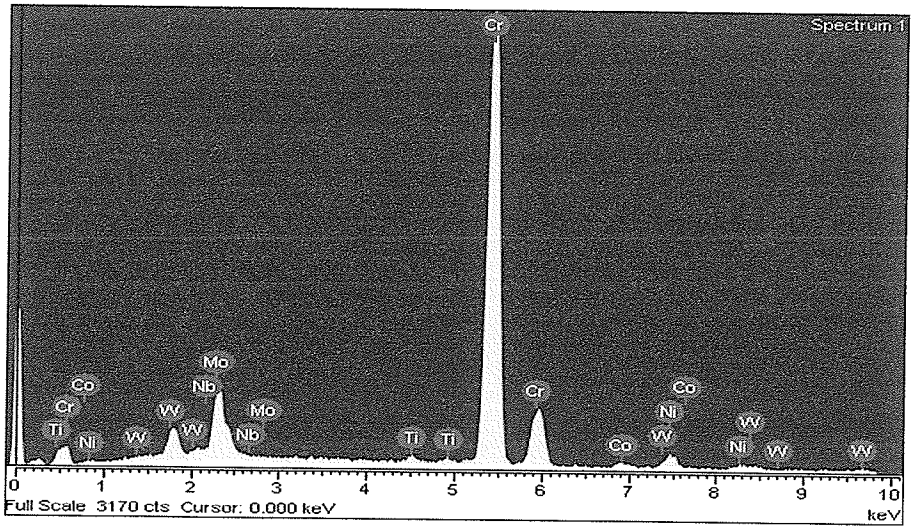
Spectrum 1
Cr
Mo
Nb
Co
Cr
Ti
Ni
V
W
Full Scale 3170 cts Cursor: 0.000 keV
keV

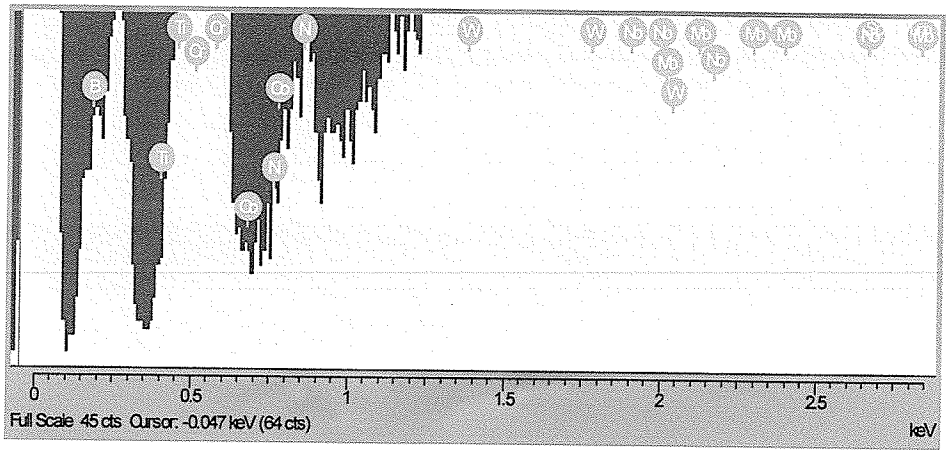
Full Scale 45 cts Cursor: -0.047 keV (64 cts)
keV

Table 4.3: Composition of metallic constituents of distinct centerline eutectic in 100 μm 'NB 150' joint bonded at 1175°C for 5 hrs.

Elements	Ni-Ti rich phase (at %)	M_2SC (sulphocarbide) -type phase (at %)	Chromium rich boride phase (at %)
Al	3.23	-	-
Ti	11.82	39.3	0.78
Cr	4.22	2.18	85.32
Co	3.84	1.0	1.47
Ni	73.25	11.0	4.53
Nb	1.96	12.68	-
Ta	1.40	2.52	-
W	0.28	0.32	1.70
Mo	-	-	6.19
Zr	-	5.0	-
S	-	26.02	-

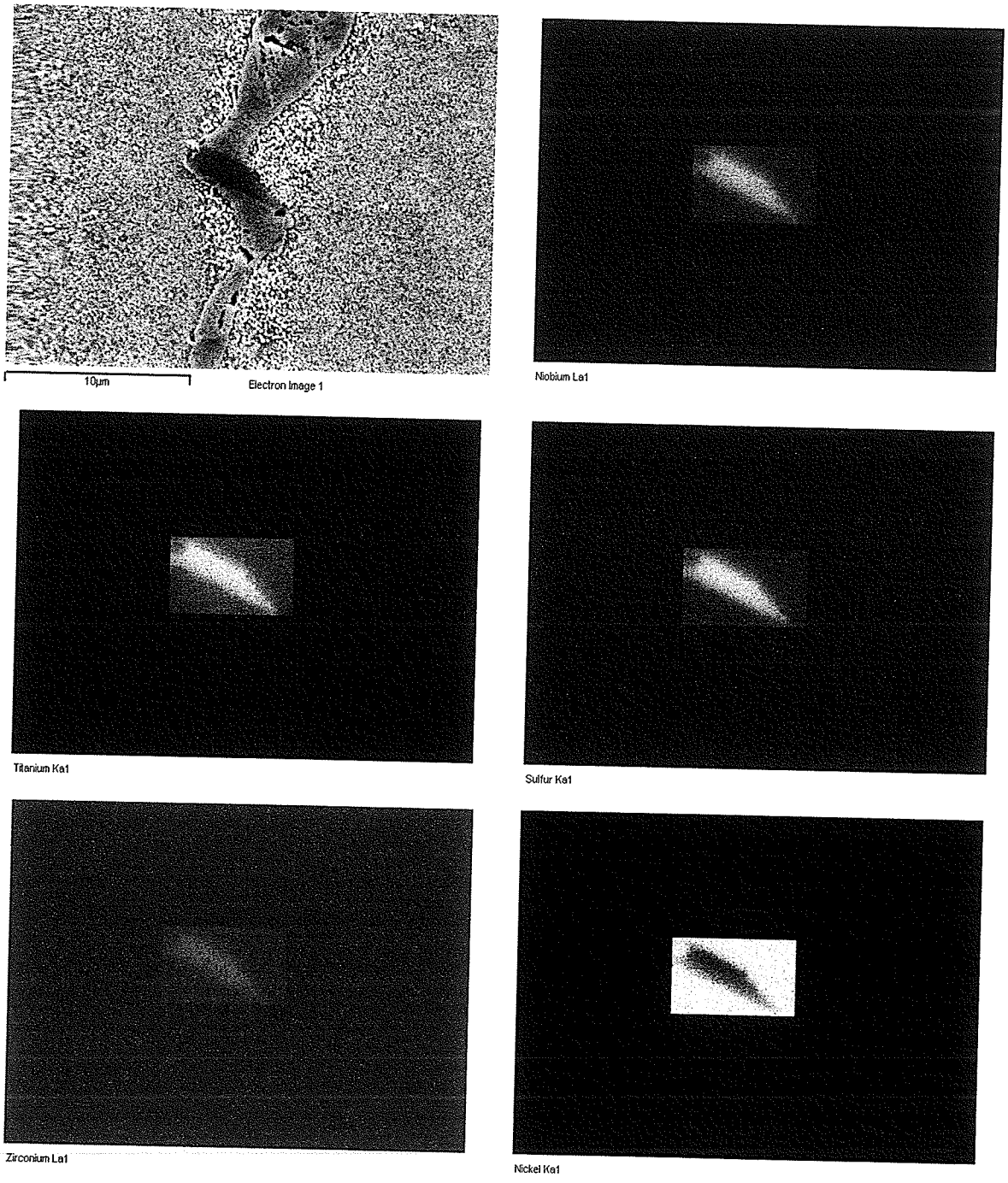

Fig. 4.8: EDS-Xray maps analysis of M_2SC-type phase observed in the centerline eutectic constituents formed in 100 µm gap-sized joint bonded at 1160^{0}C for 5 hrs.

different centerline eutectic constituents, characteristic of those shown in Fig. 4.1 were observed in the joints (i.e. the joints consisted of Ni-rich boride, Cr-rich boride, and γ-solid solution phases). SEM-EDS compositional analyses of the centerline eutectic regions in specimens bonded for 1-3 hrs at 1130°C, 1145°C and 1160°C also revealed that the average concentration of base alloy solute elements Ti, Nb and Zr in the eutectic increased with brazing temperature and time (Table 4.4).

4.1.2 Discussion

Transient Liquid Phase bonding is a widely used technique for joining of heat resistant alloys. This is because a complete isothermal solidification of the liquid interlayer results in the formation of a solid solution phase. When this phase is homogenized, it produces joints that have microstructure and mechanical properties that are comparable to those of the base alloy. However, there will be a limitation to the commercial application of this technique if a complete isothermal solidification could not be achieved within a reasonable time, as this will increase the cost of repairing damaged components, if optimum joint properties are required. In order to shorten the time that is required for a complete isothermal solidification, one of the factors that are commonly controlled is the composition of the filler alloy. Melting point depressants like boron, which is an interstitial element with high diffusivity, are usually incorporated into the filler alloys employed for TLP bonding of Ni base heat resistant alloys. However, certain elements like Al and Ti are deliberately excluded or restricted in amount from the interlayer because they can form deleterious phases during bonding [5], and also prolong the time required for the completion of isothermal solidification. For example, it has been reported

Table 4.4: Variation in the average concentration of Ti, Nb and Zr in the eutectic with bonding temperature and time (for 100 μm gap size).

Bonding Temperature (°C)	Bonding Time (hrs)	Elemental Concentration (at %)		
		Ti	Nb	Zr
1130	0	-	-	-
	1	1.99	0.24	-
	2	2.48	0.35	-
	3	2.81	0.53	-
1145	0	-	-	-
	1	2.40	0.42	-
	2	2.89	0.54	-
	3	3.21	0.57	0.06
1160	0	-	-	-
	1	3.04	0.49	-
	2	4.57	0.99	-
	3	6.33	1.55	0.49

[5] that despite a 24 hr bonding cycle at 1171°C, complete isothermal solidification could not be achieved during TLP bonding of Udimet-700 sample by using an experimental interlayer alloy of composition (wt%) Ni-15Cr-10Ti-5Si. Thus, it is essential that TLP models be developed which will successfully predict the possible effects of each, or combination of, element(s) incorporated in the filler alloy on isothermal solidification behavior. Most analytical and numerical TLP models [36, 37, 56, 62-64] are based on the use of pseudo-binary phase relationships in predicting isothermal solidification behavior. However, in industrial applications, commercial alloys and fillers are multicomponent systems, and the phase relationships encountered when joining them do not always lend themselves very well to the extrapolation of the binary-system based analysis [5]. Sinclair et al [10, 11] proposed a mechanism for the isothermal solidification process in a two-phase ternary system. It was suggested that in most situations, in contrast to the binary case, the composition of the liquid is required to change continuously as isothermal solidification progresses [11]. Thus, if the solubilities and/or diffusion coefficients of the two solute elements present in the liquid interlayer are very different, the solidification stage will be divided into two parabolic regimes [11]. The first regime would be dominated by the 'faster' solute, and the second dominated by the 'slower' diffusing solute in the liquid. Also, it has been suggested [11] that a lack of complete isothermal solidification reported by Ramirez and Liu [63] might be due to the presence of a second solute, which might be present as an impurity in the base material or in the interlayer. In this regard, only a few models have been reported in the literature [10, 11], which were able to predict the possible effects of a second solute element in the filler alloy on isothermal solidification rate. This is because the concentration path that such an

interlayer takes during solidification is far more complex, as it is dependent on the relative diffusivities and phase relationships between the elements [49]. It should be noted that although the manufacturers of filler alloys can preclude/control the concentrations of solute elements that can negatively affect the kinetics of isothermal solidification, however, most of these solute elements are used as alloying additions in the commercial alloys, which need to be brazed. Therefore, there is a possibility of enrichment of the liquefied filler with these solute elements from the base alloy during TLP bonding. This could conceivably alter the final microstructure of the filler [69] and result in a similar reduction in isothermal solidification rate as observed when the starting composition of the filler alloy was not properly controlled. An enrichment of the liquid interlayer with base metal solute element(s), and the subsequent modification of its concentration have been reported [40] during the TLP bonding of NiAl with a Ni-Si-B filler alloy. In that work, a rapid increase in the Al concentration of the eutectic (residual liquid interlayer) with bonding time, which was originally Al-free, was observed. After bonding at 1065°C for 1 min and 20 mins, respectively, the average concentration of Al in the eutectic was found to be 6 at % and 12 at %, respectively. Similar observations were also reported in a separate work on diffusion brazing of NiAl/Ni-Si-B/Ni couple [39]. At a brazing temperature of 1065°C, the average Al concentration in the eutectic increased from 2 at % after 5 mins, to 6 at % after 20 mins of brazing. It should be also noted that it took about 1260 mins (≈ 21 hrs) to completely solidify a NiAl/Ni-Si-B/NiAl couple [39]. The analysis of the isothermal solidification profile showed that approximately 44 μm wide liquid isothermally solidified within the first 100 mins (1.67 hrs), thereafter, it took around 19.33 hrs to solidify the remaining 14 μm of liquid. This

suggests that there might exist two different isothermal solidification regimes during their experiments.

In the present work, it is seen from Fig. 4.3 that isothermal solidification occurred under two different regimes at bonding temperatures of 1160°C and 1175°C. The rate at which isothermal solidification occurred in the first regime was fast as compared to the second regime, which commenced at time t_2^0 and led to an increase in the time required for a complete isothermal solidification. An enrichment of the liquid interlayer at all the bonding temperatures of 1130°C, 1145°C, 1160°C, and 1175°C with base alloy solute elements such as Ti, Nb and Zr, and a continuous modification of the liquid interlayer composition was observed as the solidification progressed (Table 4.4). Although, initial composition of the filler alloy was (at %) Ni-15Cr-3.5B, it was seen that the average concentration of Ti, Zr and Nb in the eutectic (residual liquid interlayer) after 3 hrs of bonding at 1160°C, was 6.33, 1.55 and 0.49 (at %), respectively. These elements are known to be melting point depressants and have equilibrium partitioning coefficients that are less than 1 in IN 738LC superalloy [23]. This would suggest that they might selectively partition into the liquid as solidification progresses, and induce the observed second slow solidification regime when their concentration reaches a critical amount in the residual liquid interlayer after a bonding time t_2^0. The time t_2^0 was observed to decrease with an increase in bonding temperature. This is because the concentration of the enriching base alloy solute elements increased in the liquid interlayer with an increase in the bonding temperature. Further evidence of the enrichment of the liquid interlayer with base alloy solute elements, and its continuous modification as solidification

progressed, was noted from the differences in the nature and composition of the phases formed in the centerline eutectic constituents, in both regimes, at different bonding temperatures. For example, centerline ternary eutectic constituents of Ni-rich boride, Cr-rich boride and γ-solid solution phases, termed 1st regime-type eutectic constituents, and typical of those shown in Figs. 4.1 c and d, were observed within the first hour of bonding at 1160°C and 1175°C, respectively. However, at the same bonding temperatures, centerline eutectic constituents consisting of distinctly fine $\gamma - \gamma'$ eutectic-type resolidification product, Ni-Ti rich phase, Cr-rich boride, and M_2SC-type sulphocarbide phase, termed 2nd regime-type eutectic constituents, and typical of those shown in Figs. 4.5 and 4.6, were observed after 5 hrs of brazing. The nature and composition of the 2nd regime-type eutectic constituents reflect the enrichment of the residual liquid interlayer in the aforementioned base alloy solute elements prior to athermal solidification. Thus, it is suggested that isothermal solidification was completed before the critical composition was reached at 1130°C and 1145°C, respectively. Therefore, the effects of the enriching base alloy solute elements could be minimized by ensuring that their concentrations were very low in the liquid.

4.2 Effects of Joint Gap Size on Isothermal Solidification Rate

4.2.1 Results

To study the effects of joint gap size on the rate of isothermal solidification, 25 μm, 50 μm, 75 μm, and 100 μm gap-sized coupons were bonded using Nicrobraz 150 filler, at 1160°C for varying times ranging between 1-8 hrs. The average centerline eutectic widths in 75 μm and 100 μm joints were measured using the SEM and plotted against the

bonding time (Fig. 4.9). As shown in this figure, a complete isothermal solidification of the filler in the 75 μm and 100 μm joints was achieved after 7 hrs and 8 hrs of bonding, respectively. Also, 25 μm and 50 μm gap-width joints isothermally solidified completely within 2 hrs of bonding. A secondary electron SEM image of the microstructure of the 25 μm gap-width joint after 2 hrs of bonding is shown in Fig. 4.10. It is seen that the microstructure of the joint consisted of predominantly secondary γ' precipitates, and the eutectic constituent was not observed in the joint. The secondary γ' precipitates formed within the γ-solid solution matrix after a complete isothermal solidification of the joint was achieved. The γ' precipitates were also observed in completely isothermally solidified 50 μm, 75 μm and 100 μm gap-width joints after bonding for 2, 7, and 8 hrs, respectively. Fig. 4.11 shows the microstructure of a 75 μm gap-width joint after 6 hrs of bonding. It is seen that the centerline of the joint consisted of eutectic phases, which are characteristic of those observed in the centerline of 100 μm joints bonded for 5 hrs at 1160°C and 1175°C, respectively (as shown in Figs. 4.5 and 4.6). These phases were identified to be a Ni-Ti rich phase, M_2SC-type sulphocarbide, chromium-rich boride, and $\gamma - \gamma'$ eutectic. It should be noted that similar eutectic constituents were observed in the centerline of 75 μm and 100 μm gap-width joints, which were bonded for 3-5 hrs and 4-7 hrs at 1160°C. However, below these bonding times, a different eutectic constituent made up of Ni-rich boride, Cr-rich boride and γ solid solution phase was observed in the joints.

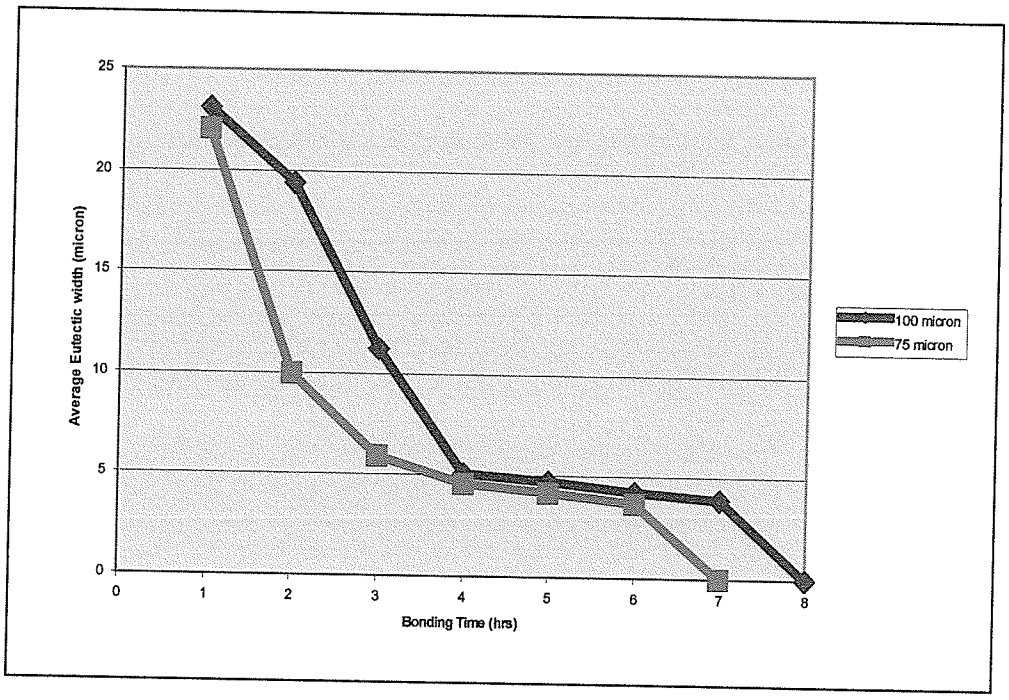

Fig. 4.9: Variation in average eutectic width with bonding time, for 100 μm and 75 μm gap sizes at 1160°C.

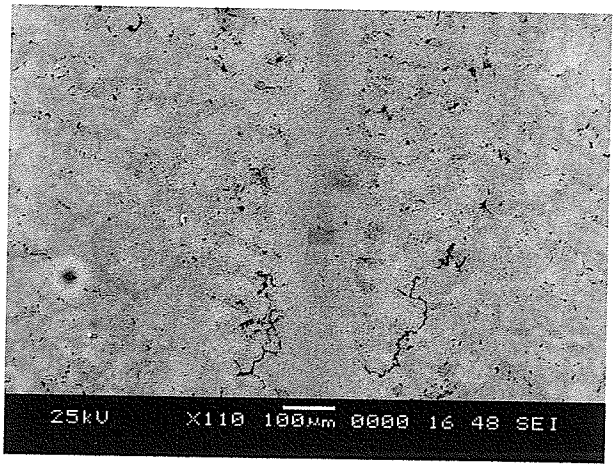

Fig. 4.10: SEM microstructure of completely isothermally solidified 25 µm joint bonded at 1160°C for 2 hrs.

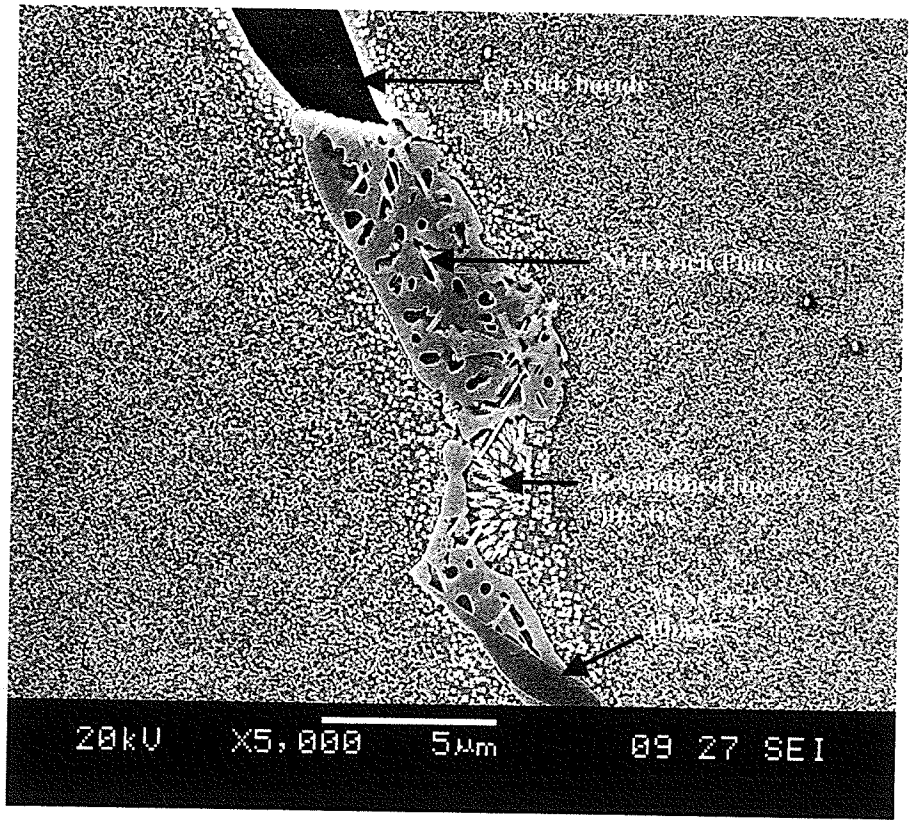

Fig. 4.11: Centerline eutectic constituents observed in 75 µm joint bonded for 6 hrs at 1160°C.

4.2.2 Discussion

Experimental results revealed that at 1160°C bonding temperature, t_2^0 increased with an increase in joint gap size. Based on the nature and composition of the phases formed in the centerline eutectic subsequent to incomplete isothermal solidification, the value of t_2^0 was deduced to be approximately less than 1hr and between 1-2 hrs for 25 μm and 50 μm joints, respectively. However, the values of t_2^0 for the 75 μm and 100 μm joints were significantly larger, approximately 3hrs and 4hrs, respectively. The observed increment in the value of t_2^0 with an increase in gap size could be due to the fact that the thicker the starting width of the liquid interlayer, the smaller would be the concentration of the enriching base metal solute elements in it. Thus, the critical composition at which the second regime sets-in at t_2^0 would be expected to be reached first in the 25 μm joint, as was observed experimentally.

A schematic illustration of the factors affecting the TLP joining process during bonding of Inconel 738LC superalloy using Nicrobraz 150 filler is shown in Fig. 4.12. It is suggested that a process of partitioning of the base alloy solute elements enriching the residual liquid interlayer occurs simultaneously as the isothermal solidification process progresses. This process becomes significant, leading to the commencement of the slower 2nd solidification regime, only when the concentration of the partitioned elements reaches a critical concentration at time $t_2^0 < t_f$, where t_f is the isothermal solidification completion time as predicted by the conventional TLP model, which depends on the bonding temperature (T_{Bp}) and the joint gap size. Thus, experimental results are in good agreement with predictions made by using the conventional TLP model, in as much as

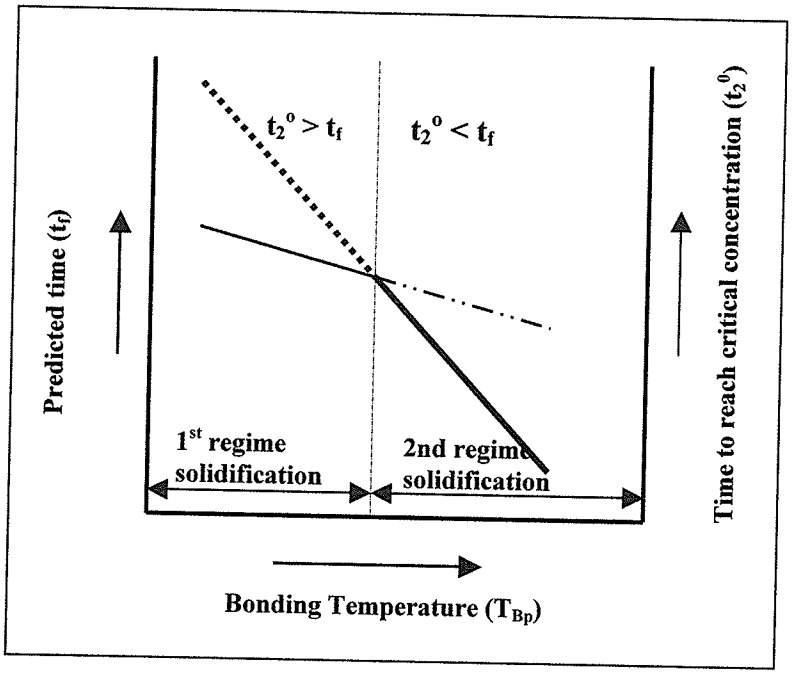

Fig. 4.12: Schematic of the factors affecting isothermal solidification process during TLP bonding of IN 738LC.

$t_2^0 > t_f$ and a complete isothermal solidification of the joint will be achieved during the 1st regime. Otherwise (i.e. when $t_2^0 < t_f$), the slower 2nd solidification regime commences; leading to a prolonging of the time required for complete isothermal solidification, and thus a significant deviation from the predictions of the conventional TLP model.

4.3 Effects of Brazing Temperature and Joint Gap Size on the nature of Interfacial Precipitates

4.3.1 Results

To study the effects of brazing temperature on the nature of interfacial precipitates, 100 μm gap-sized Inconel 738LC superalloy coupons were vacuum TLP bonded for 1 hr at temperatures of 1067^{0}C, 1160^{0}C, and 1175^{0}C, respectively. From the Ni-B binary alloy phase diagram [81] (see Fig. 4.13), the possible Ni-B binary eutectic temperatures, depending on the relative compositions of Ni and B, are deduced to be 1018^{0}C, 1093^{0}C, and 1111^{0}C, respectively. However, since the eutectic melting temperature of the filler alloy is 1055^{0}C, the brazing temperatures were chosen such that the filler alloy would melt completely, and at the same time the characteristics of the interfacial precipitates could be studied at temperatures clearly below (1067^{0}C) and above (1160^{0}C and 1175^{0}C) the quoted Ni-B binary eutectic temperatures of 1093^{0}C and 1111^{0}C. Furthermore, 100 μm and 25 μm gap-sized Inconel 738LC coupons were also vacuum TLP bonded for 1 hr at temperature of 1067^{0}C. This was done in order to study the effect of joint gap size on the nature of interfacial precipitates.

Figs. 4.14 a, b, and c show the SEM microstructure of 100 μm samples after 1 hr of bonding at 1067^{0}C, 1160^{0}C, and 1175^{0}C, respectively. It is seen that the microstructure of

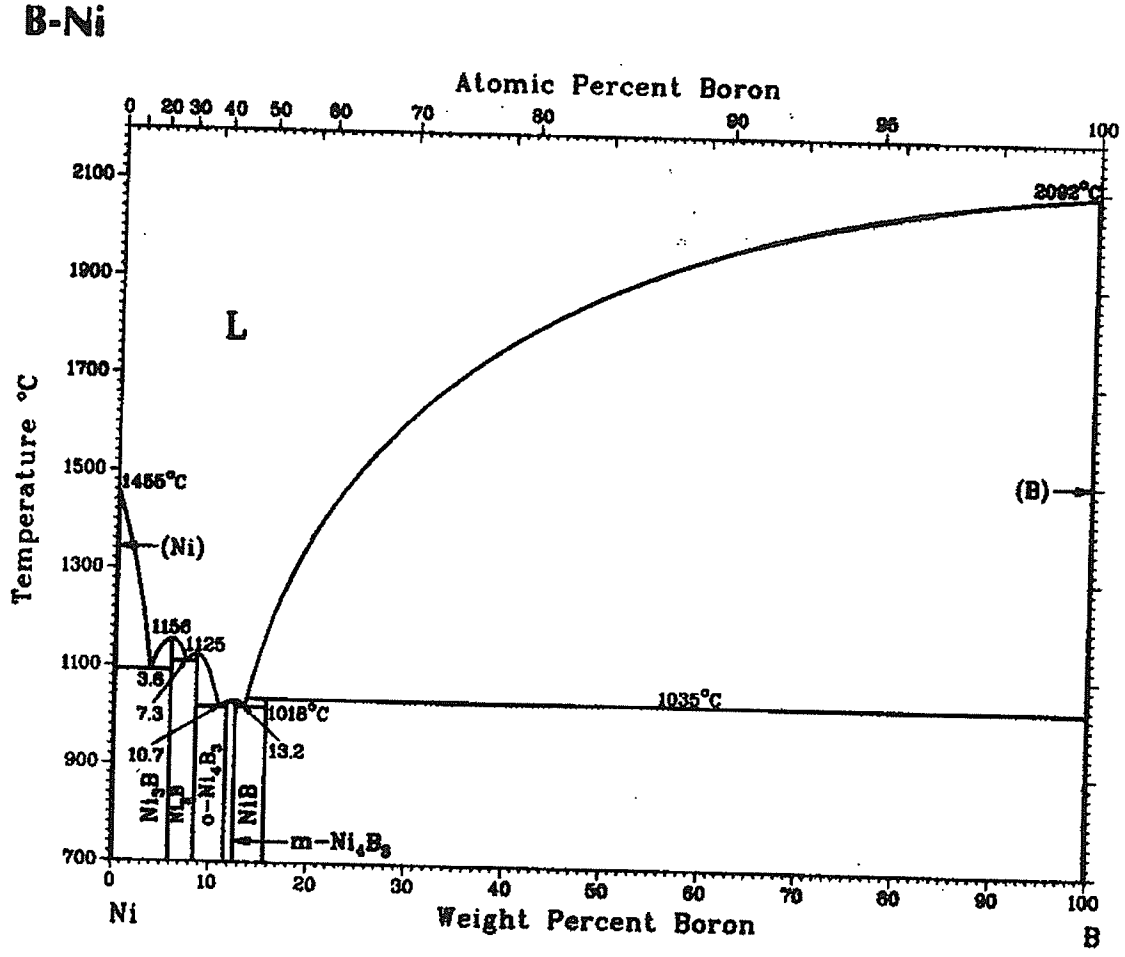

Fig. 4.13: Ni-B binary phase diagram [81]

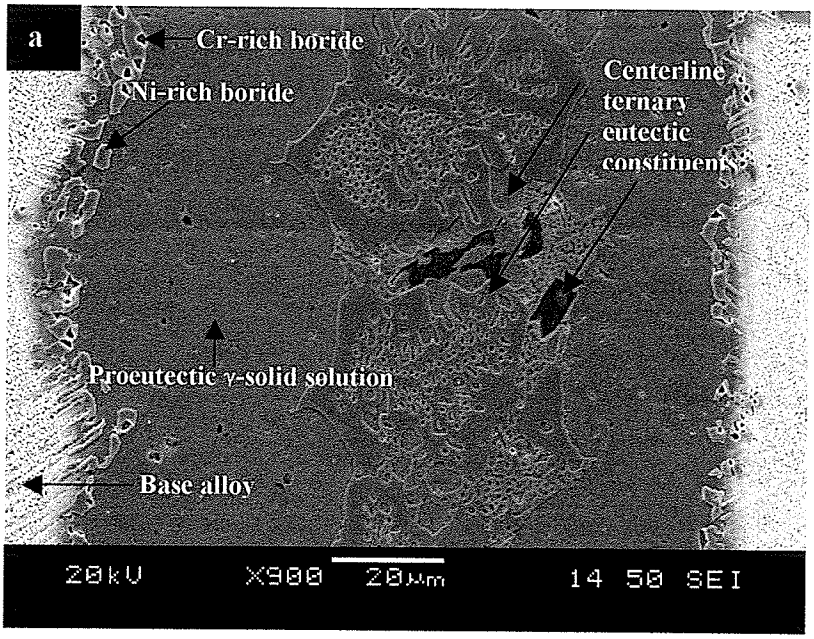

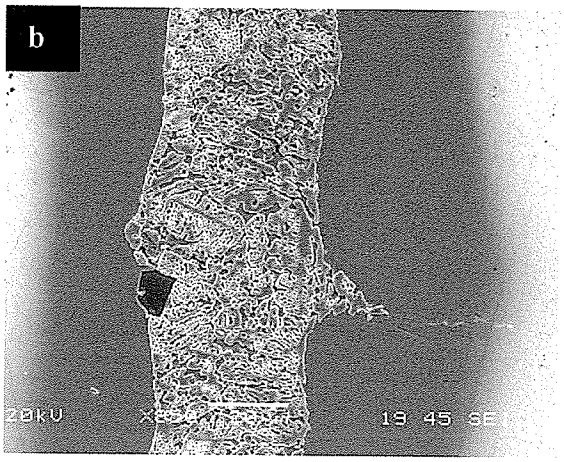

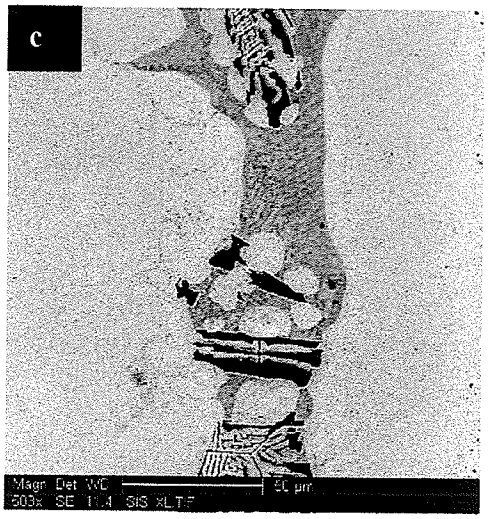

Fig. 4.14: SEM microstructure of a 100 μm joint brazed for 1 hr at a) 1067^{0}C b) 1160^{0}C and c) 1175^{0}C.

the joints, at all the bonding temperatures, consisted of similar centerline ternary eutectic constituents. These ternary eutectic constituents have been earlier identified to be nickel base γ-solid solution, nickel-rich boride, and chromium-rich boride phases (see section 4.1.1). They formed at the centerline of the joints during the athermal solidification of the residual liquid interlayer, which occurred due to incomplete isothermal solidification at the brazing temperatures [5, 9, 79, 80]. Also, as shown in Figs. 4.14 a, b, and c, the centerline ternary eutectic constituents were bordered on the two sides adjacent to the base alloy by an isothermally solidified pro-eutectic region, which has a composition similar to that of the nickel base γ-solid solution phase present in the eutectic. However, a mixture of irregularly shaped particles, which demarcated the original position of the substrate/insert interface, was observed in the 100 μm joint that was brazed at 1067^0C for 1 hr (see Fig. 4.14 a). These particles protruded from the base alloy into the isothermally solidified pro-eutectic Ni-base γ-solid solution region of the joint. Figs. 4.15 a and b show the EDS spectra of the interfacial particles. It is seen that boron was detected in both of the particles; however, its concentration could not be determined due to difficulty in quantifying the light elements with sufficient accuracy. The EDS compositional analyses of the rest of the elements (Table 4.5) suggest the particles to be nickel-rich and chromium-rich borides. It should be noted that the irregularly shaped Ni-rich and Cr-rich boride particles were not observed at the substrate/insert interfaces of 100 μm joints, which were brazed at 1160^0C, and 1175^0C, respectively (Figs. 4.14 b and c). The region essentially consisted of the pro-eutectic Ni-base γ-solid solution phase, which formed during isothermal solidification of the liquid interlayer. Fig. 4.16 shows the SEM microstructure of 25 μm joint after 1 hr of bonding at 1067^0C. It is seen that no eutectic

a

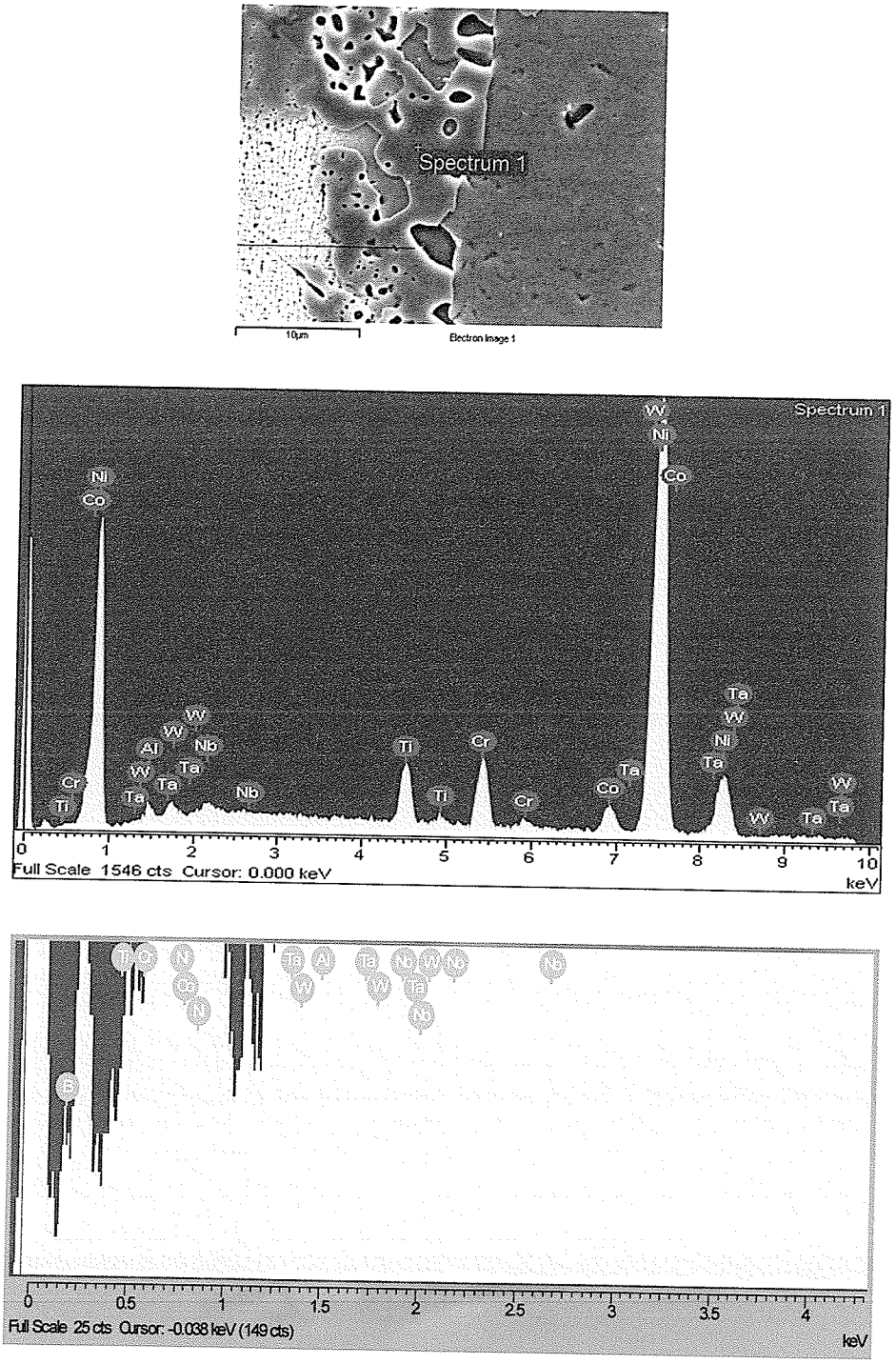

Fig. 4.15: EDS spectra of a) Ni-rich boride particle and b) Cr-rich boride particle observed at the original substrate-insert interface of a 100 µm joint brazed at 1067^{0}C for 1 hr.

b

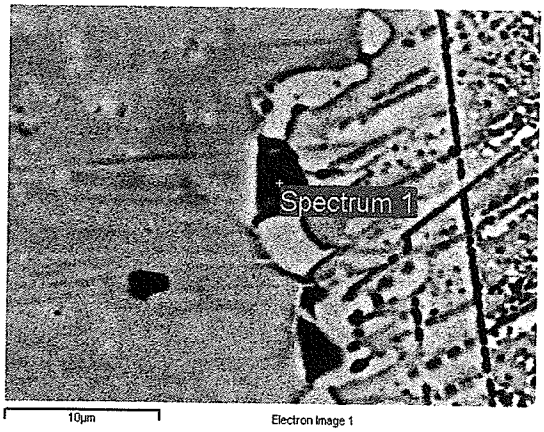
Spectrum 1
10µm
Electron Image 1

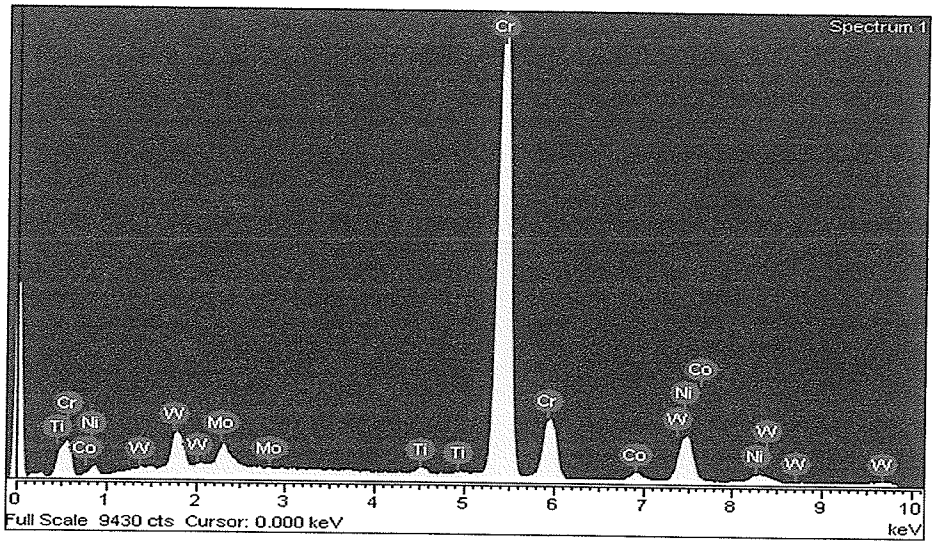
Spectrum 1
Cr
Ti
Ni
Co
W
Mo
Full Scale 9430 cts Cursor: 0.000 keV
keV

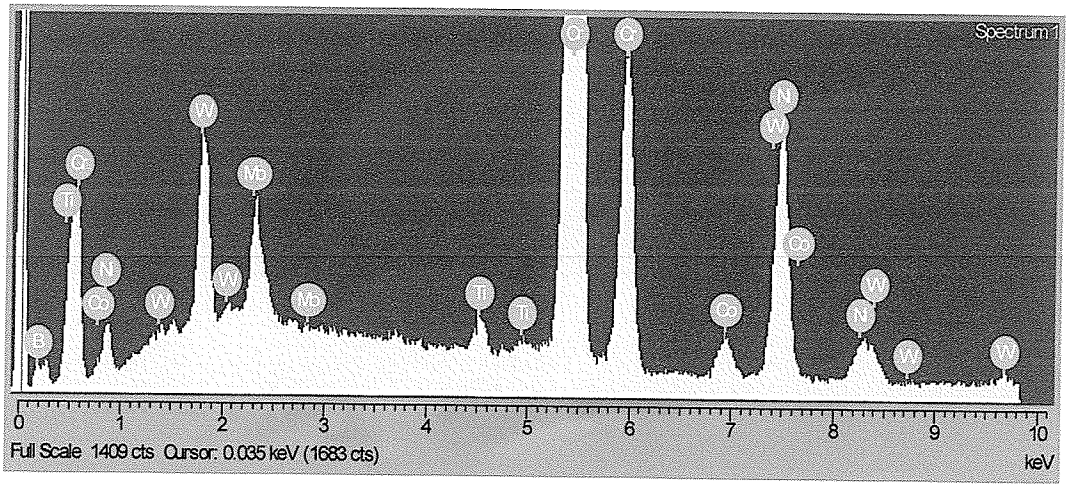
Spectrum 1
Full Scale 1409 cts Cursor: 0.035 keV (1683 cts)
keV

Table 4.5: Composition of particles observed at the original substrate/insert interface of 100 μm joint brazed at 1067°C for 1 hr.

Element	Ni-rich Boride Phase (at%)	Cr-rich Boride Phase (at%)
Al	1.78	-
Ti	4.72	0.77
Cr	6.42	78.46
Co	4.10	2.09
Ni	81.69	14.56
Nb	0.49	-
Ta	0.55	-
W	0.25	2.21
Mo	-	1.91

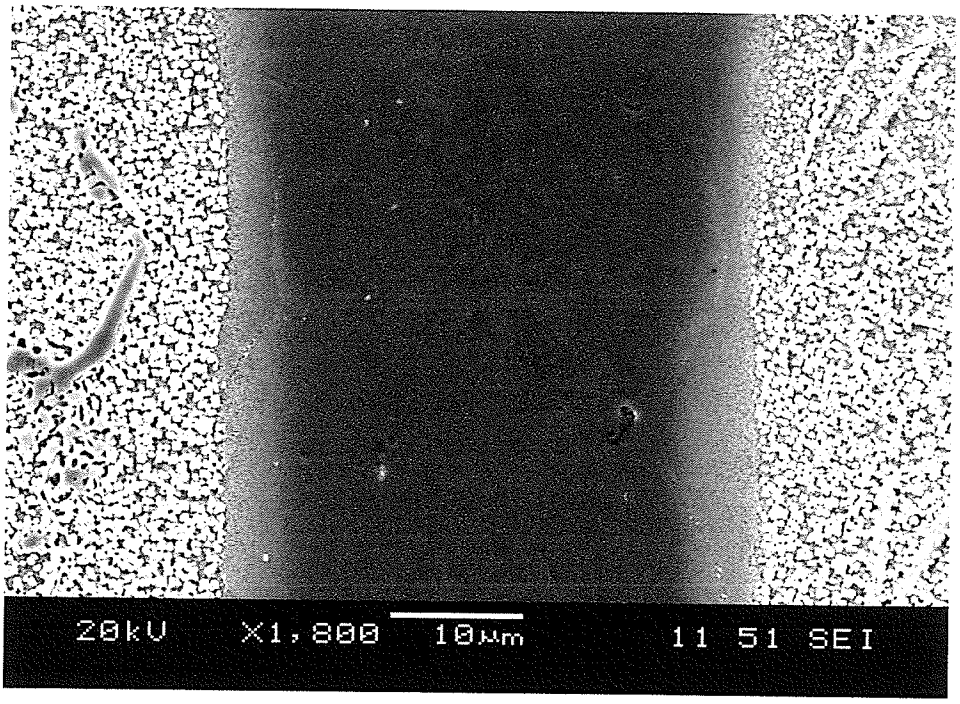

Fig. 4.16: SEM microstructure of a 25 µm joint brazed at 1067^{0}C for 1 hr.

constituent was observed in the centerline of the joint. The joint region essentially consisted of nickel base γ-solid solution phase. This suggested that a complete isothermal solidification of the liquid interlayer occurred after 1 hr of brazing. Also, neither the Ni-rich boride nor the Cr-rich boride particles was observed at the original substrate/insert interface of the joint.

4.3.2 Discussion

Conventional TLP models [37, 62, 63] have always predicted the formation of interfacial precipitate-free joints by TLP bonding. In these models, it is assumed that the solid-state diffusion of the melting point depressant (MPD), which results in isothermal solidification, starts after the equilibration of the solid and liquid phases to their respective solidus and liquidus compositions at the bonding temperature. However, Lee and North [70] and Nakagawa et al [52] have suggested a simultaneous occurrence of the solid/liquid equilibration process and the solid-state diffusion process, as against their assumed sequential occurrence. In the work of Gale and Wallach [68, 69], nickel substrates were bonded using a ternary Ni-Si-B insert. It was suggested that a significant solid-state diffusion of the melting point depressant, which was boron, occurred in the substrate before the completion of the equilibrium process. This was reported to result in the precipitation of Ni_3B boride particles at the original solid/insert interface when the solubility limit of boron was exceeded at the bonding temperature, which was below the Ni-B binary eutectic temperature.

Microstructural observations, similar to those reported by Gale and Wallach [68, 69] were also reported by Orel et al [39] during the TLP bonding of NiAl/Ni-Si-B/Ni couple at a temperature (1065°C) below the quoted Ni-B binary eutectic temperature range. In their work, boride particles were observed on the Ni substrate side immediately adjacent to the original location of the solid/liquid interface. In this work, after holding a 100 μm gap-sized coupon at 1067°C for 1 hr, a mixture of irregularly shaped Ni-rich and Cr-rich boride particles was observed, demarcating the original position of the substrate/insert interface. However, such particles were not observed in joints that were brazed at 1160°C and 1175°C respectively. The absence of the interfacial precipitates at these temperatures might be partially due to the fact that the brazing temperatures were above the Ni-B binary eutectic temperature range. However, an examination of the Cr-B binary eutectic phase diagram (see Fig. 4.17 [82]) revealed that the lowest Cr-B eutectic temperature is 1630°C. Thus, it was expected that the Cr-rich boride phase would still be formed at the original substrate/insert interface, since the brazing temperatures (1160°C and 1175°C) were far below the Cr-B binary eutectic temperature. As a result of this observation, it may be suggested that the eutectic temperature of the Cr-rich boride phase may have been significantly reduced by the presence of other alloying elements, or the solubility limit of boron in this region of the substrate might not have exceeded at these brazing temperatures. The absence of the Ni-rich and Cr-rich boride particles at the original substrate/insert interface of a 25 μm joint that was brazed for 1 hr at 1067°C was also contrary to the expectations, as the precipitation of both of these phases was expected since the brazing temperature was clearly below the Ni-B binary eutectic temperature

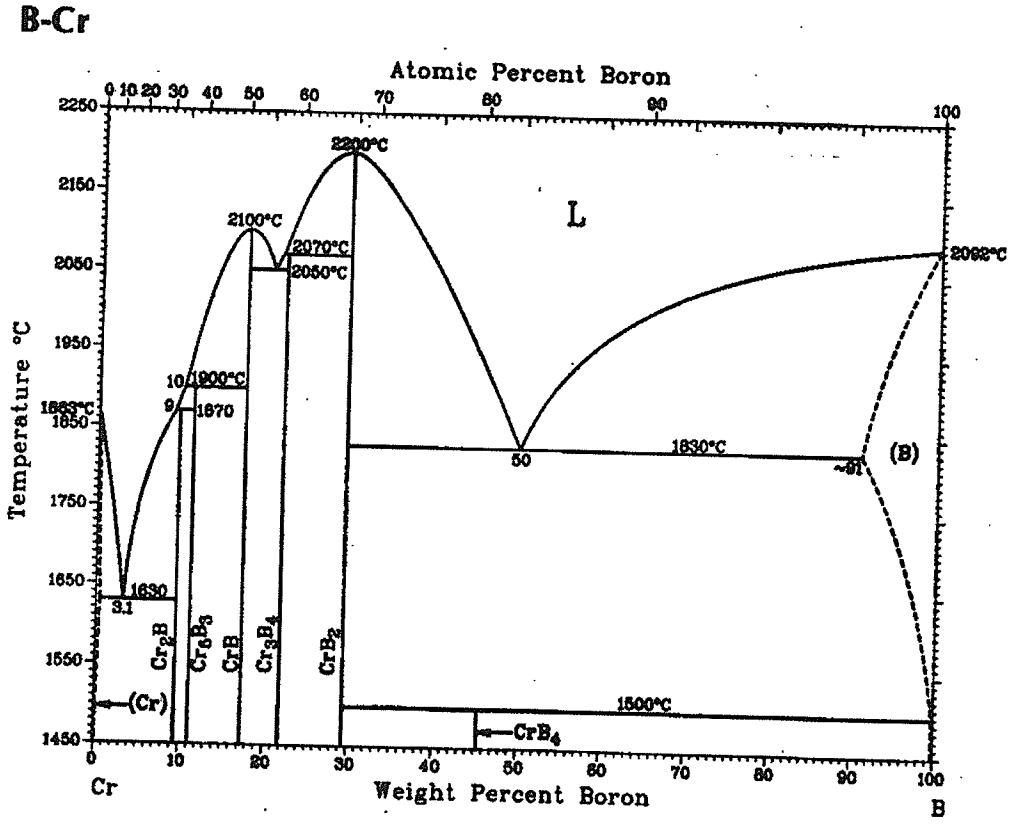

Fig. 4.17: Cr-B binary phase diagram [82]

range. It should be noted that at the same brazing temperature and time, these phases were observed in the 100 μm joint (Fig. 4.14 a). Therefore, it is likely that some diffusion-related brazing factors, like brazing temperature and joint gap size, affect the solid-state diffusion of boron prior to the completion of the equilibration process at the solid/liquid interface. If these factors are favorable, the equilibration process will occur fast enough before a significant amount of boron is diffused into the substrate. Subsequent to this, the solubility limit of boron immediately adjacent to the original substrate/insert interface will not be exceeded. Thus, second phases will not precipitate in this region. Gale and Wallach [68] have suggested that the behavior of a Ni-Si-B ternary insert used in their experiment should be similar to that assumed in the conventional TLP models, if the equilibration process is fast enough before a significant solid state diffusion has taken place. Also, in the work of Orel et al [39, 40], boride particles were not observed on the NiAl side of brazed NiAl/Ni-Si-B/Ni and NiAl/Ni-Si-B/NiAl assemblies. This was attributed to the low diffusivity of boron in NiAl substrate.

Taking an introspective look into the factors that can control the equilibration process, Nakao et al [62] modeled the kinetics of the equilibration process of a nickel base superalloy, which was brazed using a Ni-Cr-B ternary filler alloy, by using the Nernst-Brunner equation of the type:

$$n = n_s\left\{1 - \exp(\frac{-KAt}{V})\right\} \qquad (1)$$

where,

n = solute concentration in the liquid at time t

n_s = solute concentration in the liquid at equilibrium

K = dissolution rate constant, which varies with the brazing temperature

A = surface area of the solid-liquid interface

V = volume of the liquid phase

t = holding time.

Assuming that the width of the liquid zone at any instant of time (t) during the equilibration process equals the initial width of the interlayer, then, it is seen from equation (1) that the time required for the equilibration process to be half-way completed (i.e. when $n = \frac{n_s}{2}$) may be given by equation:

$$t = \frac{-W \ln(0.5)}{K} \qquad (2)$$

where,

W $\left(\approx V/A\right)$ is the half gap width of the interlayer.

Notwithstanding that the assumption leading to equation (2) may not be totally viable, because the width of the liquid interlayer actually increases during the equilibration process, the equation may provide a qualitative relationship between the equilibration time, joint gap size, and brazing temperature. It has been shown [60] that the value of K increases with temperature; thus, a decrease in the equilibration time is expected with an increase in brazing temperature. Nishimoto et al [83] have reported dissolution time of 700 secs, 300 secs, 180 secs, 60 secs, and 10 secs during the TLP bonding of single crystal CMSX-2 superalloy at temperatures of 1373, 1398, 1423, 1453, and 1523K, respectively. This suggests that the rate of the equilibration process increases with increase in brazing temperature. Also, it is seen from equation (2) that by the time

$\left(t_{25} \approx \frac{8.664x10\text{^}-6}{K}\right)$ the equilibration process is half way completed $\left(\frac{n}{n_s} = 0.5\right)$ in a 25 μm gap-sized joint, it will still be one-sixth $\left(\frac{n}{n_s} \approx 0.16\right)$ completed when a 100 μm gap width is used. Therefore, the differences in the precipitation behavior of the interfacial precipitates observed in this study might be related to the faster equilibration process achievable by brazing at higher temperatures (e.g. 1160°C and 1175°C), using a 100 μm gap-sized coupon, or at lower temperature (e.g. 1067°C), using a 25 μm gap-sized coupon. This would have resulted in a reduction in the solid-state diffusion of boron that occurred before the completion of the equilibration process.

4.4 Effects of Brazing Temperature on Grain Boundary Precipitates

4.4.1 Results and Discussion

To study the effects of brazing temperature on second phase particles that formed on the substrate grain boundaries of brazed joints, 100 μm gap-sized coupons were brazed in the vacuum furnace for 1 hr at temperatures of 1067^{0}C, 1160^{0}C, and 1175^{0}C, respectively. Figs. 4.18 a and b show the SEM microstructure of the extensive mixture of second phase particles that were observed along the substrate grain boundaries of 100 μm joints, which were brazed for 1 hr at 1067^{0}C and 1160^{0}C, respectively. These particles extended as far as 150 μm into the substrate alloy. The EDS spectra of the second phase particles, which were observed along the substrate grain boundaries of the 100 μm joints brazed for 1 hr at 1067^{0}C are shown in Fig. 4.19 and 4.20. It is seen that boron was detected in some of the particles, as shown in Fig. 4.19. The EDS compositional analyses of the rest of the

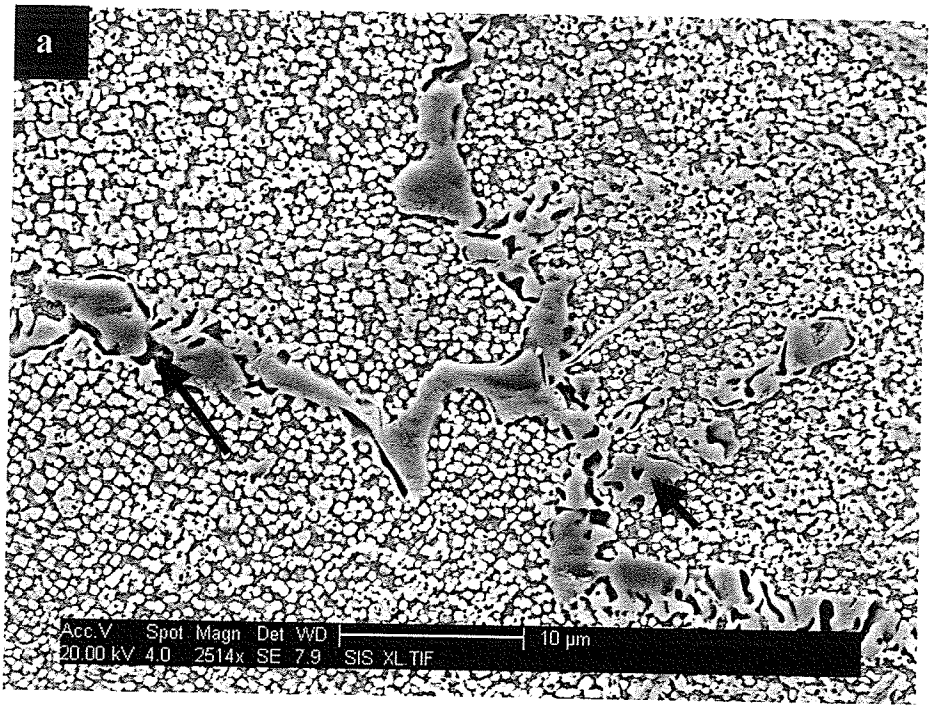

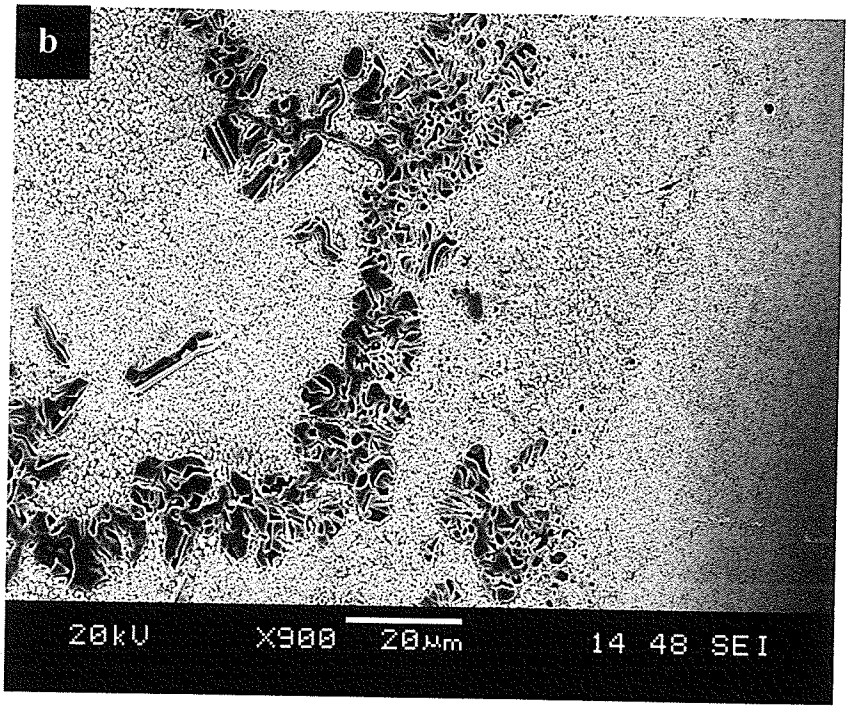

Fig. 4.18: SEM microstructure of second phase particles observed along the substrate grain boundaries of 100 µm joint brazed for 1 hr at a) 1067°C and b) 1160°C.

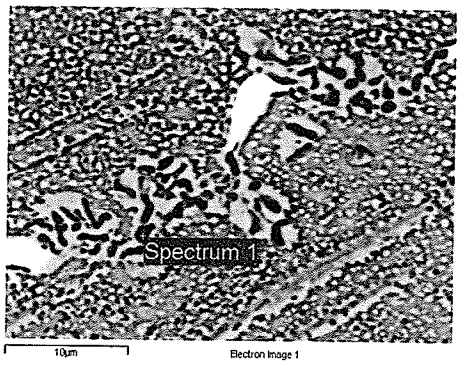

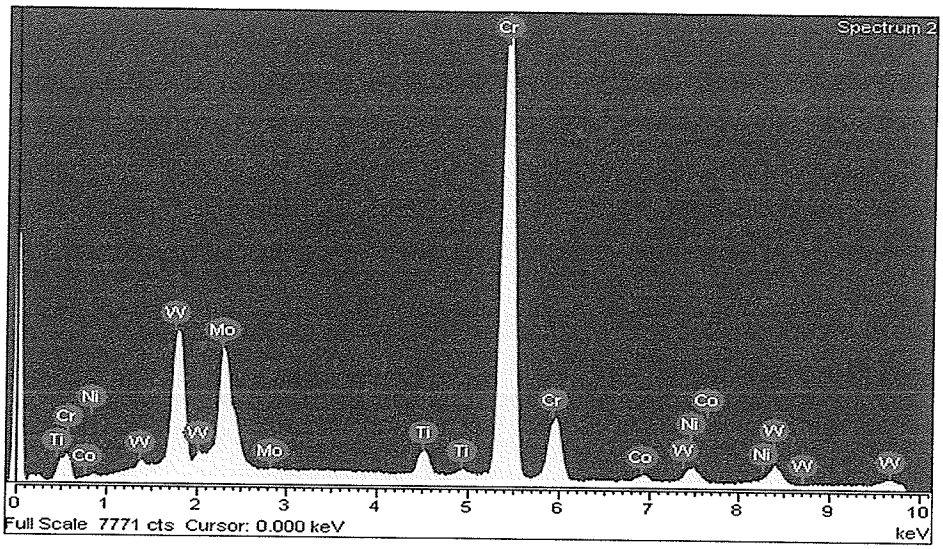

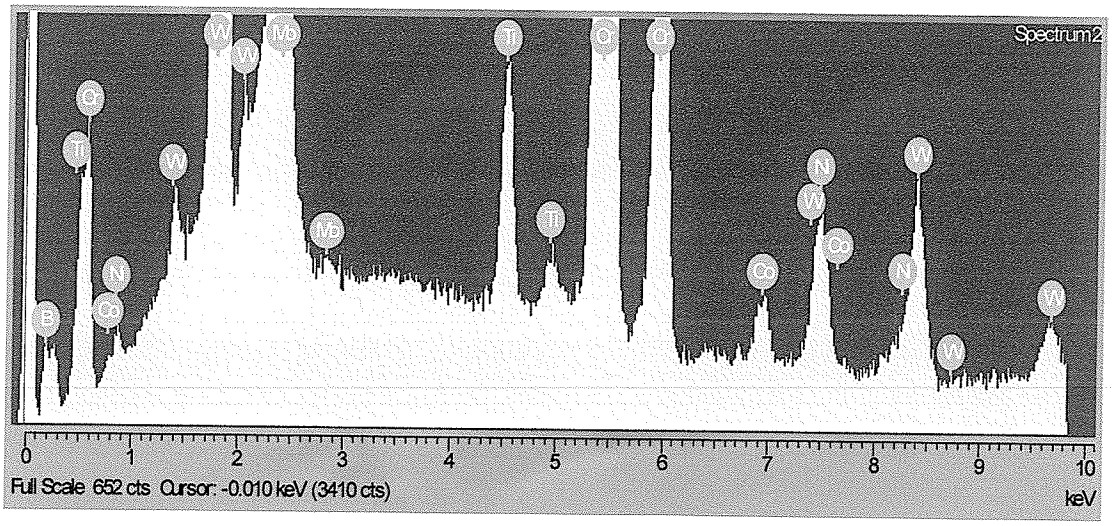

Fig. 4.19: EDS spectra of a Cr-rich boride particle observed along the substrate grain boundary of 100 µm joint brazed at 1067^{0}C for 1 hr.

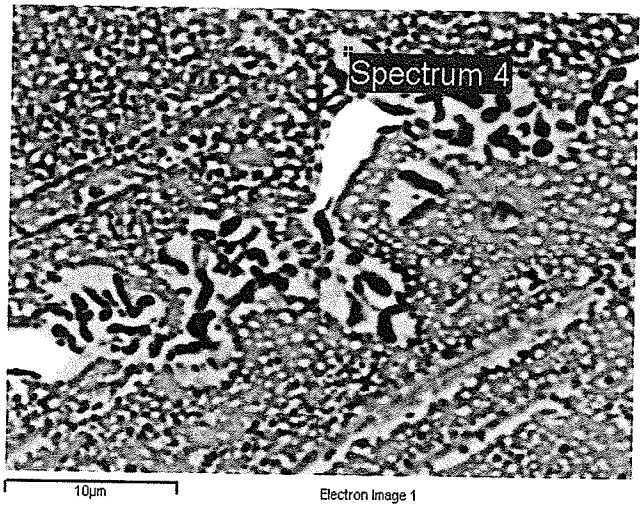

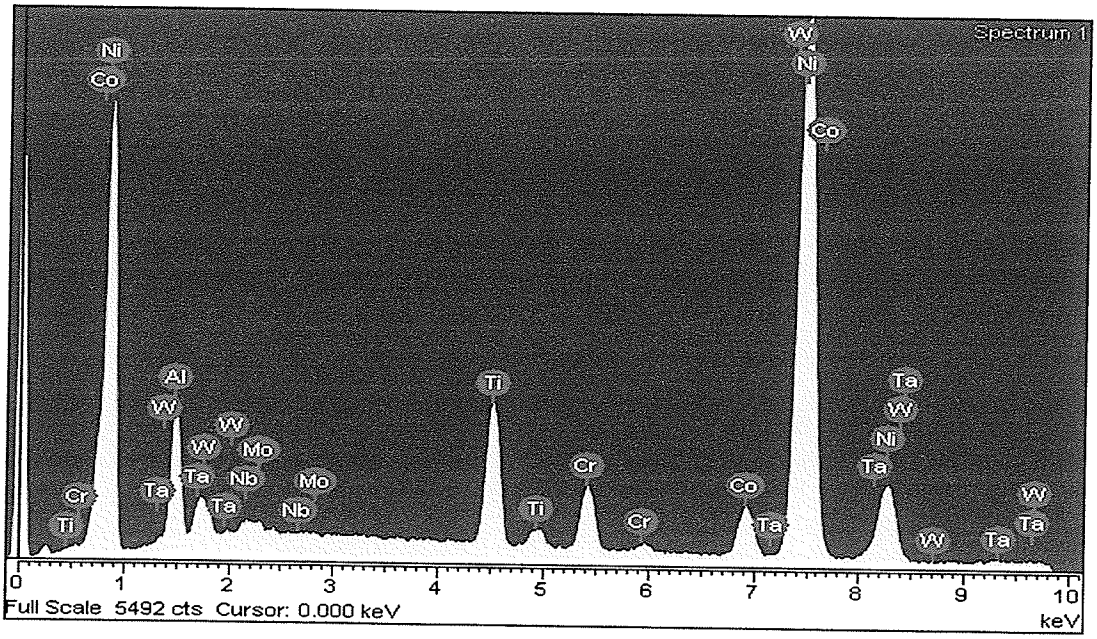

Fig. 4.20: EDS spectra of a Ni-Al-Ti rich particle observed along the substrate grain boundary of 100 µm joint brazed at 1067^{0}C for 1 hr.

elements (Table 4.6) suggest the second phase particles to be Cr-rich boride and Ni-Al-Ti rich phases.

It is known that grain boundaries provide high diffusivity paths for solute elements in comparison to volume diffusion [66] from liquid interlayer into the base alloy during isothermal solidification. This can significantly increase the TLP process kinetics, thus reducing the isothermal solidification completion time [83]. In fact, Saida et al [84] reported a progressive decrease in isothermal solidification completion time in the following order; single-crystal, coarse-grained, and fine-grained nickel base alloys. However, this can also have a detrimental effect, as the precipitation of second phase particles, as observed in the present work, is inevitable when the solubility limit of the solute element is exceeded along the grain boundaries. Fig. 4.21 shows the microstructure of the substrate grain boundaries of a 100 μm joint, which was brazed for 1 hr at 1175°C. It can be seen that at this temperature, dispersed Cr-rich boride particles were observed on the substrate grain boundaries of the joint. Also, non-equilibrium resolidified fine γ/γ' eutectic-type products formed around some of the Cr-rich boride particles. It should be noted that the Cr-rich boride particles were surrounded by Ni-Al-Ti rich particles on the substrate grain boundaries of the joints brazed at 1067°C and 1160°C, respectively. Thus, this suggests that a localized liquation of the Ni-Al-Ti rich particles took place at 1175°C, resulting in the formation of γ/γ' eutectic-type products around some of the Cr-rich boride particles.

Table 4.6: Composition of the second phase particles observed along the substrate grain boundaries of 100 μm joint brazed at 1067°C for 1 hr.

Element	Ni-Al-Ti rich phase (at %)	Cr-rich boride phase (at %)
Al	10.96	-
Ti	7.89	2.96
Cr	4.12	74.94
Co	5.51	1.66
Ni	69.20	4.22
Nb	0.51	-
Mo	0.17	9.45
Ta	1.11	-
W	0.53	6.79

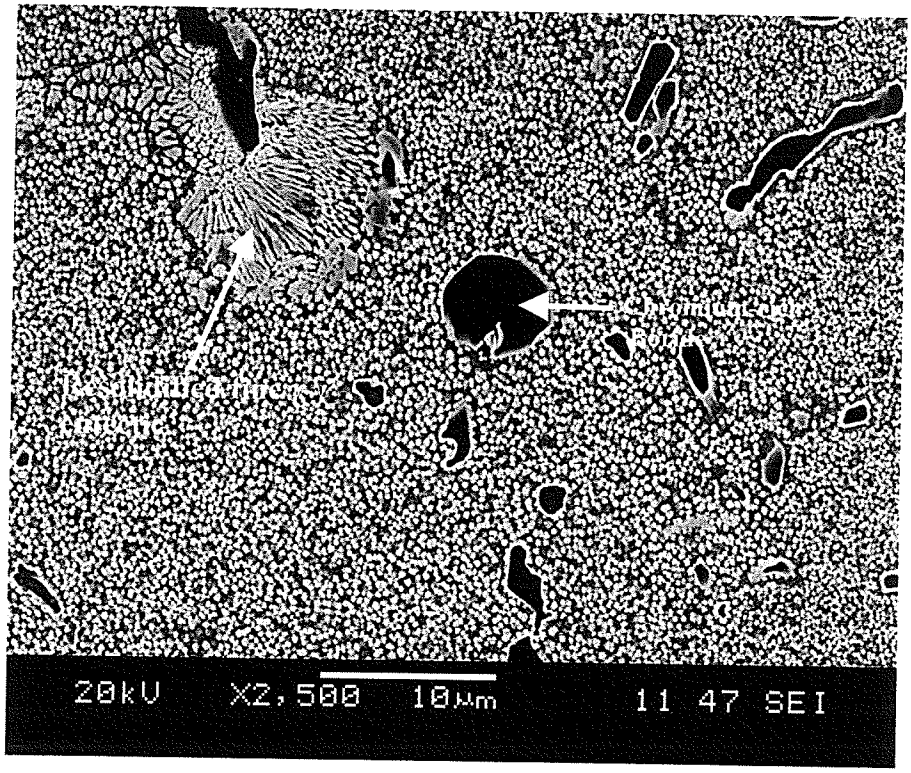

Fig. 4.21: SEM microstructure of dispersed Cr-rich boride particles and fine resolidified γ/γ' eutectic-type products observed on the substrate grain boundaries of 100 µm joint brazed at 1175^{0}C for 1 hr.

Chapter 5

CONCLUSIONS

The effects of bonding temperature and joint gap size on isothermal solidification rate, and on the nature of interfacial/grain boundary particles formed during the transient liquid phase (TLP) bonding of IN 738LC superalloy using a ternary Ni-Cr-B filler alloy, Nicrobraz 150, were investigated. The results of this investigation showed that:

1) The residual liquid after incomplete isothermal solidification at the bonding temperatures transformed into centerline eutectic-type constituents. Isothermal solidification was however achieved after bonding for 6 hrs, 5 hrs, and 8 hrs at 1130°C, 1145°C and 1160°C, respectively.

2) The current TLP model successfully predicted the time required for a complete isothermal solidification of the interlayer liquid in the joints at bonding temperatures of 1130°C and 1145°C. However, significant deviation occurred at 1160°C and 1175°C.

3) Isothermal solidification rate was observed to have two different regimes at the brazing temperatures of 1160°C and 1175°C. The nature and composition of eutectic phases formed during the two regimes were different from each other. In the 1st regime, eutectic constituents consisted of Ni-rich boride, Cr-rich boride, and γ-solid solution phases. While in the 2nd regime, they consisted of $\gamma - \gamma'$ eutectic-type

products, Ni-Ti rich phase, Cr-rich boride phase and M_2SC-type sulphocarbide phase. This is attributed to the substantial enrichment of the liquid interlayer with some of the base alloy solute elements and the continuous modification of its composition as isothermal solidification progressed.

4) Boride phases formed at the original substrate/insert interface of 100 μm gap-sized coupon, which was brazed for 1 hr at 1067°C. Their formation can be prevented by brazing at a suitable temperature and/or gap size in which the solid/liquid phase equilibration process is fast enough. This would prevent the diffusion of a significant concentration of boron into the substrate before the completion of the equilibration process.

5) Extensive amount of Cr-rich boride and Ni-Al-Ti rich particles were observed on the substrate grain boundaries of 100 μm joints that were brazed for 1 hr at 1067°C and 1160°C, respectively. However, brazing at 1175°C resulted in the localized liquation of the Ni-Al-Ti rich particles, as resolidified fine γ/γ' eutectic type products were observed around some of the Cr-rich boride particles.

Chapter 6

SUGGESTIONS FOR FUTURE WORK

1) From the present work, it is seen that the presence of a second solute element in the liquid interlayer, either due to solute enrichment from the base alloy, or due to its presence in the filler alloy, may significantly affect isothermal solidification completion time. This has not been generally considered in the existing TLP models, where a binary phase relationship is usually assumed between the base and the filler alloys. Therefore, it is expedient that a TLP model be developed, which will take this factor into consideration. Although, the problem might become more complicated, as the phase relationships encountered during such situation may not lend themselves to simple extrapolations.

2) Further systematic work needs to be done to investigate the effects of base alloy composition on isothermal solidification rate by brazing a multicomponent alloy with a filler, and comparing the isothermal solidification profile with that of a pure base metal brazed using the same filler and the brazing cycle.

3) Conventional TLP models have always predicted the formation of interfacial particle-free joints during TLP bonding. However, experimental observations which are contrary to the predictions of the TLP models have been reported in the literature. Thus, the understanding of the mechanisms of formation of the interfacial particles during TLP bonding is still an emerging subject in the

literature. Due to the limitation of SEM, which was used for the microstructural observations in this work, the quantitative chemical composition and crystallographic relationships between the interfacial particles could not be established. It is believed that a significant contribution will be made if proper interfacial studies were to be carried out using Transmission Electron Microscopic and EDS-TEM techniques.

4) In the present work, microstructural features, which contribute to the inferiority of TLP-bonded joints, compared to the base alloy, were observed at the centerline, interface and grain boundaries of IN 738LC TLP-bonded joints. Further work needs to be done to investigate the contribution of each and/or combination of these features to the degradation of the mechanical properties (tensile and stress-rupture strengths) and corrosion resistance of the TLP-bonded joints.

5) Following a complete isothermal solidification, a thermal treatment of TLP bonded part is necessary to produce a seemingly microstructural/chemically homogeneous joint. Thus, further work needs to be done in designing a suitable post-braze heat treatment operation for the TLP-bonded IN 738LC superalloy. This will result in the optimization of the mechanical properties of the bonded part.

REFERENCES

[1] Mattheij, J.H.G, Role of brazing in repair of superalloy components – advantages and limitations, Mater. Sci. and Tech., Vol 1 (No. 8), 1985, p 608-612.

[2] Duvall, S.D., and Owczarski, W.A., Further Heat-Affected-Zone Studies In Heat Resistant Nickel Alloys, Weld. J., Vol 46 (No. 9), 1967, p 423s – 432s.

[3] Haafkens, M.H., and Matthey, G.H., A new approach to the weldability of nickel-base as-cast and powder metallurgy superalloys, Weld. J., Vol 61 (No. 25), 1982, p 25-30.

[4] Ojo, O.A., Richards, N.L., and Chaturvedi, M.C., Contribution of constitutional liquation of gamma prime precipitate to weld HAZ cracking of cast Inconel 738 superalloy, Scripta Mater., Vol 50, 2004, p 641 – 646.

[5] Duvall, S.D., Owczarski, W.A., and Paulonis, D.F., TLP Bonding-a New Method for Joining Heat Resistant Alloys, Weld. J., Vol 53 (No. 4), 1974, p 203 – 214.

[6] Humpston, G., and Jacobson, D.M., Principles of Soldering and Brazing, ASM International, 1996, p 128 - 129.

[7] Thamburaj, R., Wallace, W., and Goldak, J.A., Post-weld heat-treatment cracking in superalloys, Int. Mater. Rev., Vol 28 (No. 1), 1983, p 1 – 22.

[8] Nishimoto, K., Saida, K., Kim, D., and Nakao, Y., Transient liquid phase bonding of Ni-base single crystal superalloy, CMSX-2, ISIJ Int., Vol 35 (No. 10), 1995, p 1298 –1306.

[9] Ojo, O.A., Richards, N.L., and Chaturvedi, M.C., Effect of Gap Size and Process parameters on Diffusion Brazing of Inconel 738, Sci. Technol. Weld. JOI., Vol. 9, (No. 3), 2004, p 209 – 220.

[10] Sinclair, C.W., Modeling Transient Liquid Phase Bonding in Multicomponent Systems, J. Phase Equilib., Vol 20 (No. 4), 1999, p 361 – 369.

[11] Sinclair, C.W., Purdy, G.R., and Morral, J.E., Transient Liquid Phase Bonding in Two-phase Ternary Systems, Metall. Trans. A., Vol 31A, 2000, p 1187 – 1192.

[12] Johnson, R., Welding J., 60, 10, 1981, p 185s-193s.

[13] Lugscheider, E., Schmoor, H., and Eritt, U., Optimization of repair-brazing processes for gas turbine blades, Proc. Conf. 'Brazing, High Temperature Brazing and Diffusion Welding,' Aachen, Germany, 27-29 June 1995, p 259-262.

[14] Donachie, M.J., and Donachie, S.J., Superalloys – A Technical Guide, 2nd ed., ASM International, 2002.

[15] "Alloy IN-738: Technical Data," INCO, New York, p 1 – 11.

[16] Mishima, Y., Ochai, S., Hamao, N., and Suzuki, T., Solid Solution Hardening of Nickel – Role of Transition Metal and B – subgroup Elements, Trans. JIM, 27, 9, 1986, p 656 – 664.

[17] Thakur, A., MSc Dissertation, University of Manitoba, 1997.

[18] Hoffelner, W., Kny, E., Stickler, R., McCall, W.J., Z Werktoff, 10,1979, p 84.

[19] Madeleine Durand-Charre, The microstructure of superalloys, translated by Davidson, J.H., Gordon and Breach Science Publishers, 1997.

[20] Garosshen, T.J., and McCarty, G.P., Metall. Trans., Vol. 16A, 1985, p 1213.

[21] Sims, C.T., Stoloff, N.S., and Hagel, W.C., Superalloys II, High Temperature Materials for Aerospace and Industrial Power, John Wiley and Sons, New York, 1987, p 165.

[22] Qiu, Y.Y., Scripta Materialia, Vol 33, No 12, 1995, p 1961.

[231] Taha, M.A, and Kurz, W., About Microsegregation of Nickel Base Superalloys, Z. Metallkd, Vol 72 (No. 8), 1981, p 546 –549.

[24] Lacaze, J., Chehaibou, A., and Lesoult, G., Microsegregation during directional solidification of a Ni – Al – Ta alloy, Z. Metallkde, 80, 1, 1989, p 15 – 20.

[25] Rosenthal, R., West, D.R.F., Continuous gamma' precipitation in directionally solidified IN738 LC alloy, Matr. Sci. Technol., Vol 15 (No. 12), 1999, p 1387-1394.

[26] Sallemark, R., Progress Report 2, Cost 50 Programme Sweeden, 1975.

[27] Zhu, Y., Zhang, S., and Xu, L., Superalloys 1988. The metal Society/AIME, 1988, p 703.

[28] Decker, R.F., and Sims, C.T., The Superalloys, Sims, C.T. and Hagel, W.C., eds., John Wiley and Sons, New York, 1972.

[29] Ardell, A.J., Metall. Trans., Vol 16A, 1985, p 2131.

[30] Eagar, T.W., Energy Sources used for Fusion Welding, ASM Handbook, Vol 6, 1993, p 3 – 6.

[31] Davis, J.R. (ed.), Joining, Metals Handbook, 2nd ed., ASM International, 1998, p 1049 – 1053.

[32] Mahoney, M.W., and Bampton, C.C., Fundamental of Diffusion Bonding, ASM Handbook, Vol 6, 1993, p 156 – 159.

[33] Schwartz, M.M., Brazing, 2nd ed., ASM International, 2003, p 1 – 382.

[34] Jahnke, B., and Demny, J., Thin Solid Films, 110, 1983, p 225 – 235.

[35] Bernstein, L., J. Electrochemical Soc., 113, 1966, p 1282 – 1288.

[36] MacDonald, W.D., and Eagar, T.W., Isothermal Solidification Kinetics of Diffusion Brazing, Metall. Trans. A, Vol 29A, 1998, p 315 – 326.

[37] Tuah-Poku, I., Dollar, M., and Massalski, T.B., Metall. Trans. A, Vol 19A, 1988, p 675 – 686.

[38] Maddrell, E.R., and Wallach, E.R., In Proc. Conf. Recent Trends in Welding Science and Technology, David, S.A., and Vitek, J.M. (eds.), 1990, Materials Park, OH, ASM International.

[39] Orel, S.V., Parous, L., and Gale, W.F., Diffusion Brazing of Nickel Aluminides, Weld. J., Vol 74, (No. 9), 1995, p 319s – 324s.

[40] Orel, S.V., Parous, L., and Gale, W.F., Transient Liquid Phase Bonding of NiAl using Ni-Si-B interlayers, Advanced Joining Technologies for New Materials II, 2-4 Mar 1994 (Florida), American Welding Society, 1994, p 5-19.

[41] Wells, R.R., Weld. J. Res. Supp., Vol 53, 1976, p 20.

[42] Venkatraman, R., Wilcox, J.R., and Cain, S.R., Metall. Trans. A, Vol 28, 1997, p 699.

[43] Manente, D., Brazing of Heat-Resistant Alloys, Low-Alloy Steels, and Tool Steels, ASM Handbook, Vol 6, 1993, p 925 – 930.

[44] Gove, K.B., Braze Repair of Aero-engine Components, 1989, p 341 – 345.

[45] Funk, E.R., and Udin, H., Weld. J. Res. Supp., Vol. 6, 1952, p 310s – 316s.

[46] Gale, W.F., and Wallach, E.R., Wetting of Nickel Alloys by Nickel based Brazes, The Institute of metals, 1990, p 170 – 175.

[47] Ambrose, J.C., Jenkins, S., and Nicholas, M.G., 1987, British Association for Brazing and Soldering, Preprint.

[48] Ambrose, J.C., Nicholas, M.G., and Stoneham, A.M., Kinetics of Braze Spreading, Proc. Conf. British Association for Brazing and Soldering, 1992, Coventry, U.K.

[49] MacDonald, W.D., and Eagar, T.W., Transient Liquid Phase Bonding Processes, The Metal Science of Joining, Cleslak, M.J., Perepezko, J.H., Kang, S., and Glicksman, M.E., Eds., The Minerals, Metals & Materials Society, 1992, p 93 – 100.

[50] Zhou, Y., Kuntz, M.L., and Corbin, S.F., Prediction of the Completion Time for Isothermal Solidification in TLP Bonding, Proc. Conf. Joining of Advanced and Specialty Materials, 7 – 9 October 2002, Columbus, OH, ASM International, 2003, p 75 – 82.

[51] Niemann, J.T., and Garrett, R.A., Eutectic Bonding of Boron–Aluminum Structural Components, Part 1, Welding Journal, 53, 4, 1974, p 175s – 183s.

[52] Nakagawa, H., Lee, C.H., and North, T.H., Modelling of Base Metal Dissolution Behaviour during Transient Liquid Phase Brazing, Metall. Trans. A, Vol 22A, 2, 1991, p 543 – 555.

[53] Lommel, J.M., and Chalmers, B., The Isothermal Transfer from Solid to Liquid in Metal Systems, Trans. AIME, Vol 215, 1959, p 499 – 508.

[54] Gale, W.F., Applying TLP Bonding to the Joining of Structural Intermetallic Compounds, JOM, 1999, p 49-52.

[55] Macdonald, W.D., and Eager, T.W., Annu. Rev. Mater. Sci., Vol 22, 1992, p 23-46.

[56] Zhou, Y., Gale, W.F., and North, T.H., Modeling of Transient Liquid Phase Bonding, International Materials Reviews, Vol 40, No. 5, 1995, p 181-196.

[57] Zhou, Y., PhD Dissertation, University of Toronto, 1994.

[58] Langer, J.S., and Sekerka, R.F., Acta Metall., Vol 23, 1975, p 1225-1237.

[59] Onzawa, T., Suzamura, A., and Kim, J.H., J. Jpn. Weld. Soc., Vol 8, No. 4, 1990, p 74.

[60] Ikawa, H., and Nakao, Y., Trans. Jpn. Weld. Soc., Vol 10, No. 1, 1979, p 24.

[61] Lesoult, G., Center for Joining of Materials Report, Carnegie Mellon University, Pittsurgh, PA, Sept. 1976.

[62] Nakao, Y, Nishimoto, K., Shinozaki, K., and Kang, C.Y., Theoretical research on transient liquid insert metal diffusion bonding of nickel base alloys, Trans. Jpn. Weld. Soc., Vol 20 (N0. 1), 1989, p 60-65.

[63] Ramirez, J.E., and Liu, S., Diffusion Brazing in the Nickel-Boron System, Weld. J., Vol 71, 1992, p 365s – 375s.

[64] Liu, S., Olson, D.L., Martin, G.P., and Edwards, G.R., Modeling of Brazing Processes that Use Coatings and Interlayers, Weld. J., Vol 70 (No. 8), 1991, p 207s –215s.

[65] Zhou, Y., Analytical Modeling of Isothermal Solidification during Transient Liquid Phase (TLP) bonding, J. of Mat. Sci. Letters, Vol 20, 2001, p 841-844.

[66] Shewmon, P., Diffusion in Solids, 2nd ed., 1989, p 19-23.

[67] Sakamoto, A., Fujiwara, C., Hattori, T., and Sakai, S., Weld. J., Vol 68, 1989, p 63.

[68] Gale, W.F., and Wallach, E.R., Microstructural Development in Transient Liquid-Phase Bonding, Metall. Trans. A., Vol 22A, 1991, p 2451-2457.

[69] Gale, W.F., and Wallach, E.R., Influence of Isothermal Solidification on Microstructural Development in Ni-Si-B filler Metals, Mater. Sci. Tech., Vol 7, 1991, p 1143-1148.

[70] Lee, C.H., and North, T.H., 71st American Welding Society Convention, Anaheim, CA, April 1990, Preprint, AWS, Miami, FL., 1990, p 273-276.

[71] Crank, J., The Mathematics of Diffusion, 2nd ed., Oxford University Press, Oxford, United Kingdom, 1975, p 37.

[72] Ojo, O.A., Richards, N.L., and Chaturvedi, M.C., Isothermal Solidification during Transient Liquid Phase Bonding of Inconel 738 superalloy, Sci. Technol. Weld. JOI., (in press).

[73] Bell, S.R., Materials Science and Technology, Vol 1, No 8, 1985, p 629-634.

[74] Juergens, W., Wide gap brazing in the maintenance of turbine guide vanes, DVS Berichte (Deutscher Verband fuer Schweisstechnik), Vol 98, 1985, p 78-82.

[75] Le Blanc, A., and Mevrel, R., Diffusion brazing study of DS247/BNi-3/Astroloy, Proc. Conf. on High Temperature Materials for Power Engineering, Sept. 24-27 1990, p 1451-1460.

[76] Wu, X., Chandel, R.S., and Li, H., Evaluation of transient liquid phase bonding between nickel-base superalloys, Journal of Materials Science, Vol 36, No 6, 2001, p 1539-1546.

[77] Li, W., Jin, T., Sun, X., Guo, Y., Guan, H., and Hu, Z., Transient liquid phase bonding of Ni-base single crystal superalloy, Journal of Materials Science and Technology, Vol 18, No 1, 2002, p 54-56

[78] Khan, T.I. and Wallach, E.R., Journal of Materials Science, Vol 30, No 20, 1995, p 5151-5160.

[79] Ojo, O.A., MSc Dissertation, University of Manitoba, 2002.

[80] Ohsasa, K., Shinmura, T., and Narita, T., Numerical Modeling of the Transient Liquid Phase Bonding Process of Ni using Ni-B-Cr Ternary filler metal, J. of Phase Equlib., Vol 20 (No. 3), 1999, p 199-206.

[81] Liao, P.K., and Spear, K.E. (1991): Alloy Phase Diagrams, ASM Handbook, Vol 3, ASM International, 1992, p 2.83.

[82] Liao, P.K., and Spear, K.E. (1986): Alloy Phase Diagrams, ASM Handbook, Vol 3, ASM International, 1992, p 2.81.

[83] Kokawa, H., Lee, C.H., and North, T.H., Metall. Trans., Vol 22A, 1991, p 1627-1631.

[84] Saida, K., Zhou, Y., and North, T.H., Influence of base metal grain size on isothermal solidification during transient liquid-phase brazing of nickel, Journal of Materials Science, Vol 28, No 23, 1993, p 6427-6432.